

Fermi National Accelerator Laboratory

TM-1656

**Technical Assessment
of the
Loma Linda University Proton Therapy Accelerator**

F. Mills, Chairman
*Fermi National Accelerator Laboratory
P.O. Box 500
Batavia, Illinois 60510*

October 1989



Operated by Universities Research Association Inc. under contract with the United States Department of Energy

TECHNICAL ASSESSMENT

OF THE

LOMA LINDA UNIVERSITY PROTON THERAPY ACCELERATOR

OCTOBER, 1989

FERMI NATIONAL ACCELERATOR LABORATORY

**OPERATED UNDER CONTRACT WITH THE
UNITED STATES DEPARTMENT OF ENERGY**

PARTICIPANTS

F. Mills, Chairman

A. Bogacz

F. Cole, LLUMC

J. Crisp

C. Curtis, LLUMC

G. Dugan

D. Finley

D. Harding

M. Harrison

S. Hsueh

R. Little, SAIC

J. MacLachlan

P. Martin

P. Morton, SAIC

C. Owen

C. Schmidt

D. Swenson, SAIC

V. Visnjic

A. Visser

R. Webber

Table of Contents

- I. Introduction
F.E. Mills
- II. Recommendations
F.E. Mills
- III. Individual Reports
 - A. Injection Systems
 - 1. Ion Source and LEBT Performance (C.D. Curtis)
 - 2. Performance of the RFQ and Debuncher (C.W. Owen)
 - 3. Addendum to Ion Source and RFQ Performance (C.D. Curtis)
 - 4. Injection Matching (J.A. MacLachlan)
 - B. Synchrotron Ring - Transverse Dynamics
 - 1. Beam Observations at Injection (P. Martin)
 - 2. Space-Charge Effects at Injection (D. Finley)
 - 3. Coherent Instability Survey (A. Bogacz)
 - 4. Transverse Dynamics During Acceleration (S.Y. Hsueh)
 - 5. Beam Lifetime Due to Gas Scattering (V. Visnjic)
 - C. Synchrotron Ring - Longitudinal Dynamics
 - 1. RF Capture (F.E. Mills)
 - 2. RF Requirements and Performance (J.L. Crisp)
 - D. Synchrotron Ring - Beam Extraction
 - 1. Beam Extraction Dynamics and Performance (M. Harrison & S.Y. Hsueh)
 - 2. Beam Spill Control and Feedback Systems (J.L. Crisp)
 - E. General systems
 - 1. Power Supply Requirements and Performance Implications (A.T. Visser)
 - 2. Diagnostics and Beam Measurement (R.C. Webber)

Introduction

In April 1986, officials of Loma Linda University requested that Fermilab design and construct a 250 MeV proton synchrotron for radiotherapy, to be located at the Loma Linda University Medical Center. In June 1986 the project, having received all necessary approvals, commenced. In order to meet a desirable schedule providing for operation in early 1990, it was decided to erect such parts of the accelerator as were complete at Fermilab and conduct a precommissioning activity prior to the completion of the building at Loma Linda which will house the final radiotherapy facility. It was hoped that approximately one year would be saved by the precommissioning, and that important information would be obtained about the system so that improvements could be made during installation at Loma Linda. This report contains an analysis by Fermilab staff members of the information gained in the precommissioning activity and makes recommendations about steps to be taken to enhance the performance of the proton synchrotron at Loma Linda.

In the design of the accelerator, effort was made to employ commercially available components, or to industrialize the products developed so that later versions of the accelerator could be produced industrially. The magnets could only be fabricated at Fermilab if the schedule was to be met, but efforts were made to transfer that technology to industry. Originally it was planned to use a 1.7 MeV RFQ fabricated at the Lawrence Berkeley Laboratory as injector, but LBL would have found it difficult to meet the project schedule. After consideration of other options, for example a 3.4 MeV tandem accelerator, a supplier (AccSys Inc.) qualified itself to provide a 2 MeV RFQ on a schedule well matched to the project schedule. This choice was made, but a separate supplier was selected to develop and provide the 425 MHz power amplifier for the RFQ.

During the design of a debuncher to reduce the momentum spread of the beam from the RFQ, investigations by Fermilab and AccSys staff predicted that the tightly bunched beam emerging from the RFQ would gain a large momentum spread from the space charge forces in the beam. Calculations indicated that this could partly be offset by employing a debunching cavity in the beam line. Because of this, the project accepted a design intensity of $5 \cdot 10^{10}$ protons per pulse. Subsequent beam measurements have verified the prediction of momentum spread growth.

Recommendations

1. Power Supplies

Power supplies have been the most difficult aspect of the commissioning work at Fermilab. In order to carry out this activity, it was necessary to use magnet power supplies borrowed from the Research and Accelerator Divisions, because the power supplies purchased for the accelerator could not be received in time. In most cases, the borrowed power supplies are inadequate for the purpose, typically having poor ripple and regulation properties in the region where they must be operated. For example, where it would be desirable to have a quadrupole tuning current of one amp, the ripple current is comparable to the tuning current, because the current is so much less than full scale. Further, the unipolar nature of the supplies in many cases does not allow the use of desirable tuning ramps for correction elements.

*At Loma Linda, the purchased supplies go most of the way toward correcting these shortcomings, with the exception of solving the problem of extracted beam modulation, as noted in LL-306. **There will be a continuing need to develop means to remove extracted beam modulation at Loma Linda in preparation for future use of beam-scanning systems.***

Careful attention should be paid to the quality of regulation of the new supplies during ramp down and return to injection field level.

The Holec current transducer provides adequate measure of the ring dipole current to program the RF system VCO, but **care must be taken to prevent noise pick-up by the transducer on the signal path to the VCO.**

Noise pick-up on the current program to the dipole supply must be controlled. With the present program level of 250 A/volt, even a few millivolts of noise will cause significant problems at the injection level.

2. Injector

A. The momentum spread from the RFQ is larger than 1%, which is too large for efficient injection into the ring. The technical specifications supplied by the vendor do not include a specification for momentum spread after space charge spreading and debunching.

B. The peak current surviving the 180° bend is about two thirds the current specified by the vendor.

C. The beam from the ion source does not seem to be properly matched into the RFQ, which can have serious effects on RFQ performance. It is not clear that this is a tractable problem without extensive new diagnostics. **The matching should be studied further with the new Fermilab diagnostics before the source is shipped to Loma Linda. (See addendum A3 below)**

D. The performance of the debuncher has not yet been verified and will require further work at Loma Linda.

E. To obtain present performance, it is necessary to supply almost 250 kW to the RFQ, considerably more than the vendor specification. There are problems with sparking at fields even smaller than the design gradient, and at this level, sparking is frequent. This problem needs further investigation. **The RFQ should be returned to ACCSYS for disassembly and inspection for spark damage. The sparking problem should be monitored carefully during the commissioning at Loma Linda.**

The RFQ Power Amplifier was more than one year late in delivery, so it was necessary that the RFQ be operated with a borrowed supply at low power for most of the commissioning period. Since the RFQ power amplifier was received, it has been a continuing source of trouble, requiring a large amount of work by many Fermilab rf experts. Recently, after considerable hardening and upgrading, the amplifier has run more reliably.

The commissioning experience at Fermilab has demonstrated that the RFQ is not the optimum injector accelerator for a small synchrotron. Even if an RFQ operated as designed, the momentum spread would be too large for the synchrotron ring., partly because of

longitudinal space charge in the tight bunches, which increases the momentum spread even more. Any future synchrotrons of this design should utilize a tandem electrostatic generator or some other dc device with very small output momentum spread and much higher reliability. Such an injector was considered during the design of the Loma Linda synchrotron. A tandem electrostatic generator producing a 25-mA pulse 20 μ sec long (the Loma Linda synchrotron requires only 1 μ sec) of 3.5 MeV protons was built for DESY at the National Electrostatics Corporation, so the technology is proven. The higher injection energy is of course an advantage for space-charge problems in the ring.

If the experience with the RFQ and its power amplifier continue to be disappointing at Loma Linda, replacement of the RFQ by a tandem might be considered if it can be fitted into the building. Some rebuilding of injection-line magnets would be needed to upgrade them to 3.5 MeV.

3. Magnets

The commissioning has demonstrated that the chromaticities of the beam are quite large, as large as 20 horizontally at 2500 Amp. It appears that these large values arise from the sextupole fields of the main dipole magnets, although the measured values of chromaticity are still approximately 50% larger in magnitude than the values calculated from the measured dipole fields. These chromaticity effects are much exacerbated by the large dispersion of the ring.

The main bending magnets should be reshimmed at Fermilab to compensate the sextupole fields causing the chromaticity values. Since the chromaticity varies with excitation, the correction should be effected at mid-field. This should leave some compensation for the chromaticity due to eddy currents at low fields, which is of the opposite sign. Further, the shims should be such as to allow modification in the field.

4. Vacuum

The vacuum system has operated successfully at pressures sufficiently low to obtain lifetimes of a half second at injection. There were problems with large amounts of outgassing material in the injection septum, but a new septum with much better outgassing

properties has now been installed and operated. **The system should be rid of any remaining outgassing materials before it is reassembled.**

5. RF System

Both the low level and the high level systems operate satisfactorily, however They do not provide the capability to operate at fixed frequency with open loops on flat top. **Fixed frequency capability may be needed to help correct extracted beam current modulation.**

6. Diagnostics

A. **The system needs a monitor which displays the total charge in the accelerator.**

B. **An extracted beam current monitor is needed with sufficient bandwidth to be used for feedback control of the extracted beam.** This will help provide a highly desirable state of independence between the accelerator and the end use facility for purposes of control and safety. A gas scintillation chamber has been designed and built for the treatment-room diagnostics that would meet the requirements, but it is considered that this device would generate too much scattering in the beam.

C. **Kickers are needed to "ping" the beam to measure tunes during ramping as well as on flat top or flat bottom or fixed field injection studies..** At present, one of the beam-position monitors is disconnected and used as an electrode to ping the beam.

D. **Moveable jaw scrapers in the 2 MeV beam line and the ring** would be useful to help understand the injector performance, 2 MeV transport, injection and capture processes in the ring, and ring acceptance apertures.

7. Extraction Components

The extraction components seem to perform as designed, but **the electrostatic septum should be operated at higher voltage.** A power supply capable of higher-voltage operation will be available at Loma Linda.

There does not seem to be evidence for strong skew field components from the Lambertson magnet.

Considerably more experimental work is needed to understand extraction losses and nonuniformity.

Magnet measurements showed a chromaticity large enough to be uncomfortable at lowest and highest magnet excitations. Beam measurements showed even higher chromaticity, causing important degradation of accelerator performance.

Sufficiently many many subsystems were complete to proceed with precommissioning in late 1988. The most notable exceptions were the magnet power supplies, the RFQ power amplifier, the control system, the clock system, and the low level RF system. The power supplies used were from spares in the Research and Accelerator Divisions. The AccSys Corporation generously lent the use of their RFQ power amplifier for most of the precommissioning period. The temporary clock system was created from standard Laboratory timing equipment. The control and low level RF systems were built during precommissioning.

The preconditioning can be considered to have been a success. The operation schedule has been accelerated by more than one year, compared to a schedule which would call for installation to begin next winter. The accelerator has operated at $2.5 \cdot 10^{10}$ protons per pulse, half the design goal, with 70% extraction efficiency. The accelerator has carried out successful experiments in shielding and an R & D program in development of components for the beam delivery nozzle. Beam measurements at Fermilab lead to definite recommendations to improve operation at Loma Linda. The rest of this report consists of the recommendations and technical papers written by Fermilab staff addressing the issues arising from the precommissioning.

A.1 ION SOURCE AND LEPT PERFORMANCE

C.D. CURTIS

Requirements

A goal of 1.6×10^{11} protons per pulse at full energy in the synchrotron requires an injected beam of 26mA for one usec. If one allows for 65% (probably too optimistic) capture and acceleration efficiency because of momentum spread and other problems, the required 2-MeV beam from the RFQ is 40 mA. If one uses a reduced goal of 5×10^{10} protons per pulse, the required beam from the RFQ is 12.5 mA, an approximate value which has been used for many recent beam studies. Our hope had been to reach 40-50 mA from the RFQ.

The calculated transverse acceptance of the RFQ is 1.1π mm-mrad (normalized) for a 25-mA beam at the design gradient, increasing to 1.35π for a gradient 15% higher. The acceptance decreases to 0.8π at the design gradient for a 50-mA beam. The Accelerator Systems RFQ is designed for 30 mA with a current limit of ≈ 60 mA.

Match to the RFQ requires a strongly convergent beam to pass through a 9.5-mm aperture 22 mm upstream of the vanes, which have an aperture of approximately 4mm. Calculations have shown that a 70-mA beam of 1π mm-mrad emittance and uniform charge density will just clear the upstream aperture and match to the required α and β .

If one assumes an 80% transmission of the RFQ at the 50-mA current level and that 90% of the input beam falls within the acceptance, then the total ion-beam current required from the source for 90% proton percentage is 77 mA.

Source and Transport Line Description

Layout of the source and transport line is shown in Fig. 1. Beam from the plasma expansion cup of a Duoplasmatron ion source passes through a 2-gap accelerating column into a 30-in long line with two d.c. solenoid focusing lenses for matching to the RFQ input acceptance ellipses. Two sets of horizontal and vertical steering magnets in the drift space between lenses adjust the beam in position and angle at the entrance to the RFQ. Two toroids measure beam current out of the column and into the RFQ. Because of space limitations, the orthogonal beam-profile wires and emittance measuring probe are located only near the center of the line. Each solenoid is 6.33 in. long with an aperture of 2.5 in. The I.D. of the beam pipe is $2 \frac{1}{8}$ in.

Performance

The ion source has been tested to a current of 100 mA. Normal operating currents have been in the 60-75-mA range. Proton fraction depends on source operating parameters and reaches 90%. Maximum beam out of the transport line has read ≈ 60 mA. Most operation has been with 40-55 mA at the entrance to the RFQ. Table 1 gives one example of operating values for the source, transport line and RFQ.

It is impractical to measure emittance at the exit of the column, at the center of the line and at the exit of the line at the same time. Measurements were made at the column exit only on the source test bench and at the exit of the transport line only before the RFQ was put in place. At the exit of the line, measurements with the second solenoid excited to full field for proper match were limited because of inability to record the larger angles with existing instrumentation. Values of emittance for lesser lens excitation could be observed, however. Examples of measurements under various beam conditions are shown in Figures 2-15 for beam currents of 30-75 mA.

Most emittance measurements (90% contour) at the exit of the column have given values of $(0.3-0.5)\pi$ mm-mrad. Values at the exit of the line were mainly $(0.5-1.0)\pi$ with varying amounts of distortion and for beam currents of ~ 40 mA. Values in the line after the first lens have values of $(0.8 - 1.4)\pi$ before correction for molecular ions and noise, which increase the values. The emittance for protons only appears to be $\sim 1 \pi$ in general but with some spherical aberration. Trim lines in the emittance program to eliminate most of the unwanted signal would correct the emittance values closer to their true values.

Because one cannot measure the beam properties at the match point of the RFQ with the RFQ in place, the best diagnostic tool for determining the quality of the match should be the RFQ itself, if it is performing properly. How well are we doing? The answer shows the problem. Fig. 16 shows the transmitted beam through the RFQ and the 2-MeV beam (around the 180° bend). Recent similar plots show these curves approaching each other as the RFQ gradient is increased to ~ 0.53 (the threshold for 2-MeV beam is ≈ 0.43 V) as though it may be approaching a proper operating level. The beam current is still rising very steeply, however, and is only a fraction of the input beam. The highest transmitted beam has been 18 mA at a gradient of 0.55 V. At this time the input beam was ≈ 40 mA.

Explanation of Results-Work on Improvements

A number of factors could contribute to the poor RFQ transmission. Further studies are required to be sure of their relative importance and what improvements may be possible.

1. Emittance too large for acceptance. There is emittance growth in the line, caused in part by spherical aberration of the small aperture lenses. Some improvement in brightness may be possible by installation of a smaller anode aperture in the source to enable higher arc current, and hence high proton percentage, for lower current beams of smaller diameter.

2. Mismatch of beam to the RFQ. Various adjustments in alignment with subsequent changes in steering magnet currents, well within their limits, led to little change in performance. It is unlikely that steering is the problem. Further beam studies using different relative strengths of the lenses is still in order to determine the optimum strengths. It is interesting to note, however, that the beam optics calculation in Fig. 17 based on emittance measurement of a 70-mA beam in the middle of the line succeeded in matching the required α and β at the RFQ with complete space charge neutralization assumed in the line and with lens strengths close to those actually used. The beam envelope fits within the beam pipe radius of 27mm. Another possible solution with higher lens strengths and 60% neutralization is shown in Fig. 18.

3. Wrong injection energy. Some brief tests with a column voltage higher than the 30.5kV maximum of the present power supply have indicated potential for some improvement. A 40-kV supply controllable through the computer will be installed on July 3rd to answer this question.

4. Insufficient rf power. More rf power certainly helps although, as stated earlier, we may be close to a proper operating level. Higher gradient means larger acceptance and more accelerated beam for an input beam of large emittance or mismatched. It may be worth noting, however, that the calculated percentage increase in acceptance along a constant 25-mA curve of acceptance versus gradient is less than 55% of the percentage increase in observed 2-MeV beam versus gradient. The question of adequate power is perhaps still open.

5. Emittance program improvements. This does not directly affect beam performance. However, providing trim lines and connecting beam percentages with plotted contours would contribute to our knowledge of beam distribution in the phase plane and of the effective emittance.

TABLE I

One Set of Operating Parameters
-Ion Source, LEBT & RFQ

Filament Current	19.8A
Filament Voltage	2.3A
Magnet Current	2.5A
Arc Modulator Voltage	153.V
Arc Current	16.5A
HV #1 (total column voltage)	30.1kV
HV #2 (2nd column gap voltage)	5.2kV

Solenoid Lens #1 Current	452A
Solenoid Lens #2 Current	506A
Steering Magnet #1 Current	2.4A
Steering Magnet #2 Current	-1.6A
Steering Magnet #3 Current	2.0A
Steering Magnet #4 Current	1.3A
RFQ Gradient	0.525V(Higher value needed)
RFQ Power	238kW(Higher value needed)

Measured Beam Currents:

Ion Source(column out)	57mA
RFQ Input	52mA
RFQ Output	16.5mA
180° Magnet Output	15.2mA(Debuncher on)

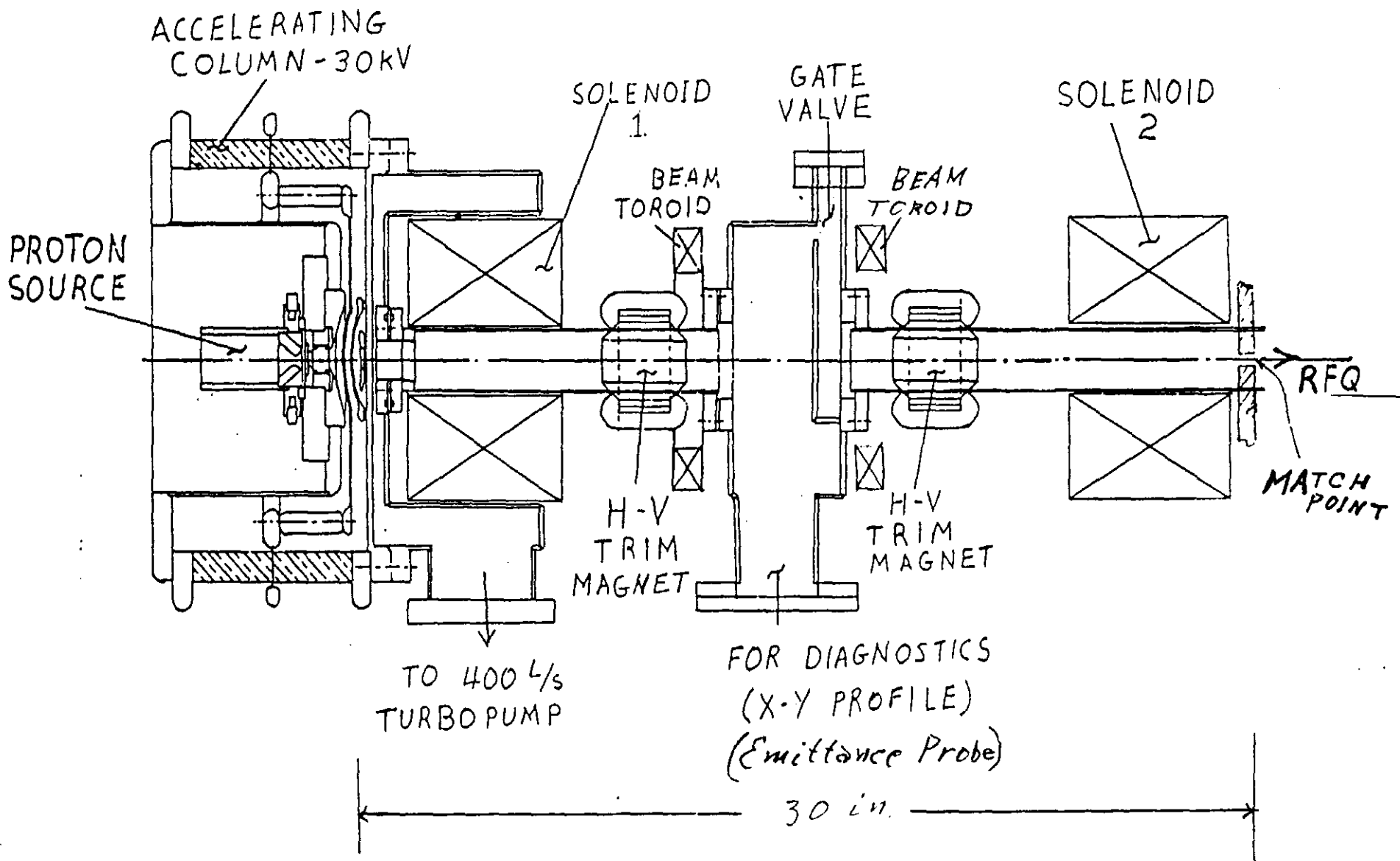


Fig 1

Test Bench

Data taken: Thu Apr 14 13:10:19 1988

Current 29.5 mA
Kinetic Energy, 0.0436 MeV

RMS Quantities

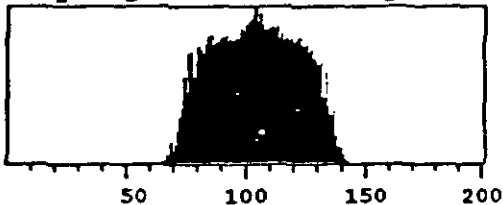
Normalized Emittance 0.404 pi mm-mrad

Alpha -1.82

Beta 0.331 mm/mrad

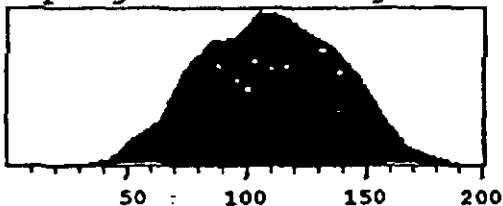
Gamma 13 mrad/mm

projection along x



sigma x = 1.86 mm

projection along x'



sigma x' = 11.7 mrad

Proj. Emittance (pi mm-mrad)

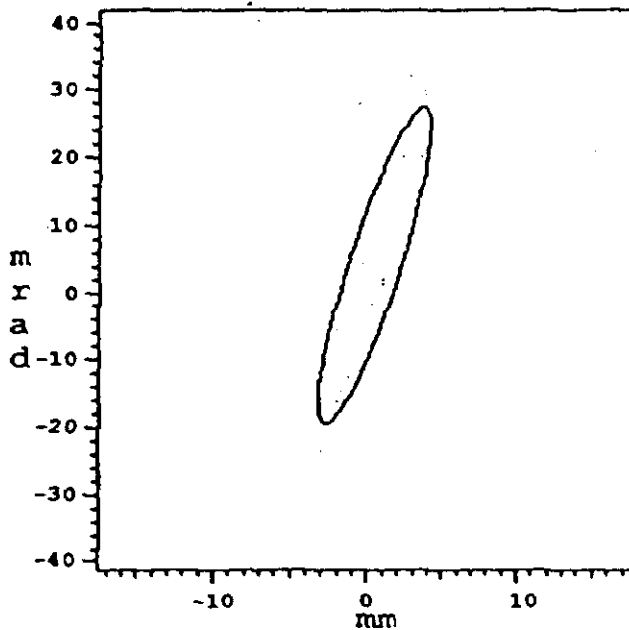
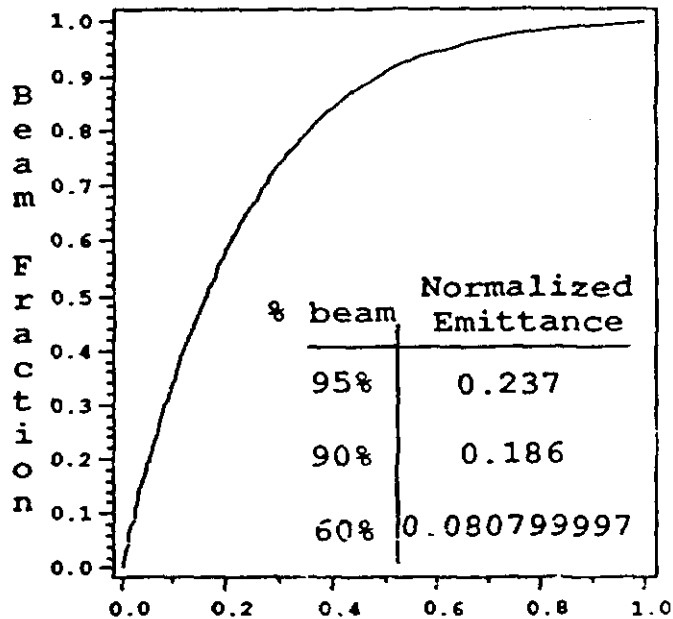


Fig. 2

20-Strif probe

Test Bench

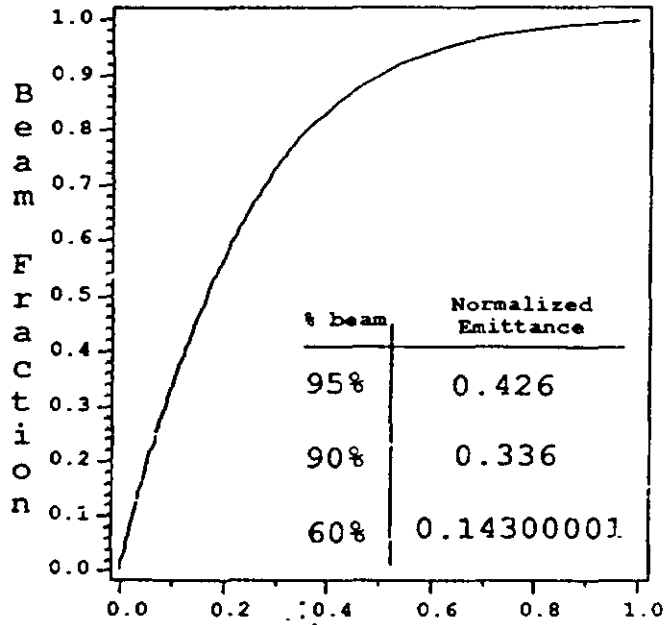
Data taken: Thu Nov 19 13:12:40 1987

Current 31.4 mA
Kinetic Energy 0.0443 MeV

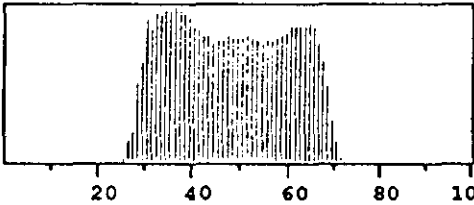
RMS Quantities

Normalized Emittance 0.472 pi mm-mrad
Alpha -3
Beta 0.491 mm/mrad
Gamma 20.4 mrad/mm

Projection Emittance (pi mm-mrad)

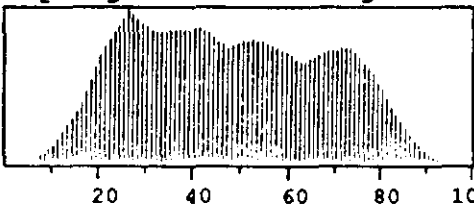


projection along x



sigma x = 2.44 mm

projection along x'



sigma x' = 15.7 mrad

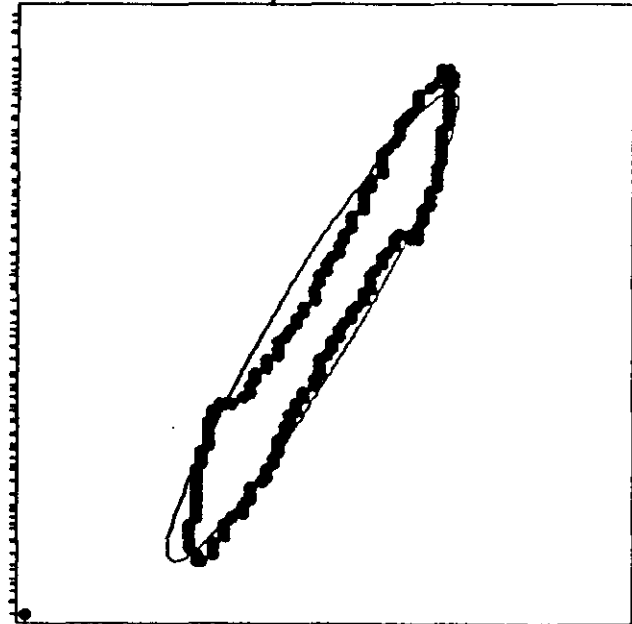


Fig. 3

Test Bench

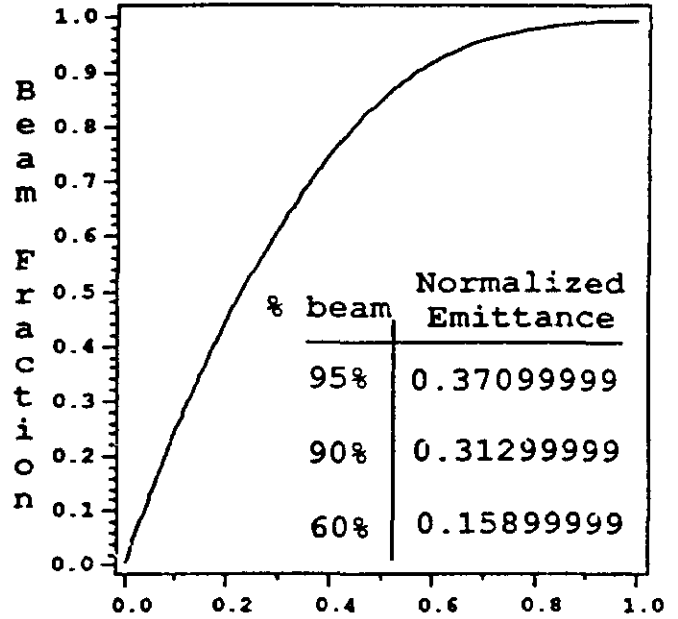
Data taken: Fri Mar 18 13:09:09 1988

Proj. Emittance (pi mm-mrad)

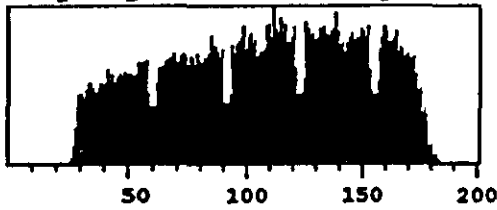
Current 77.199997 mA
 Kinetic Energy 0.0285 MeV

RMS Quantities

Normalized Emittance 5.05 pi mm-mrad
 Alpha -0.0477
 Beta 0.307 mm/mrad
 Gamma 3.27 mrad/mm

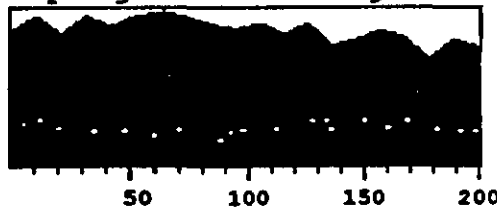


projection along x



sigma x = 7.05 mm

projection along x'



sigma x' = 23 mrad

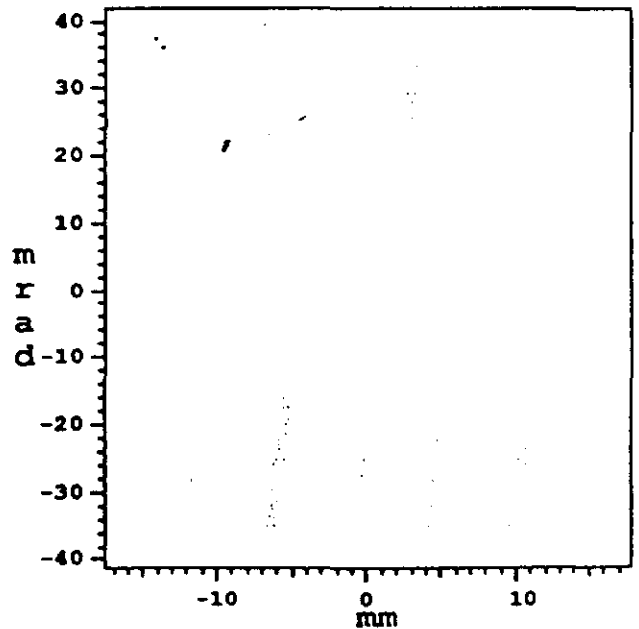


Fig. 4

Multibank Probe

Total Voltage : 31.2 kV
 Exit Voltage : 15.6 kV

LEBT Exit

IEI-312

Mon Oct 31 15:02:20 1988

ϵ_{rms} 0.988 π mm-mrad
 α_{rms} 0.814
 β_{rms} 0.323 mm/mrad
 γ_{rms} 5.14 mrad/mm
 KE 0.0314 Mev
 Toroid 50.8 mA
 Sol. #1 500.8 Amps
 Sol. #2 -4.297 Amps

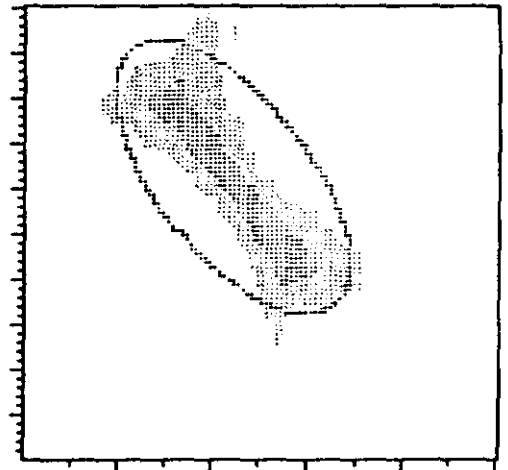
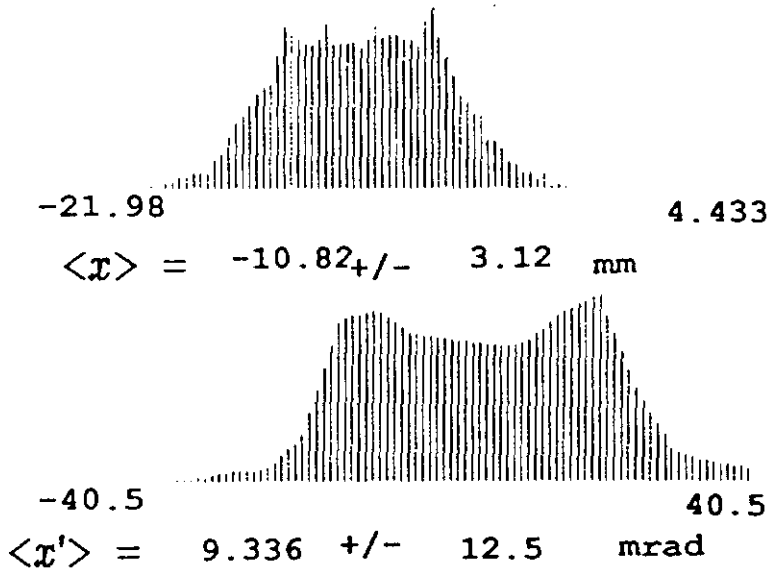
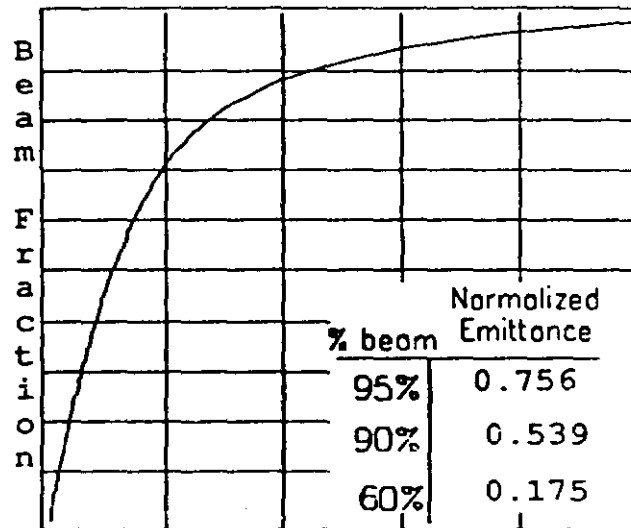
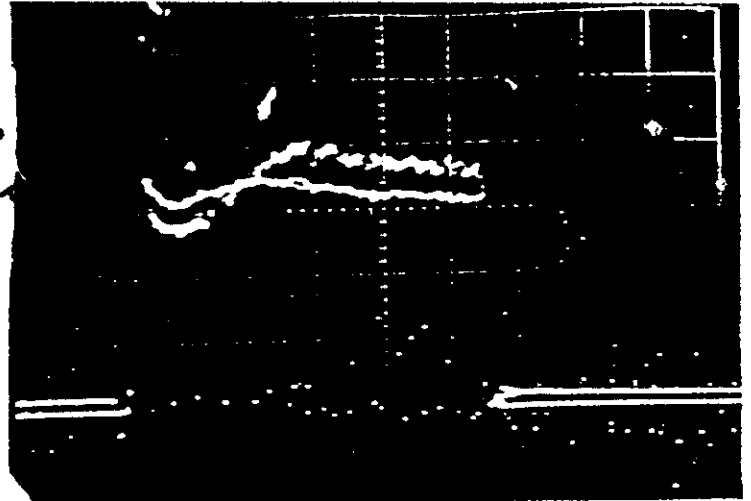


Fig. 5

10/31/88 1715

```

FILE -FILAMENT CUR 21.57 A
ARCMOD-ARC MOD VOLTS 116.5 V
MAG1 -MAGNET CURRENT 1.736 A
ISCH3 -
MV1 -HIGH VOLTS #1 31.81 KV
MV2 -HIGH VOLTS #2 15.32 KV
ISOL1 -SOLENOID 1 499.5 AMP
ISOL2 -SOLENOID 2 -3.979 AMP
FILV FILAMENT VOLTS 2.317 V
ARCI ARC CURRENT 20.2 A
ISTOR SOURCE TOROID 58.35 MA
IFARC FARADAY CUP -124.9 NA
    
```



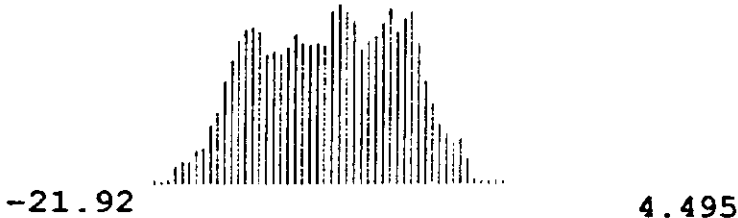
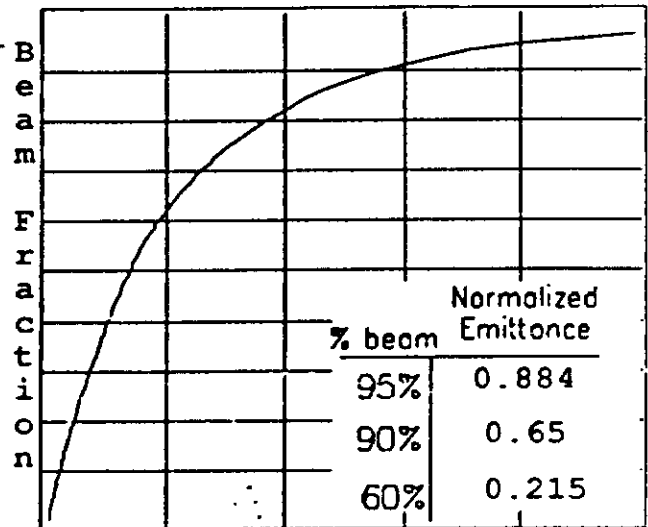
T: 20 mA/div G: 10 mA/div

Raised Arc Current

Mon Oct 31 16:52:23 1988 I B1-25

ϵ_{rms} 1.12 π mm-mrdd
 α_{rms} 0.71
 β_{rms} 0.244 mm/mrdd
 γ_{rms} 6.16 mrdd/mm
 KE 0.0313 Mev

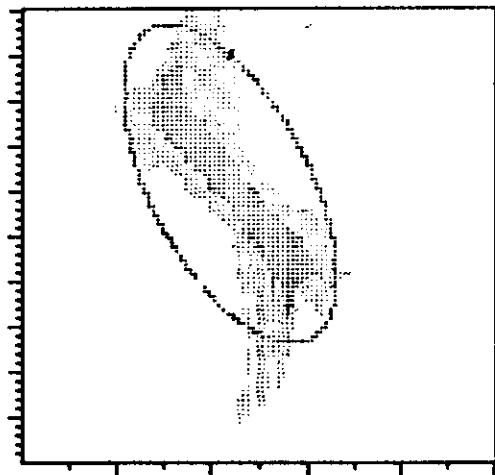
Toroid 58 mA; 35 mA in F. cup
 Sol. #1 499 Amps
 Sol. #2 -4.297 Amps



$\langle x \rangle = -10.64 \pm 2.89$ mm



$\langle x' \rangle = 8.429 \pm 14.5$ mrad



LEBT Exit

Fig. 6

IBI-7

LEBT Exit

Thu Oct 27 10:47:50 1988

ϵ_{rms} 1.74 π mm-mrad
 α_{rms} -0.234
 β_{rms} 0.179 mm/mrad
 γ_{rms} 5.91 mrad/mm

KE 0.0307 Mev

Toroid 64.2 mA

Sol. #227.8 Amps

Sol. #21517.8 Amps

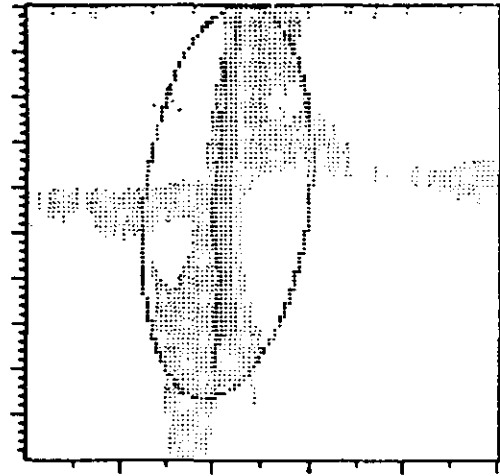
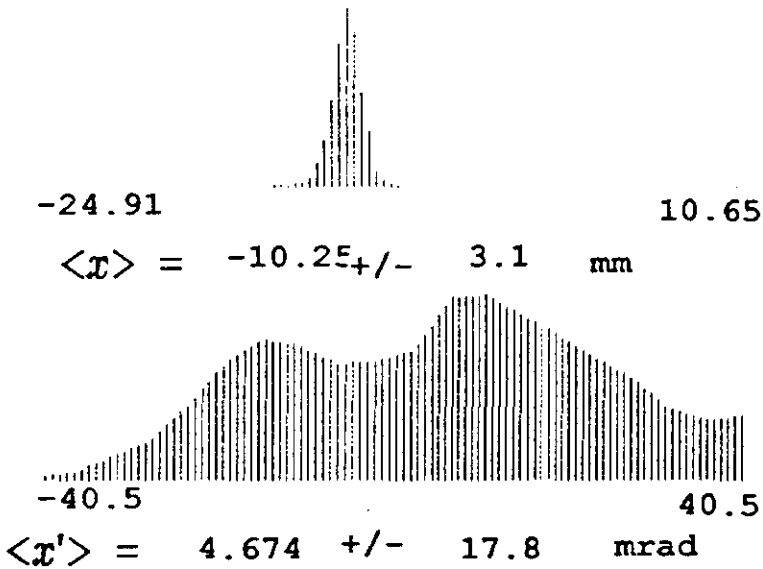
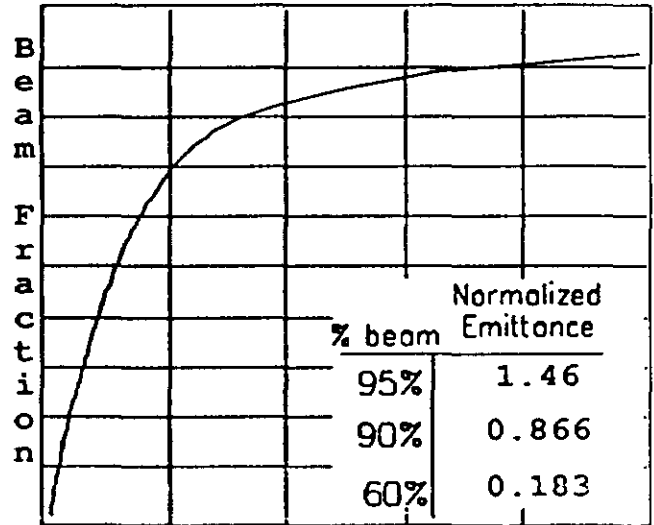


Fig. 7

IB1-10

LEBT Exit

Thu Oct 27 11:32:17 1988

ϵ_{rms} 2.64 π mm-mrad
 α_{rms} -1.02
 β_{rms} 0.461 mm/mrad
 γ_{rms} 4.41 mrad/mm
KE 0.0309 Mev
Toroid 64.5 mA
Sol. #1 314 Amps
Sol. #2 559.7 Amps

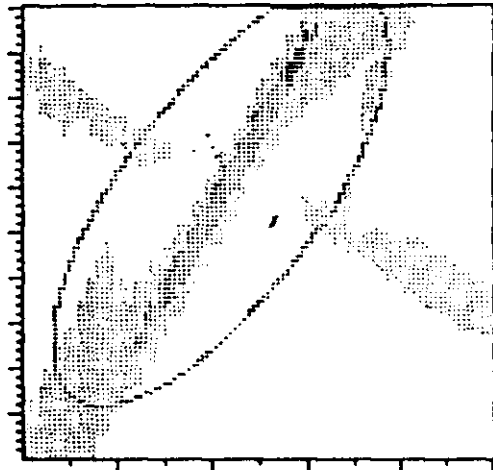
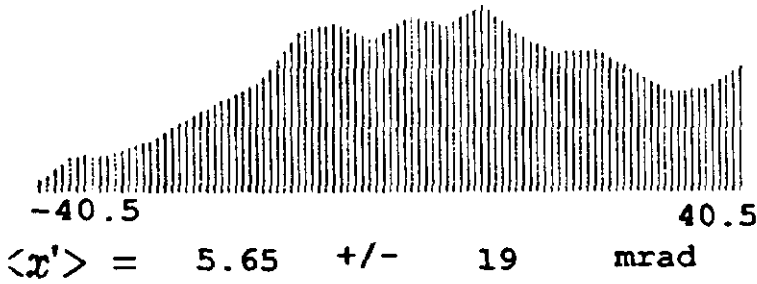
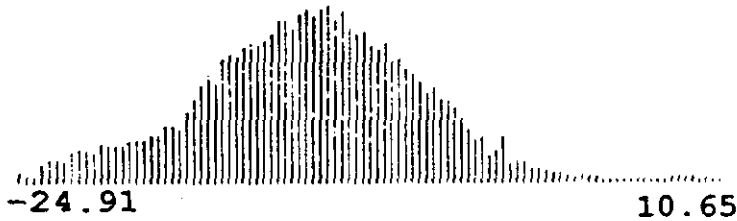
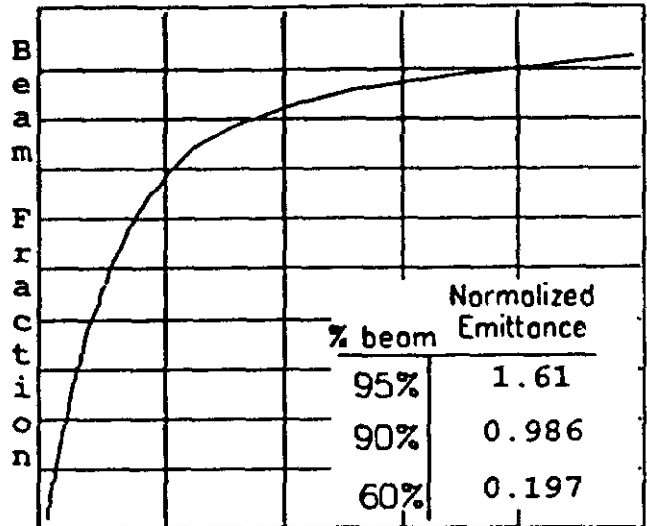
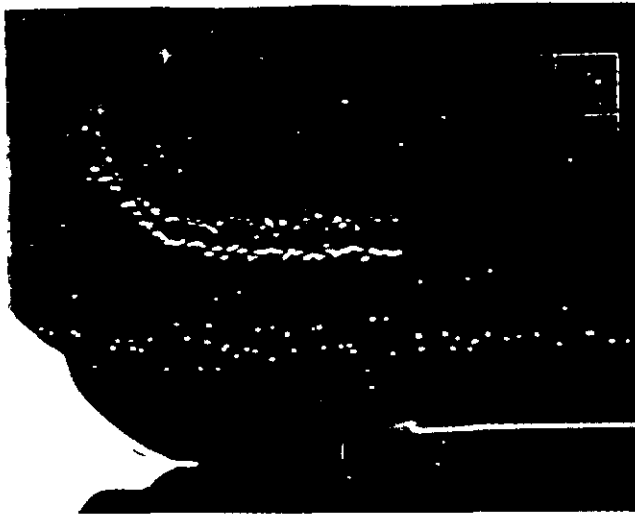


Fig. 8



```

11/01/88 1722
FILE -FILAMENT CUR 21.43 A
ARCND3 -ARC MED VOLTS 112.6 V
MAG1 -MAGNET CURRENT 1.73 A
ISCH3 -
NV1 -HIGH VOLTS 01 30.33 KV
NV2 -HIGH VOLTS 02 3.354 KV
ISOL1 -SOLENOID 1 591.9 AMP
ISOL2 -SOLENOID 2 642 AMP
FILV -FILAMENT VOLTS 2.293 V
ARC1 -ARC CURRENT 16.33 A
ISTOR SOURCE TOROID 53.55 MA
IFARC FARADAY CUP -124.9 MA
A. 17:05Z ISOL2
  
```

LEBT Exit

IEI-26

Tue Nov 1 17:07:17 1988

ϵ_{rms} 1.03 π mm-mrad
 α_{rms} 0.016
 β_{rms} 0.0623 mm/mrad
 γ_{rms} 16 mrad/mm
 KE 0.0305 Mev
 Toroid 53.8 mA
 Sol. #1 592.1 Amps
 Sol. #2 642.1 Amps

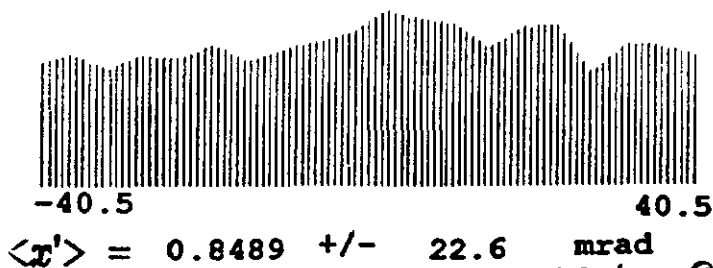
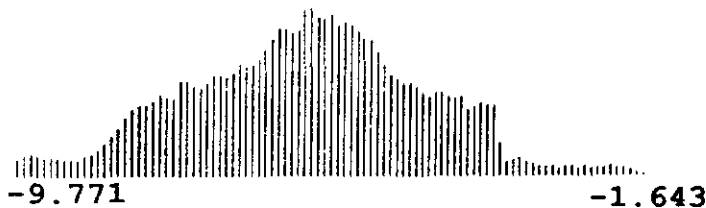
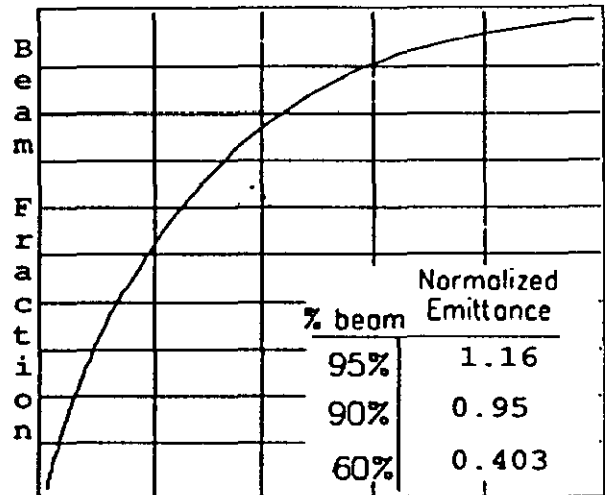
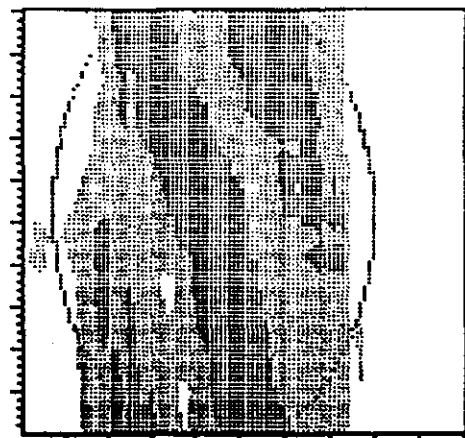


Fig. 9



Multi-bank Probe

Center of Line

Save Data

Take Data

New Data

Main Menu

Plot Data

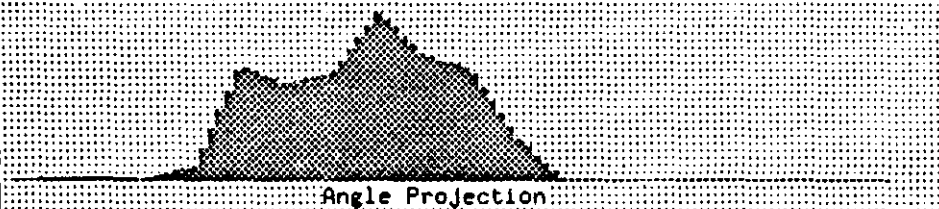
RMS Quantities

Norm' zed Emit.	3.12	pi mm-mrad
Alpha	0.518	
Beta	1.26	mm/mrad
Gamma	1.01	mrad/mm

$\langle x \rangle = -12.85 \pm 11.1$ mm

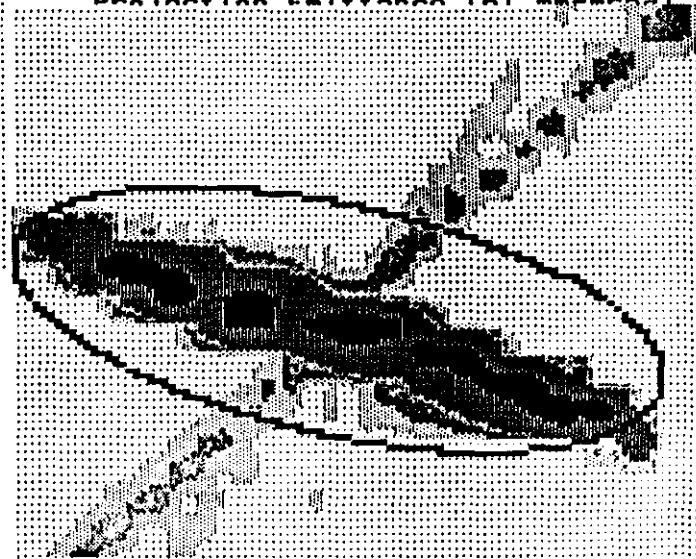
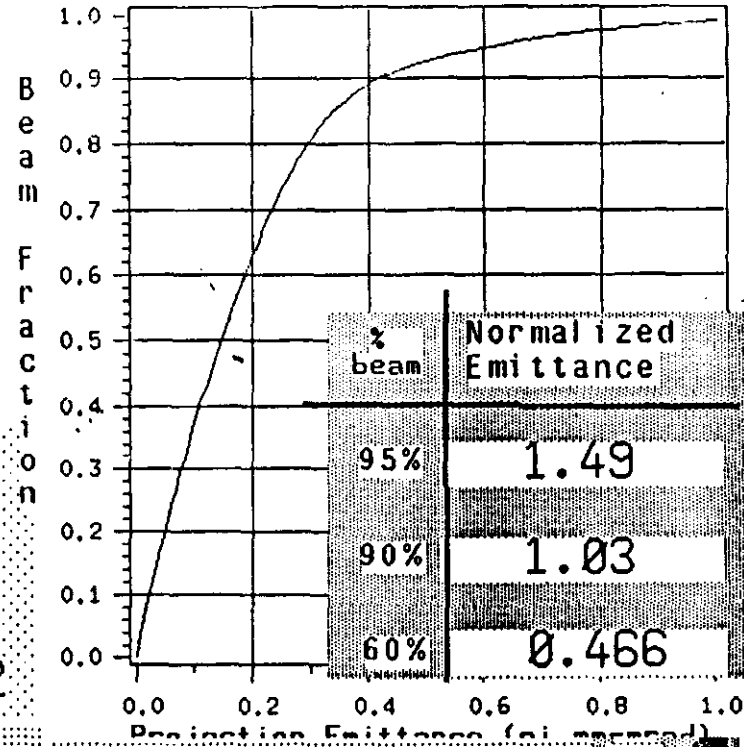


$\langle x' \rangle = -6.737 \pm 9.91$ mrad



Toroid	56.5	mA
Sol. #1	451.2	Amps
Sol. #2	504.3	Amps
KE	0.03	MeV

Fri Jun 23 11:28:33 1989



4127

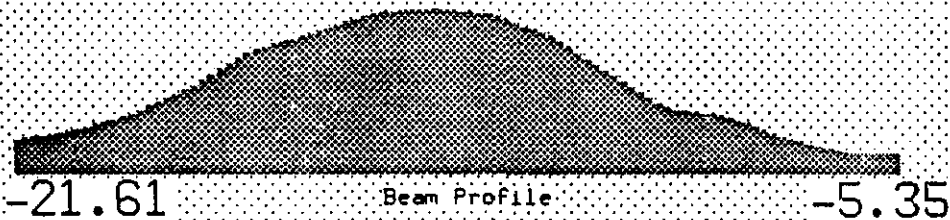
Center of Line

- Save Data
- Take Data
- New Data
- Main Menu
- Plot Data

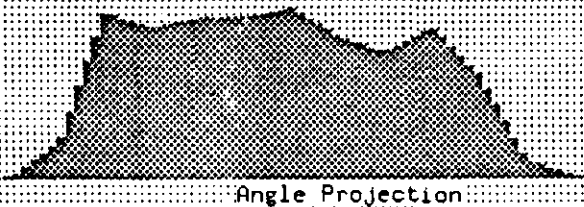
RMS Quantities

Norm' zed Emit. 0.955 pi mm-mrad
 Alpha 0.266
 Beta 0.263 mm/mrad
 Gamma 4.08 mrad/mm

$\langle x \rangle = -15.93 \pm 2.79$ mm

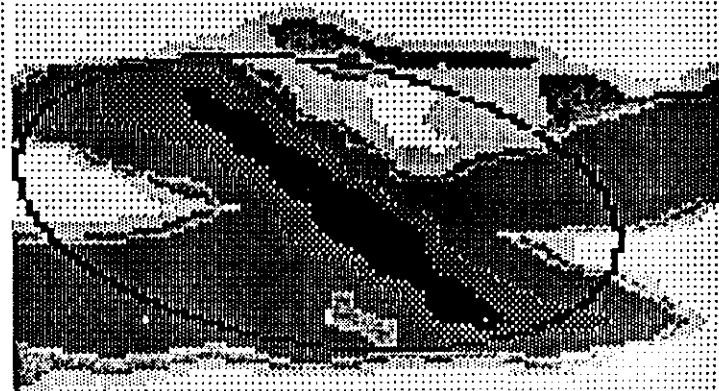
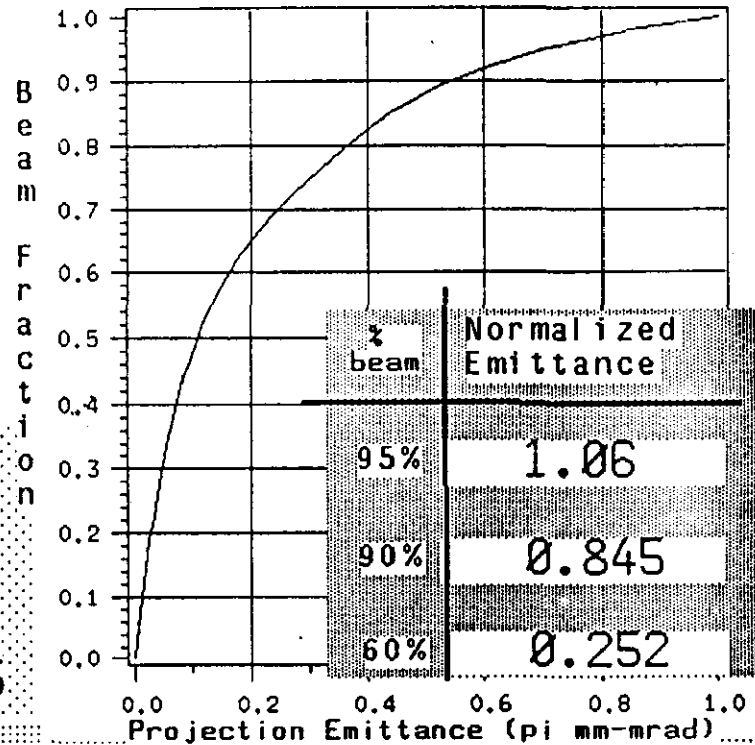


$\langle x' \rangle = -7.296 \pm 11$ mrad



Toroid 52.4 mA
 Sol. #1 530.3 Amps
 Sol. #2 504.6 Amps
 KE 0.0307 MeV

Fri Jun 23 17:55:58 1989



Center of Line

Save Data

Take Data

New Data

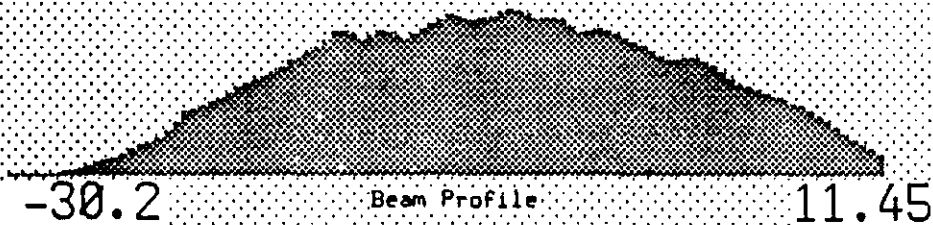
Main Menu

Plot Data

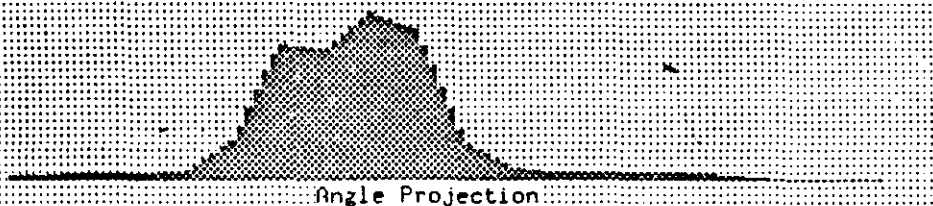
RMS Quantities

Norm' zed Emit. 2.46 pi mm-mrad
 Alpha -0.192
 Beta 0.703 mm/mrad
 Gamma 1.48 mrad/mm

$\langle x \rangle = -10.96 \pm 7.34$ mm

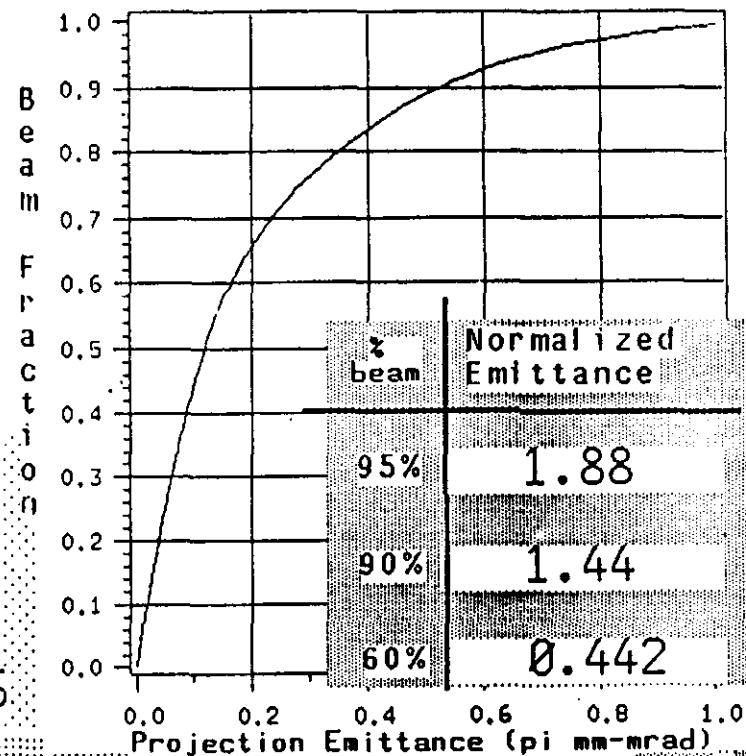


$\langle x' \rangle = -6.874 \pm 10.6$ mrad



Toroid 48.5 mA
 Sol. #1 478.5 Amps
 Sol. #2 475.5 Amps
 KE 0.0303 MeV

Fri Jun 2 17:59:15 1989



13

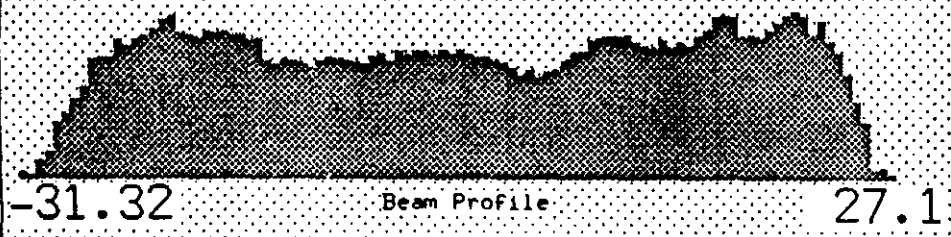
Center of Line

- Save Data
- Take Data
- New Data
- Main Menu
- Plot Data

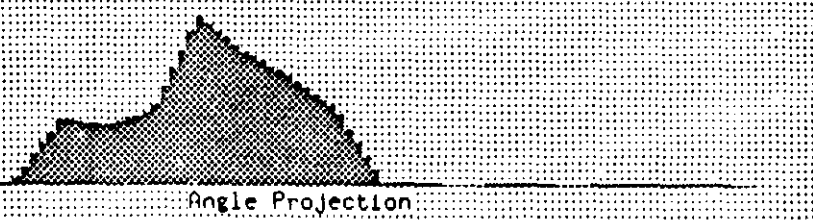
RMS Quantities

Norm' zed Emit. 4.08 pi mm-mrad
 Alpha 0.478
 Beta 1.39 mm/mrad
 Gamma 0.883 mrad/mm

$\langle x \rangle = -6.338 \pm 13.3$ mm

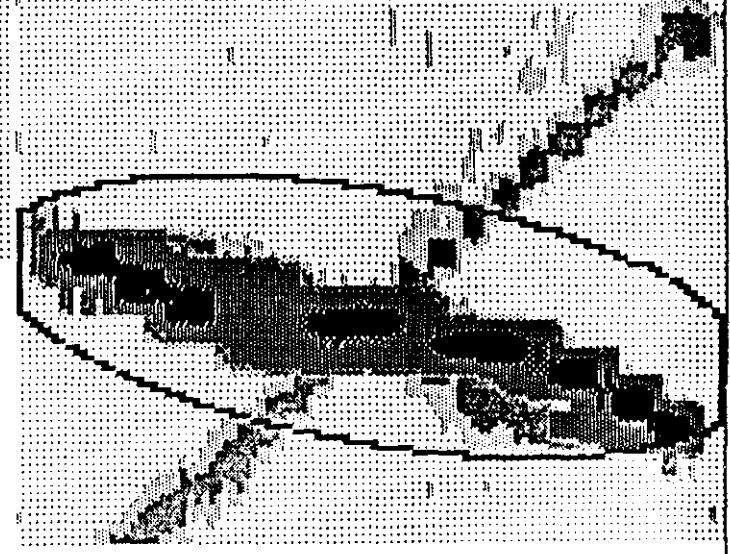
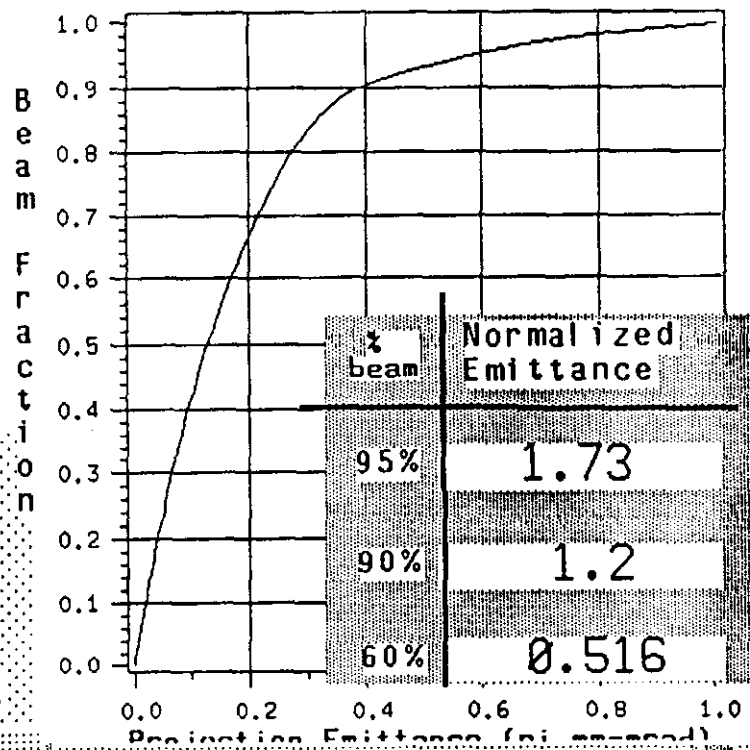


$\langle x' \rangle = -8.022 \pm 10.6$ mrad



Toroid 71.7 mA
 Sol. #1 450 Amps
 Sol. #2 461.7 Amps
 KE 0.0303 MeV

Tue Mar 14 16:18:48 1989



#1 1-1

Center of Line

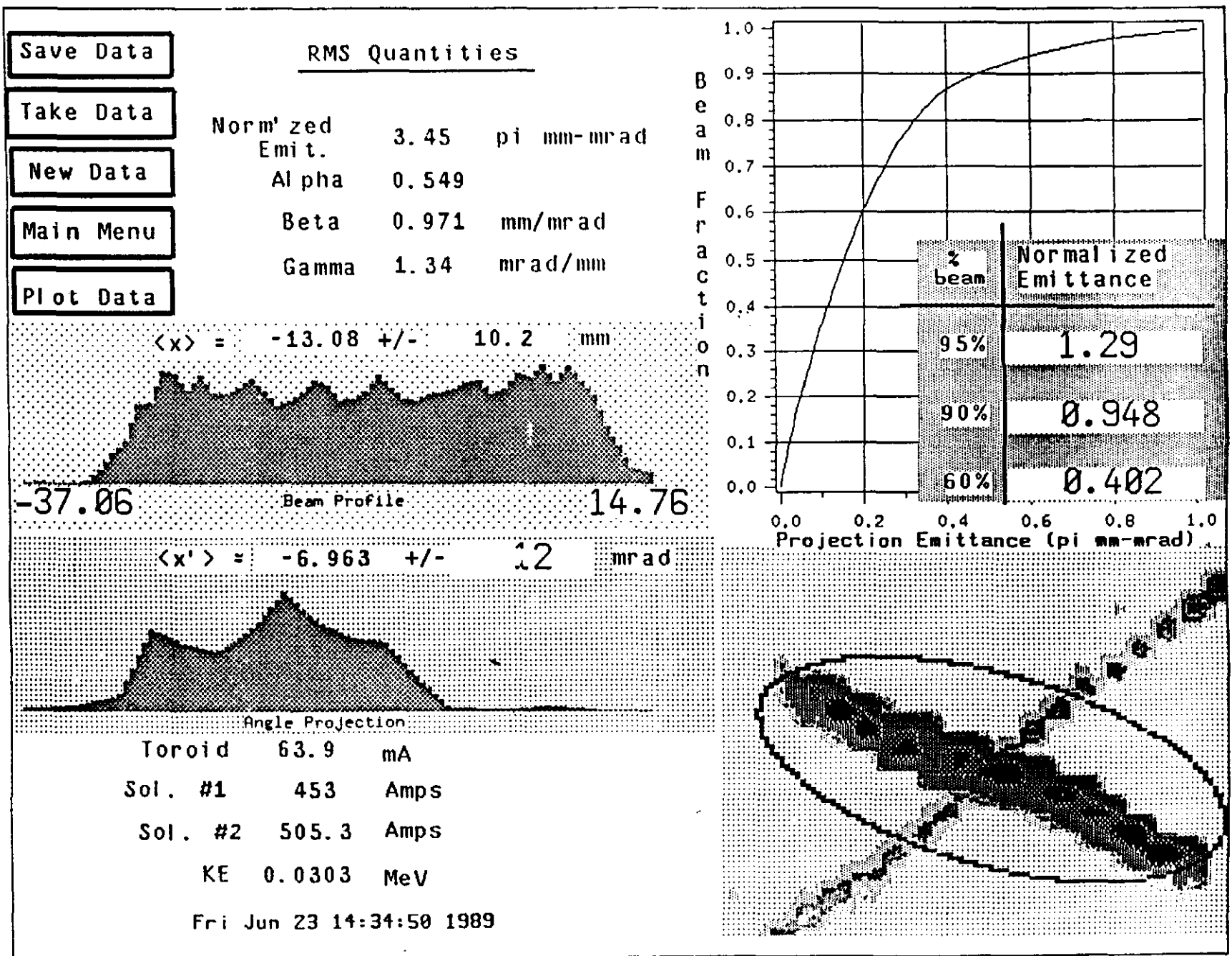


FIG. 14

114

Center of Line

Save Data

Take Data

New Data

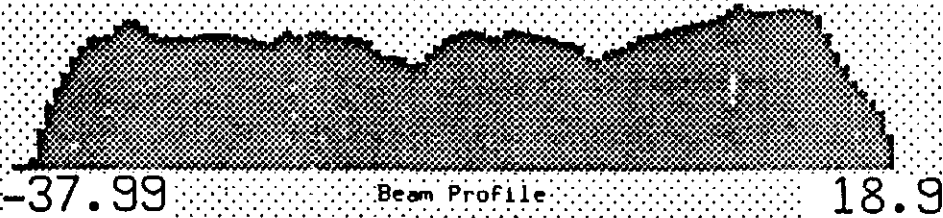
Main Menu

Plot Data

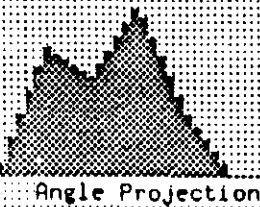
RMS Quantities

Norm' zed Emit.	2.6	pi mm-mrad
Alpha	-0.736	
Beta	2.14	m-m/mrad
Gamma	0.72	mrad/mm

$\langle x \rangle = -13.1 \pm 13.2$ mm

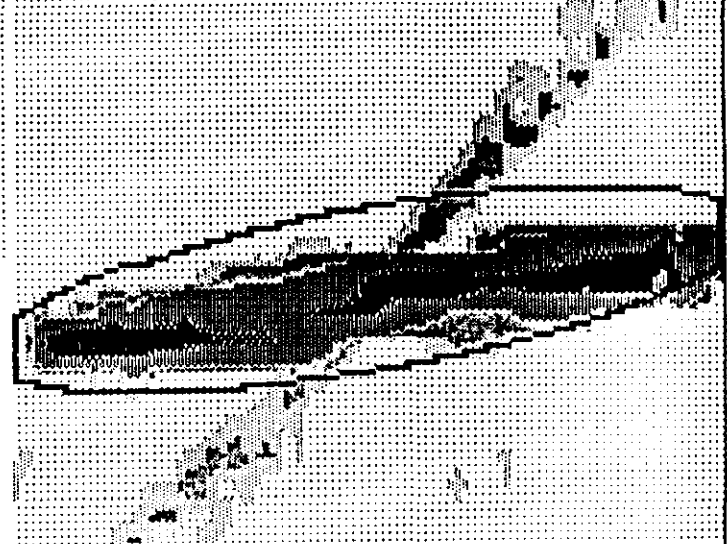
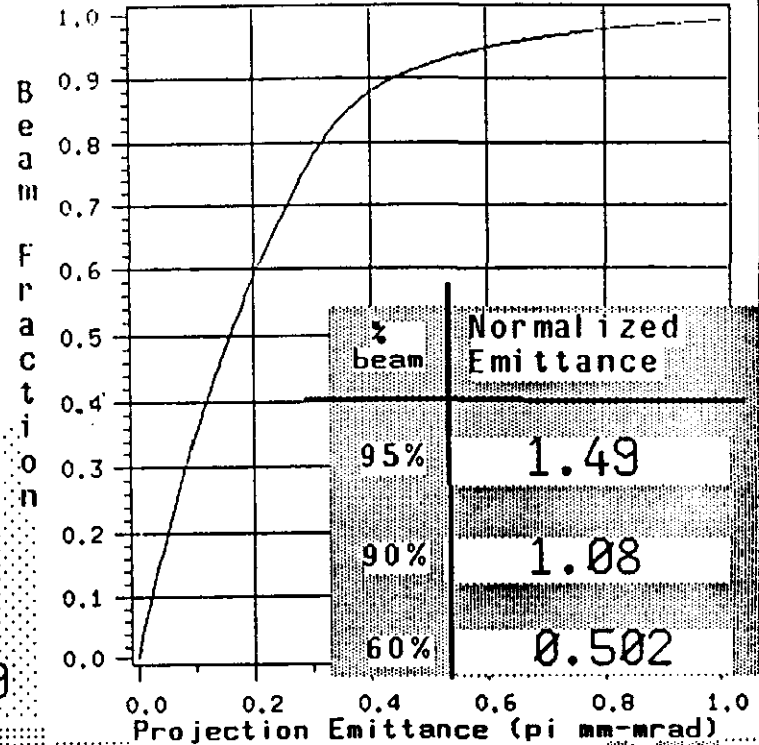


$\langle x' \rangle = -4.391 \pm 7.65$ mrad



Toroid	69.2	mA
Sol. #1	415.2	Amps
Sol. #2	505.7	Amps
KE	0.03	MeV

Fri Jun 23 12:10:19 1989



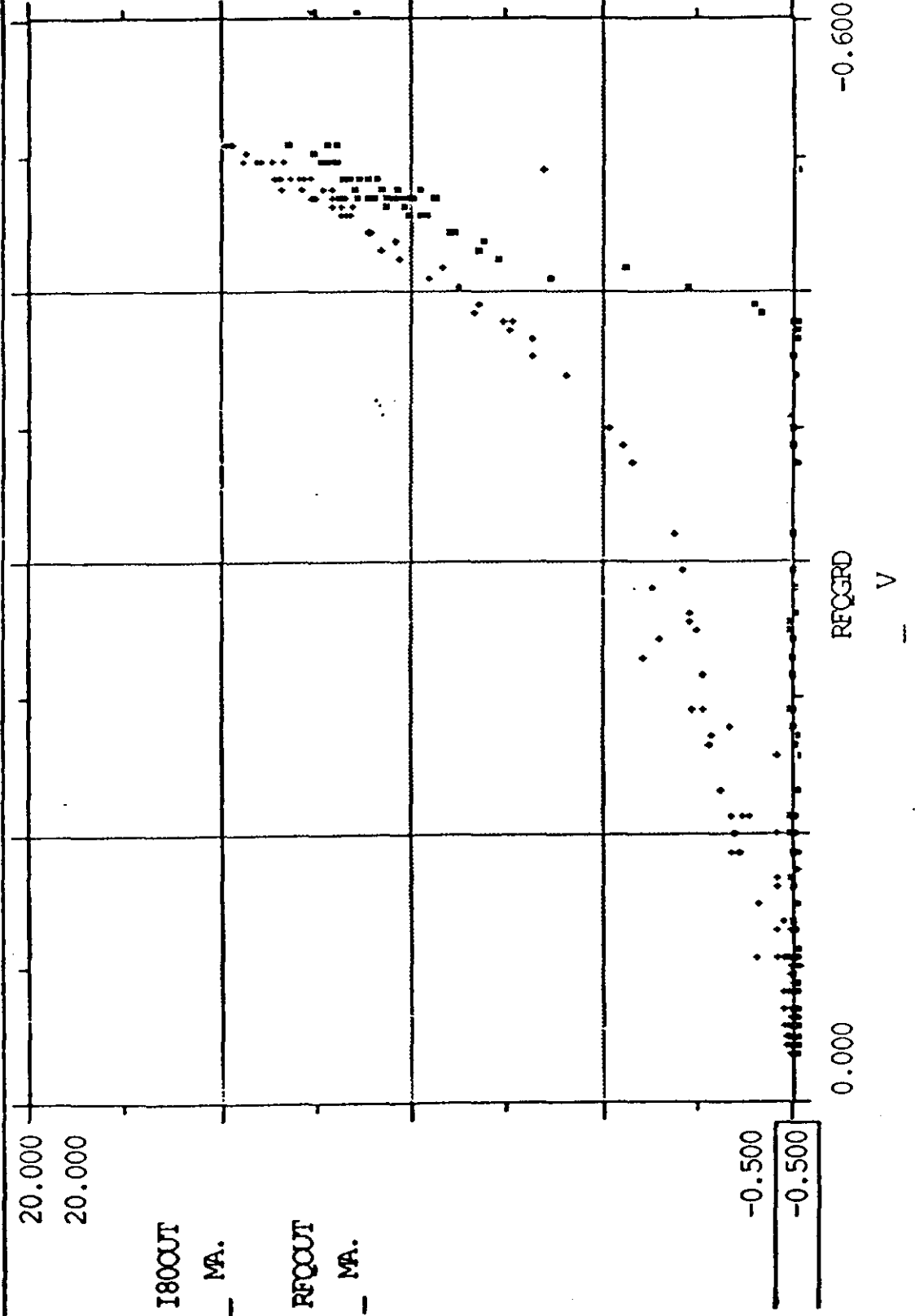
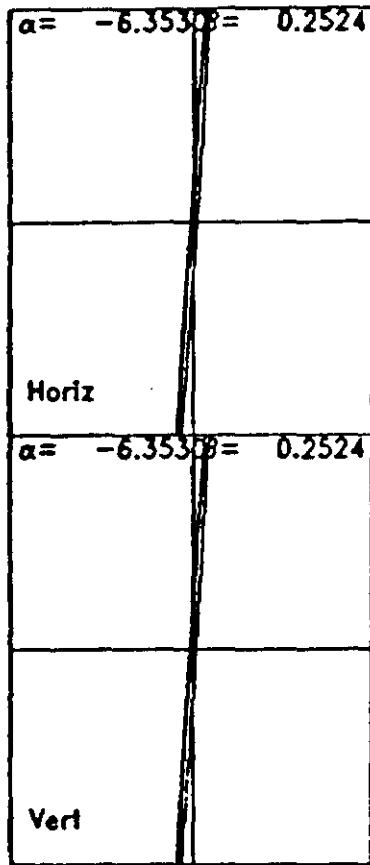


Fig. 16

Match into RFQ for 0 mA beam.



I= 0.0 0.0
 W= 0.030 0.030
 EX= 125.00 125.00
 EY= 125.00 125.00

Matching Variables

KE	MP	VALUE
3	1	4209.025
8	1	4469.601

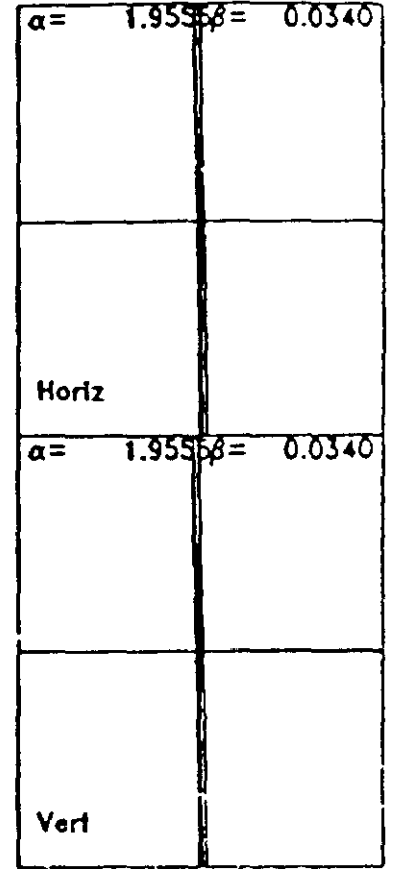
Matching Type = 7

Desired values:

ALPHA-X 1.960
 BETA-X 0.034

Mismatch factor:
 0.001

Code: TRACE v
 File: TEST_30KEV_6.DAT
 Date: 6-JUN-89
 Time: 16:49:08



50.0mm X 100.0mrad

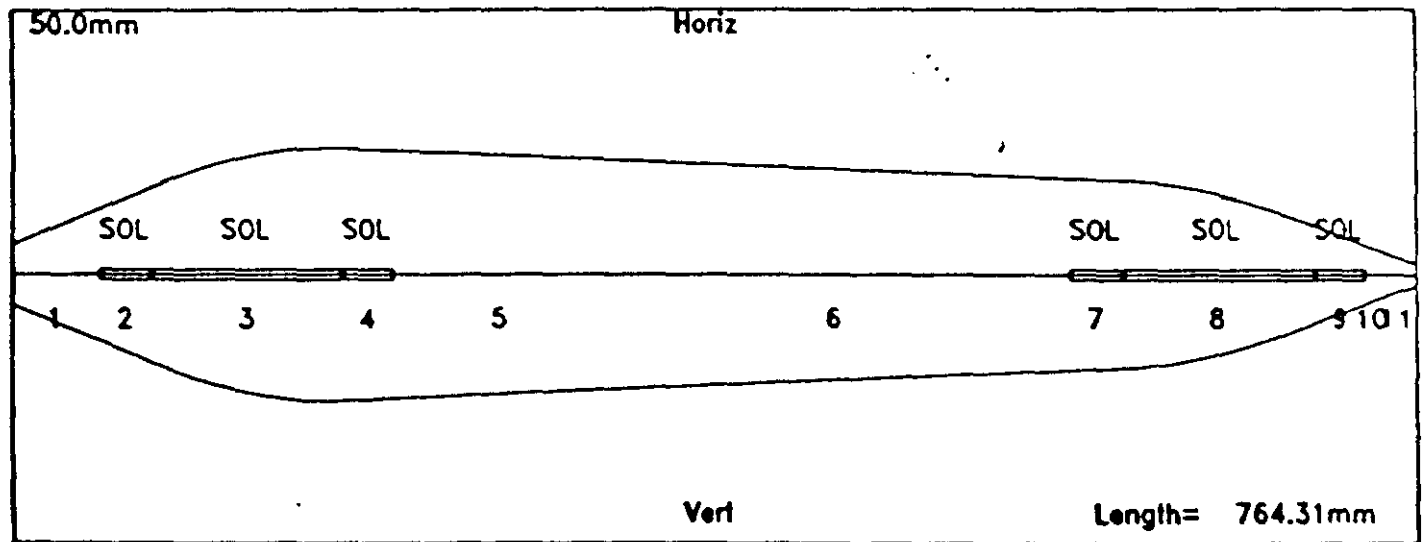
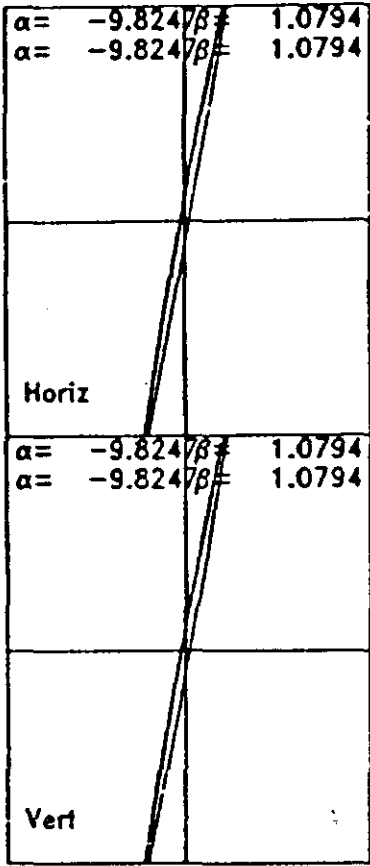


Fig. 17

Fit for 30 mA beam, show params into RFQ and at emit probe



I= 30.0 30.0
 W= 0.030 0.030
 EX= 125.00 125.00
 EY= 125.00 125.00

Matching Variables
 ME MP VALUE
 3 1 5073.608
 8 1 6725.014

Matching Type = 7
 Desired values:
 ALPHA-X 1.960
 BETA-X 0.034

Mismatch factor:
 0.002

Code: TRACE v
 File: TEST_30KEV_6.DAT
 Date: 6-JUN-89
 Time: 16:37:38

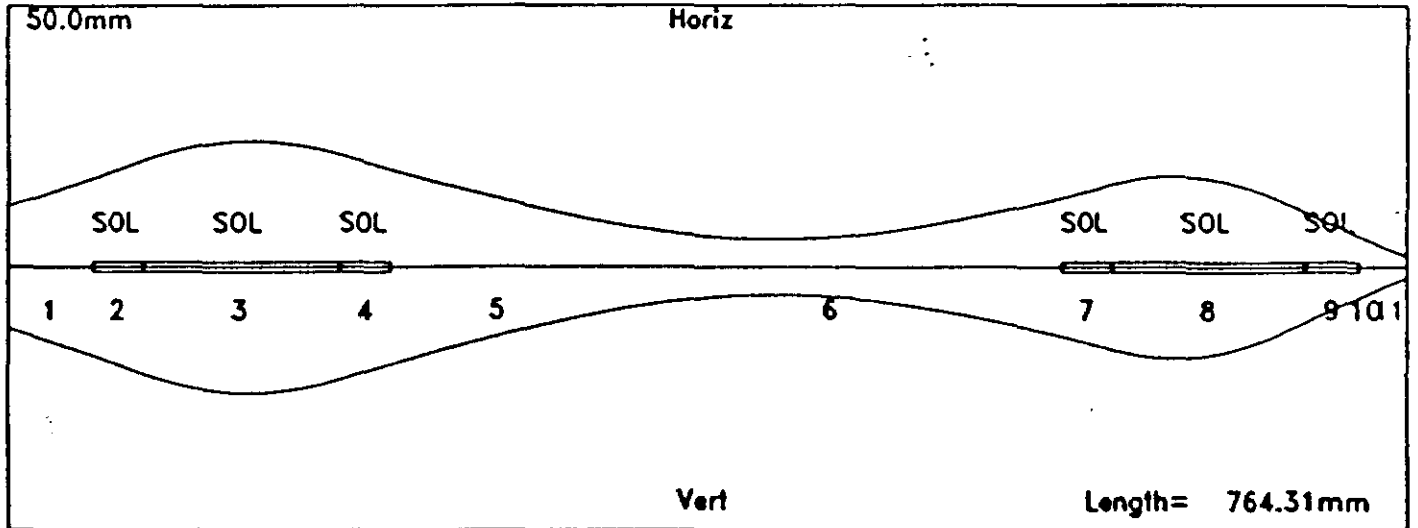
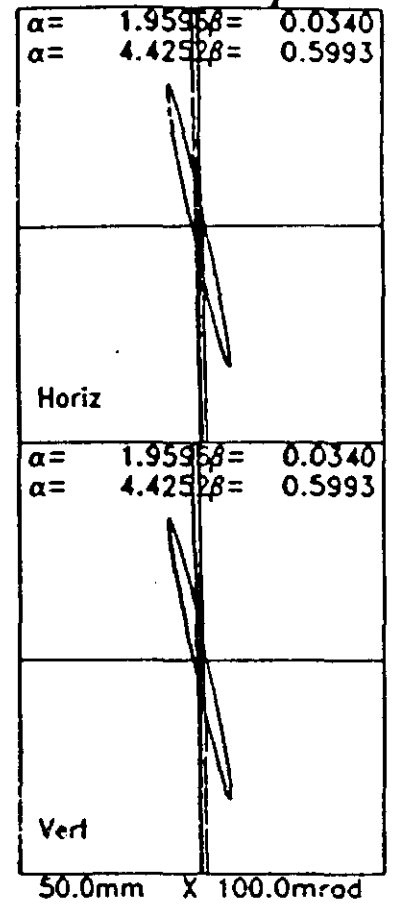


Fig. 19

A.2 PERFORMANCE OF THE RFQ AND DEBUNCHER FOR THE LLUMC ACCELERATOR

C.W. OWEN

To provide beam for injection to the LLUMC medical accelerator using, whenever possible, commercially available subsystems, we chose an RFQ and debuncher manufactured by AccSys, Inc. The RFQ is very similar to one which was brought into operation at about the time we placed the order. The debuncher was designed to provide a satisfactory longitudinal match of the beam between the RFQ and the synchrotron lattice. Exotic bunch rotation schemes could perhaps improve the match, but they would necessarily involve lots of expense and time and might not be suitable for use in a hospital environment.

AccSys also provided, under contract to Fermilab, numerical simulations to help assess the suitability of the beam for injection into the synchrotron. The transverse emittance is very small. It is so small that it will have to blow up vertically in the synchrotron in order to be stable at higher intensities.

As has been noted by C.D. Curtis in his description of the ion source, the original goal of about $1.5E 11$ protons/pulse depended on, among other optimistic assumptions, accelerating as much as 40 or 50 mA of protons in an RFQ. At the time that planning was being done, we were also expecting to have a 200 MHz RFQ built by LBL for this specific purpose.

The AccSys RFQ was built for another purpose originally. It was expected to deliver 25 mA of protons at 2 MeV. The "space charge limit" of the RFQ is about 60 mA. That is not a firm number, but rather an indication that we might expect to reach something near that number if we can match the beam to it and furnish the necessary power to it.

Because of a myriad of problems - primarily but by no means limited to the rf amplifier - we do not yet have definitive answers to the questions of the ultimate capabilities of the RFQ. We have evidence of input matching problems and voltage holding problems. Fermilab people are working on gradient and phase regulation for the RFQ/debuncher system.

The highest current achieved so far around the 180 degree magnet is approximately 18 mA. The properties and aperture of the 180 degree magnet are such that the beam that makes it that far should be accepted by the synchrotron if the apparent aperture of the synchrotron is what it was advertised to be.

Numerical simulations performed by AccSys indicate that after an 18 mA beam has traveled 2 m downstream of the debuncher, by which time it will be almost completely debunched, about 80% of the beam will lie within 15 keV of 2 MeV. For 1 microsecond the revolution time at 2 MeV, that corresponds to about $8.9E 10$ protons. For +/- 7 keV energy spread,

a number which should be reasonable for adiabatic capture in a machine with an aperture more than twice that large, there are $6.6E 10$ protons/microsecond. The number of protons within some momentum interval does not scale strictly with the current because of space charge effects and because beam loading effects become more difficult to deal with at higher currents, but in the range of currents which the RFQ manufacturer and I thought was reasonable, the deviation from linearity is not large. The calculated distributions are shown in Figure 1 for currents 18, 27, and 34 mA. Those are the currents which would result from perfectly matched 20, 30, and 40 mA beams into the RFQ. The calculations do not include the effects of neighboring bunches (which make the induced energy spread smaller) or the effects of image currents (which have the opposite effect).

Recent measurements made by P. Martin indicate that the energy acceptance of the synchrotron is only about ± 3 or 4 keV at injection energy. The amount of beam within that energy interval is about 4 or $5E 10$ at 18 mA (the highest current we have achieved so far). A more nearly typical operating current recently might be, perhaps, 12 mA. Under the present apparent conditions, we may expect to have no more than $3E10$ to have any chance of survival.

Although we still have hopes of increasing the current from the injector, I think it is entirely unrealistic to expect more than a factor of two increase of beam within the extremely narrow momentum aperture that we apparently now have. Even if we could provide more, we are apparently operating on the edge of the microwave instability.

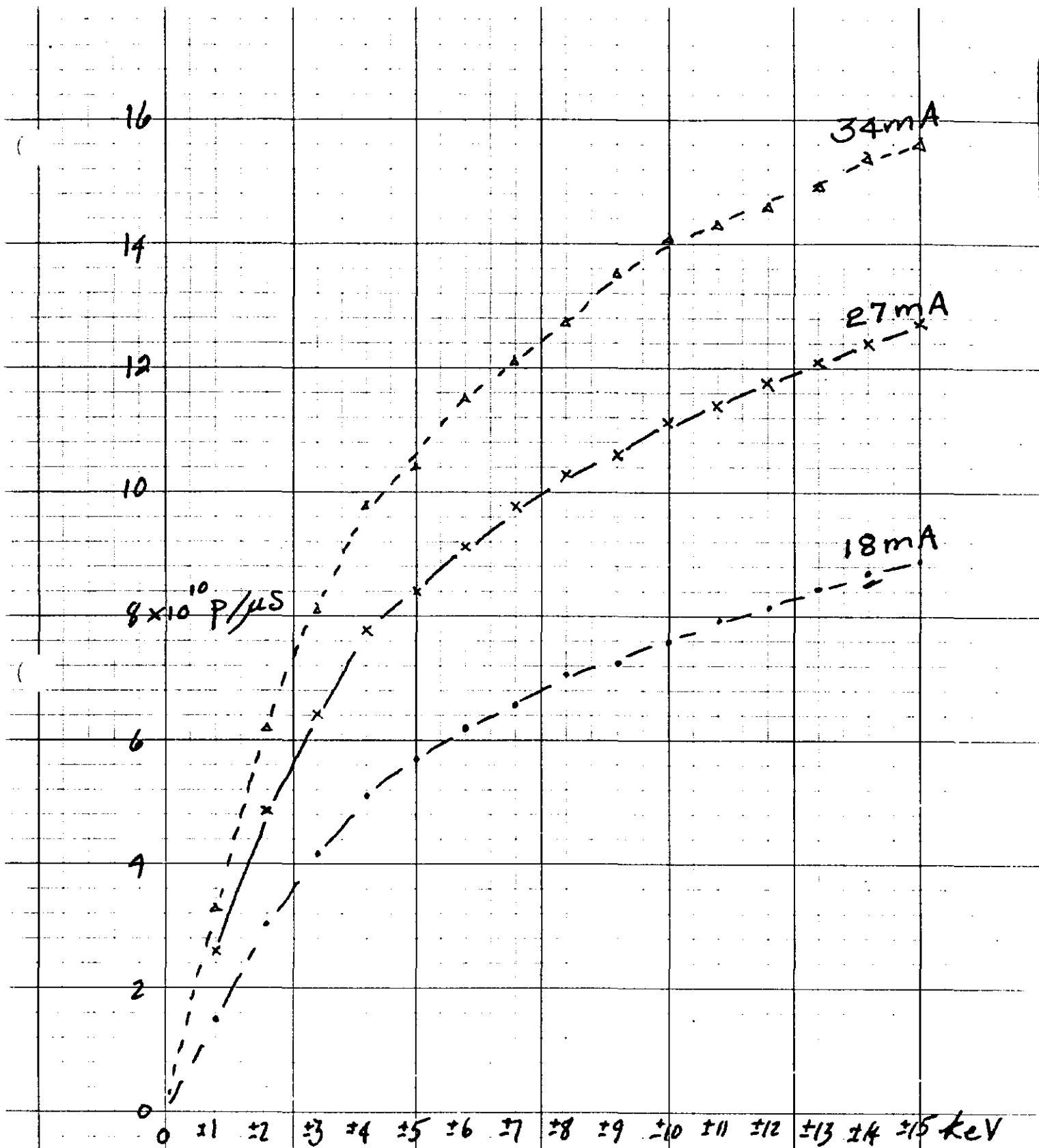


Fig. 1 Energy Spread at 2 MeV for Deunched Beam

CWO

A.3 ADDENDUM TO ION SOURCE AND RFQ PERFORMANCE REPORTS

C.D. CURTIS

Consideration of RFQ accelerator performance involves voltage holding or accelerating field (gradient) capability as well as beam performance. The latter, of necessity, involves also the ion source performance. Both parts of the system will be addressed and their performance updated.

Much of the time during studies with the synchrotron, operating gradients of the RFQ have been in the 0.5 - 0.55V range or 16-28% above the measured acceleration threshold value of 0.43V. The operating gradient varied with both voltage-conditioning status of the RFQ and status of the micom rf power supply, which often had problems. Thanks to the efforts of John Ried, Q. Kerns, C. Kerns and other rf group members, the micom supply was "hardened" to become much more reliable during the last weeks of operation. During the visit of Jim Potter from AccSys, the RFQ was conditioned to higher gradients so that during the last 36 hrs of running before shutdown, it ran consistently at a gradient of 0.57 to 0.58 with very little sparking. During the conditioning process Potter observed an inconsistent behavior of cavity field decay during sparks which suggested something wrong in the RFQ cavity. As a consequence, a decision to send the RFQ back to AccSys for inspection and testing has already been implemented. It will be opened and possibly completely disassembled, cleaned and reassembled before final rf testing.

We turn next to the subject of beam performance. Transmission of the RFQ has been observed for input beams of 10-65 mA for high RFQ gradients of 0.57-0.59. Maximum values were 60% for input currents ≤ 20 mA, 50% for currents ≤ 40 mA and 40% for currents ≤ 60 mA. The maximum beam out of the RFQ has been 24-25 mA (~60mA input) for high gradient for both the FNAL ion source and the duplicate AccSys ion source. Of this current 21-23 mA passed through the 180° bend magnet with the debuncher on and phase adjusted although not precisely adjusted for the beam current and gradient used. Operation of the debuncher at full power typically doubles beam transmitted through the 180° bend magnet. Potter will look into boosting the power level of the present debuncher power supply. Examples of transmission curves are shown in Fig. 1 and Fig. 2. AccSys achieved 24.5 mA of momentum analyzed beam from their first RFQ with a lower emittance beam of only 30 mA injected. These output beam currents are comparable for both RFQ's when running at approximately the same total power level of 240-250 kW as measured and calculated, admittedly by different people.

The accuracy and significance of rf power measurements have often been a problem. Perhaps this can be illustrated in Figures 3 and 4. Two MeV beam current is plotted as a function of the square root of normalized cavity power (proportional to gradient) in Fig. 3. The AccSys and Loma

Linda July data almost track each other but the Loma Linda September data diverges. The acceleration threshold power levels varied relatively little (116-128 kW). One may be tempted to say that the September data are the result of a brighter beam from the ion source until one looks at Fig. 4, where beam current and cavity power are plotted against gradient read-out from the cavity (via rf-rectifying diode). The slight offset in the two beam curves, which otherwise track, is probably the result of sampling the gradient 1-2 usec before maximum field in the very short power pulse of July 13, which barely leveled off. The September 13 pulse, with amplitude control loop closed, was longer and had a longer flat top. The difference in cavity power curves is not really understood. John Ried made the power determinations for each run in two ways. Power was calculated from the rf amplitude obtained by a pickup loop in the RFQ. It also was determined by subtracting beam power from the forward power measured by a directional coupler. From the fact that these two determinations were in approximate agreement, one hoped to eliminate the uncertainty of excessive electron loading.

Because of the generally higher beam current injected into the Loma Linda RFQ, one expected more 2-MeV beam from it. The question, therefore, remains, why was this expectation not achieved?

Accelerating field or gradient in the RFQ appears adequate relative to design. Acceleration threshold gradient is expected to be 84% of design gradient. For a threshold gradient of 0.44, this means a design gradient of 0.525. Because this design value is just over the knee of the transmission curve for a matched beam, a 10% higher value is recommended by AccSys for best operation. On our gradient scale, this gives a value of 0.578, a level which we held successfully during the last brief period of running.

To answer the question of the correct injection energy, we obtained RFQ transmission versus gradient curves at each of several energies from 26 keV to 36 keV. On the basis of the minimum gradient at which the curves for total transmitted beam and accelerated beam began to coalesce, we chose an energy between 30 and 32 keV. As a practical matter, however, we continue to find somewhat more accelerated beam for injection at 34 keV, possibly because of increased beam current from the source.

An important question remains. Is the ion source beam sufficiently well matched into the RFQ? The RFQ was removed on September 14 and an emittance probe installed at the end of the low energy transport line to measure emittance and distortions at full operating strength of the solenoid lenses. The new probe had a larger angular acceptance (+ 82.5mrad) than did the probe used last year (+ 40mrad). To accommodate existing vacuum-can hardware, the emittance probe plane ended up 3/8 in. upstream of the RFQ match point and the second solenoid lens had to be moved 7/8 in. upstream from its previous operating position as a result the precise orientation of the beam in the phase plane when the RFQ was in

operation was not verified. Consequently runs were taken at a range of lens strengths giving rotation of the beam ellipse as it approached the proper $\alpha + \beta$ for RFQ match. Little change in emittance values was seen during rotation.

A few examples of emittance plots are shown in Figures 5-10. Aberrations can be seen, particularly in the fringes of the beam but also somewhat in the core of the beam, so that effective emittance for a specified percentage of beam is larger than the measured value. At times, molecular beam remnants are also visible.

Table I attempts to summarize emittance values at the exit of the transport line under a variety of conditions. We may compare these values with the RFQ acceptance values calculated by AccSys in Figure 11 as a function of RFQ gradient and beam current. One sees that, for a 25-mA beam accelerated by the RFQ, the acceptance increases from about 1.11 at design gradient to 1.27 μ mm-mrad at 10% over design, where we operated for a brief period and hope to run in the future. For 45 mA accelerated these values increased from 0.87 at design gradient to 1.07 at 10% over design. From Table I, one sees that our effective 90%-contour emittances equal or exceed these acceptances, a somewhat uncomfortable comparison. On the other hand, if one considers the core of the beam (say 60% contour), one finds emittances well within the acceptance. Therefore, if one assumes only 60% of the beam is matched into the RFQ, a 25-mA beam accelerated gives a transmission of 60-70% at most for the matched portion of input beams of 60-70 mA (measured by beam toroid during operation and with Faraday cup after RFQ removal).

What else may reduce the transmission? The effect of an unmatched beam fraction on the remaining fraction that is matched, for a high current beam, is not known. Ken Crandall of AccSys is trying to model this. Another concern is the interaction of the solenoid-lens field with the mild steel end plate of the RFQ which is in close proximity to the solenoid. We hope to make some field measurements. There is a proposal to install a non-magnetic end plate. Also the 3/8-inch aperture in the half-inch thick new end plate will be tapered to reduce possible occlusion of beam.

A remark on the difference in performance of the two ion sources we have used may be in order. The beam from the AccSys duplicate of the modified FNAL source has higher angular divergence. This difference does not necessarily hamper overall performance but allows less flexibility in the usable voltage distribution on the accelerating column and in the tuning of the transport line for best performance. The solenoid lenses consequently must run at higher strength for this source. A careful measurement should be made of the extraction gap length and the inclination angle of the Pierce electrode for the two sources.

Summary

The RFQ was voltage conditioned to run consistently at 10% above design gradient for 36 hrs before shutdown with little sparking. The "hardened" Micom power supply delivered 240-250 kW of power to accelerate 23-25 mA of beam with a maximum of 23 mA around the 180° bend. Because of power decay inconsistencies during spark, the RFQ is being opened for inspection, cleaning and final testing at AccSys.

An accelerated beam of 24 mA is only 40% of an input beam of 60 mA. Emittance measurements were made at the output of the injection transport line after removal of the RFQ. Because of emittance growth and aberrations in the transport line, the effective emittance for 90% of the beam appears to exceed the calculated acceptance. Although a large fraction of the beam falls within the acceptance, there is, however, significantly less beam out of the RFQ than expected. There remains the question of possible interference with the match by solenoid field distortions at the RFQ input. Field measurements are planned. The effect of an unmatched beam fraction on the remaining matched beam fraction is also under study by AccSys.

TABLE I - SUMMARY OF EMITTANCE VALUES

Conditions	Current (mA)	Beam Fraction (%)	Normalized Emittance ($\mu\text{m-mrad}$)	
			Measured Value	Effective Value
<hr/>				
Old Source				
Normal column voltage	30-45	90	0.5-1.0	0.7-1.3
Reduced lens strength	(Oct. '88)	60	0.2-0.4	0.3-0.6
Small angle probe				
<hr/>				
New Source	45-55	90	0.9-1.4	1.1-1.6
Normal column voltage				
High lens strength		60	0.35-0.5	0.4-0.7
Large angle probe				
<hr/>				
New Source	43-72	90	0.9-1.2	1.2-1.6
Accel-Decel column				
High lens strength		60	0.3-0.4	0.5-0.7
Large angle probe				

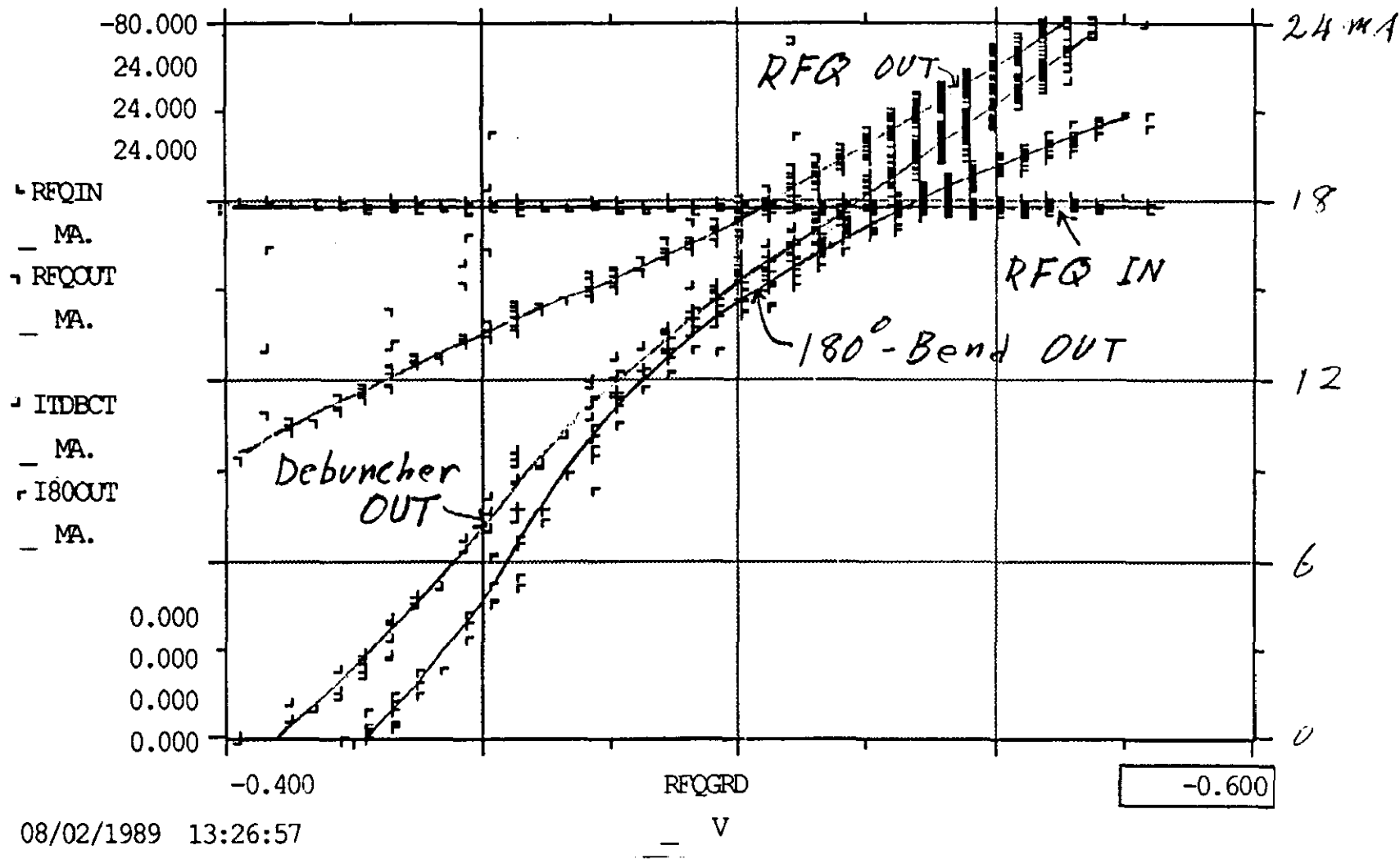
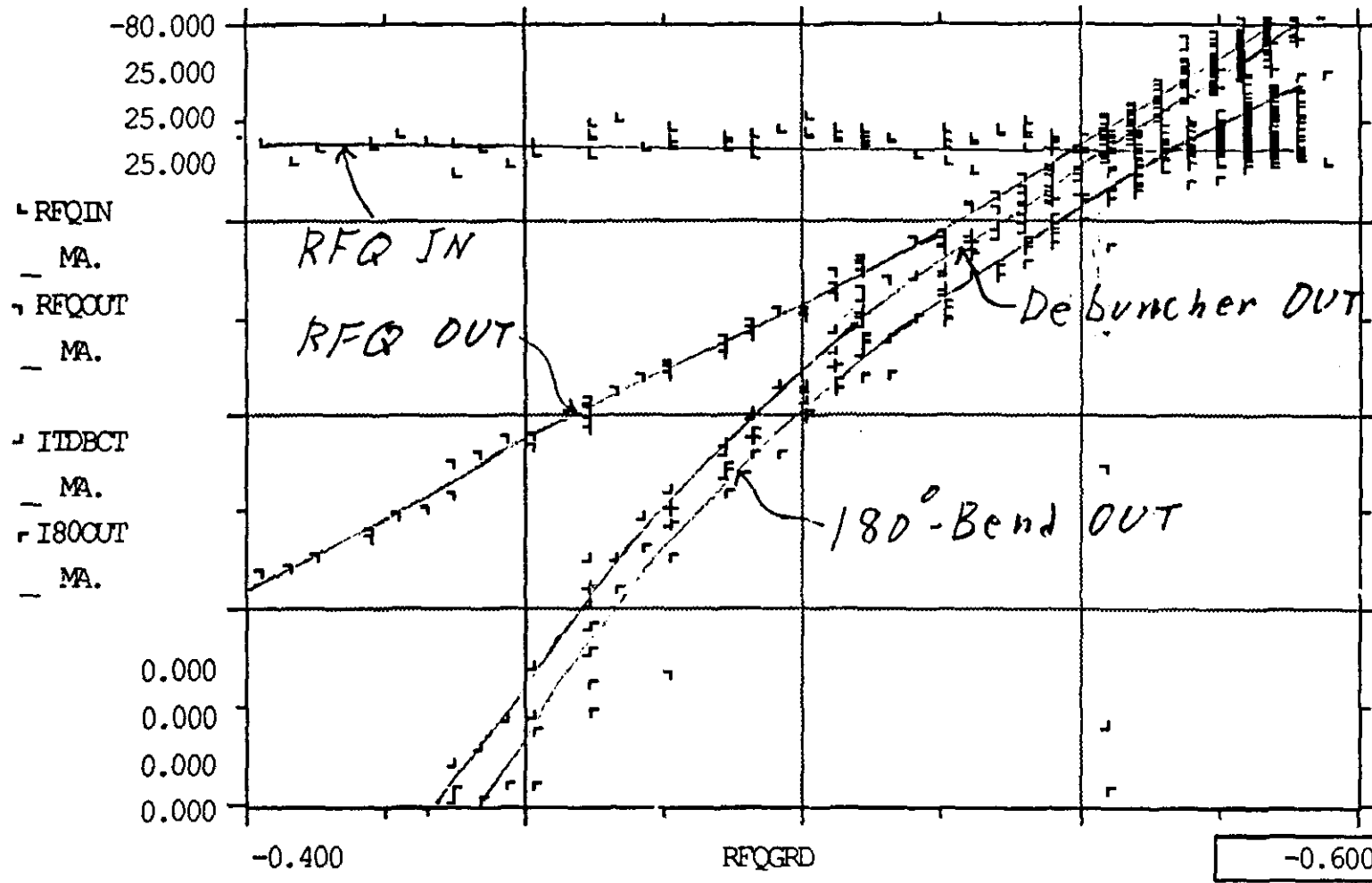


Fig. 1. Transmission Curves



09/13/1989 10:30:44

HV1 = 34.2 kV
 HV2 = -6.0 kV

Fig. 2. Transmission Curves

46 0780

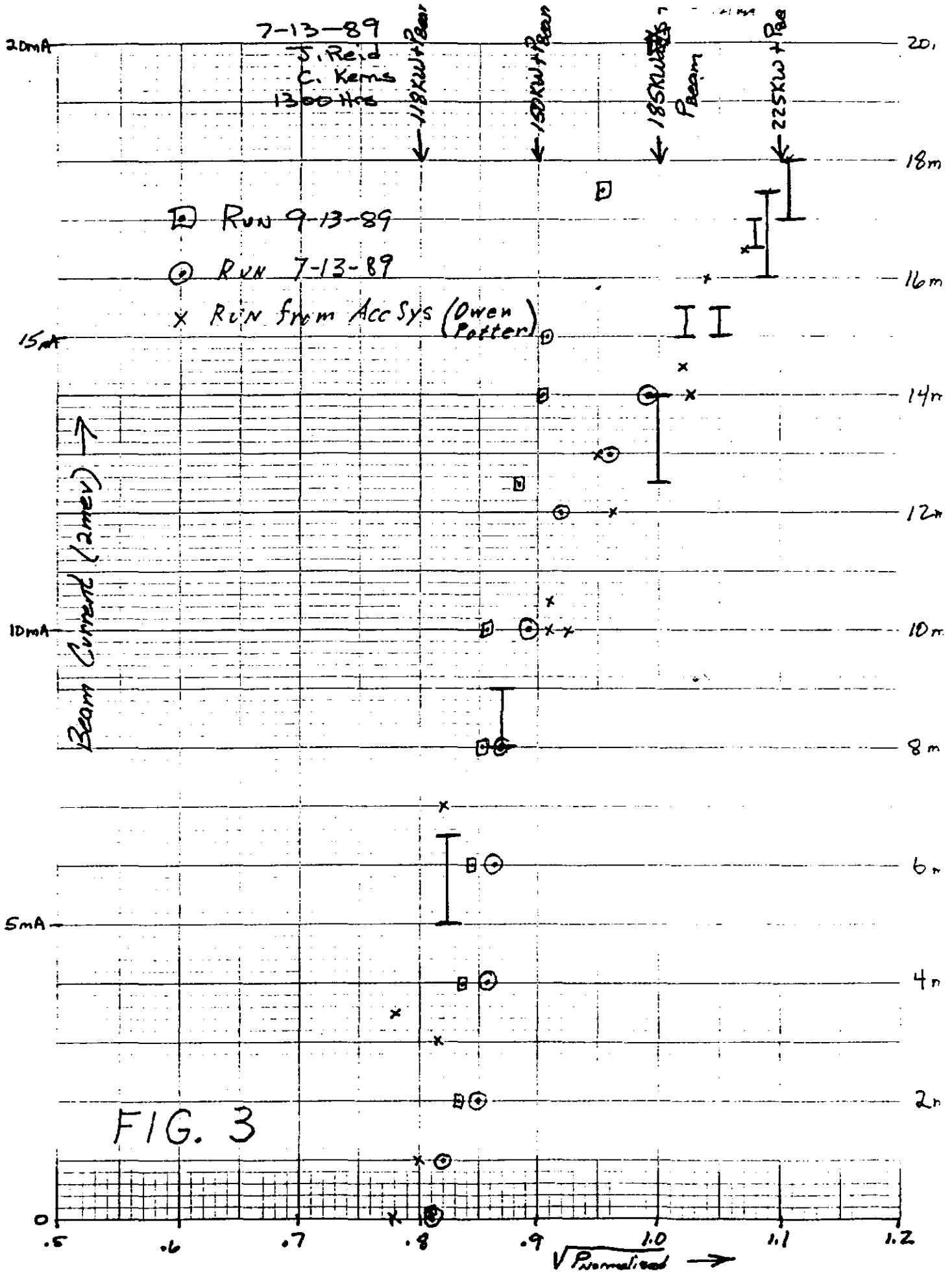


FIG. 3

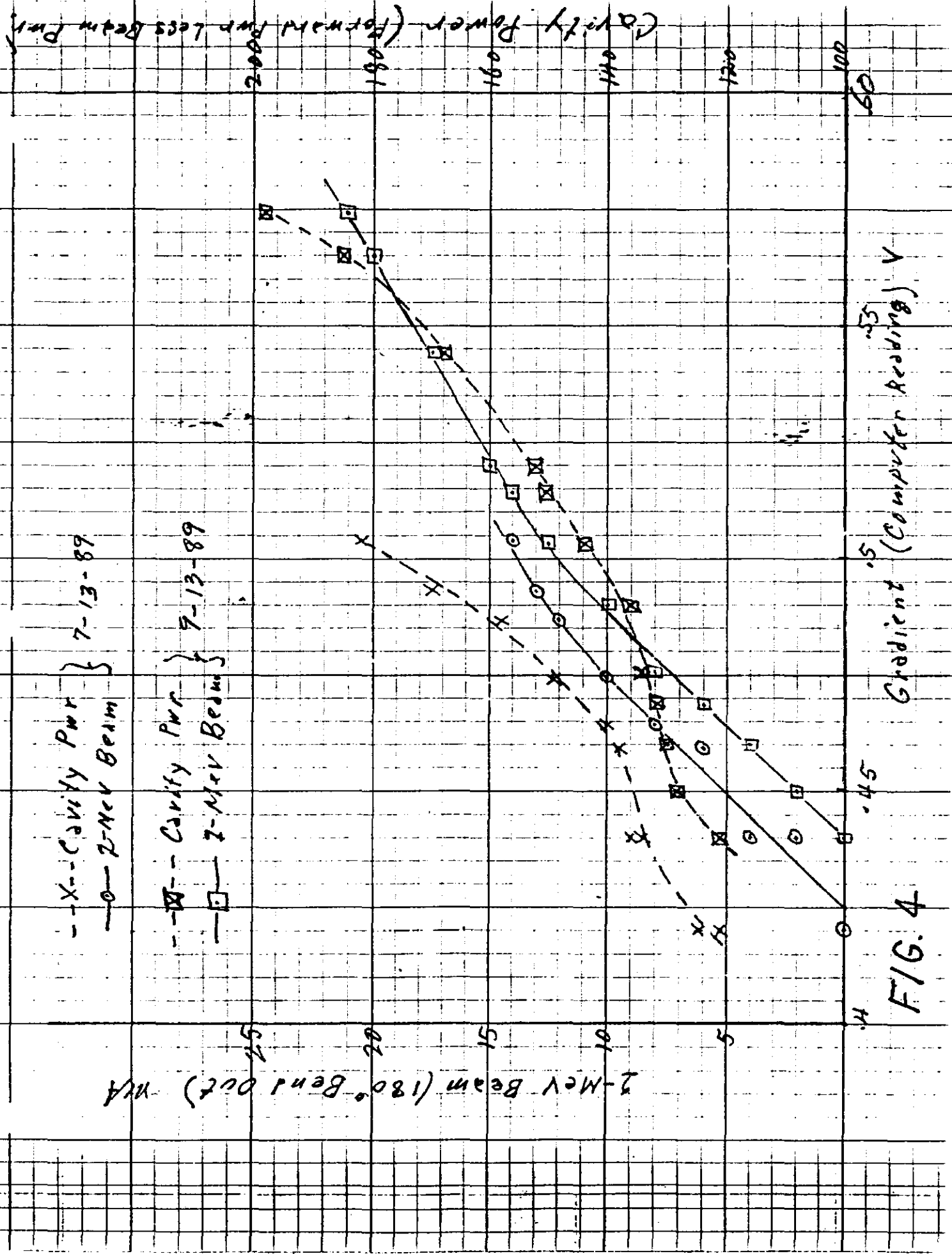


FIG. 4

Save Data

Take Data

New Data

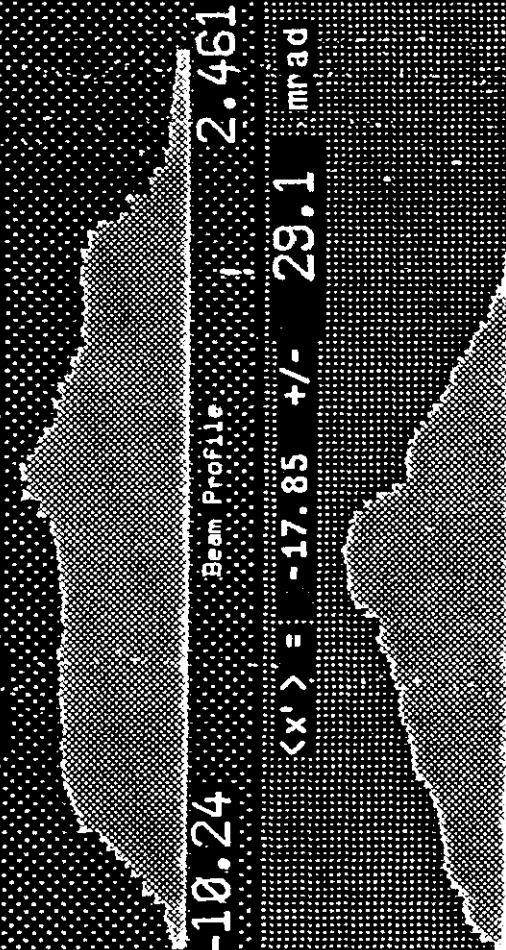
Main Menu

Plot Data

RMS Quantities

Norm' zed Emit. 1.34 pi mm-mrad
 Alpha 1.76
 Beta 0.191 mm/mrad
 Gamma 21.4 mrad/mm

$\langle x \rangle = -4.532 \pm 2.75$ mm

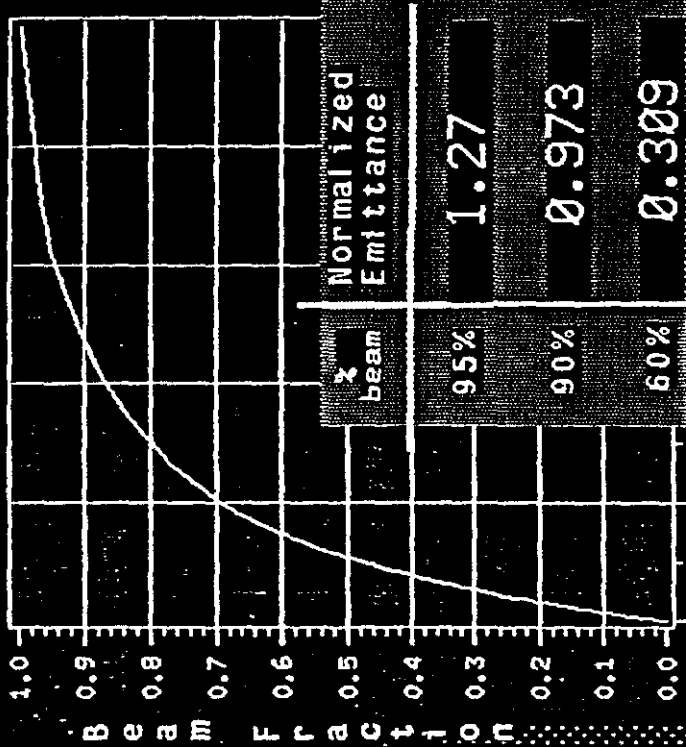


$\langle x' \rangle = -17.85 \pm 29.1$ mrad

Angle Projection

Toroid 99.7 mA
 Sol. #1 0 Amps
 Sol. #2 0 Amps
 KE 0.0335 MeV

Sat Sep 16 10:43:34 1989



Normalized Emittance

1.27

0.973

0.309

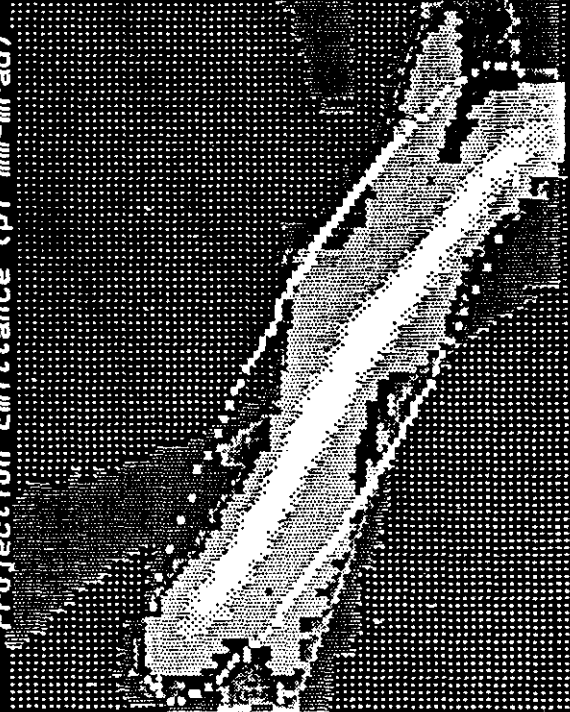
% beam

95%

90%

60%

Projection Emittance (pi mm-mrad)



60 mA-
 586 A
 560A-

FIG. 5

Save Data

Take Data

New Data

Main Menu

Plot Data

RMS Quantities

Norm'zed Emitt. 1.65 pi mm-mrad
 Alpha 0.443
 Beta 0.0395 mm/mrad
 Gamma 30.3 mrad/mm

$\langle x \rangle = -3.085 \pm 1.39$ mm

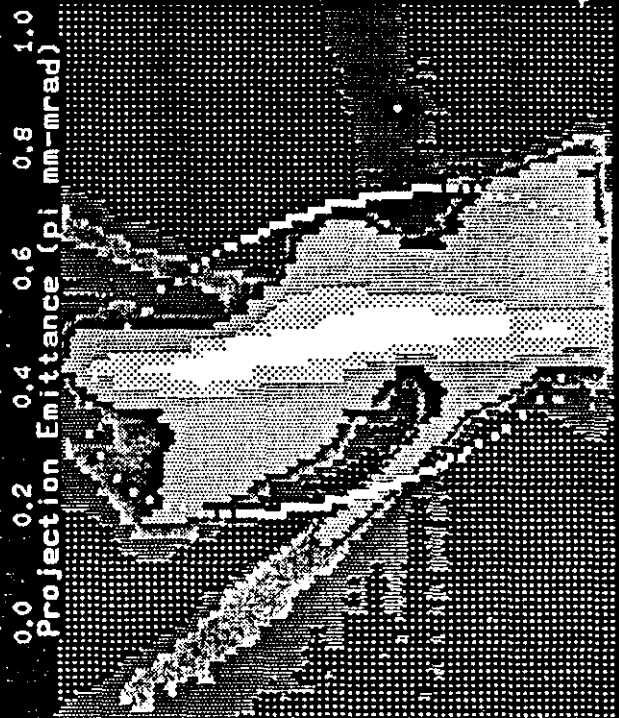
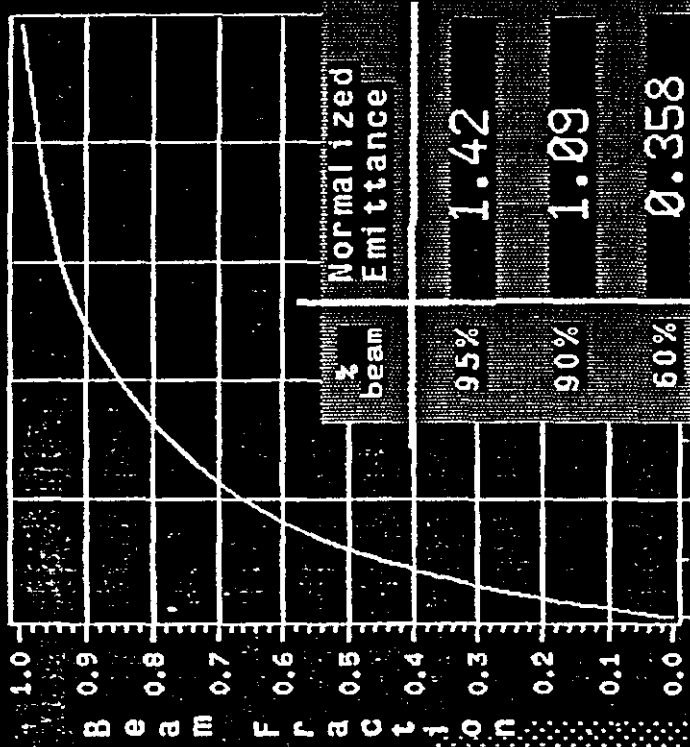
-9.429 Beam Profile 2.763

$\langle x' \rangle = -4.568 \pm 38.5$ mrad

Angle Projection

Toroid 99.6 mA
 Sol. #1 0 Amps
 Sol. #2 0 Amps
 KE 0.0335 MeV

Sat Sep 16 11:33:46 1989



63 mA
 586 A
 700 A

FIG. 6

Save Data

Take Data

New Data

Main Menu

Plot Data

RMS Quantities

Norm' zed Emitt. 1.36 pi mm-mrad
 Alpha 1.06
 Beta 0.0701 mm/mrad
 Gamma 30.4 mrad/mm

<x> = -3.567 +/- 1.68 mm

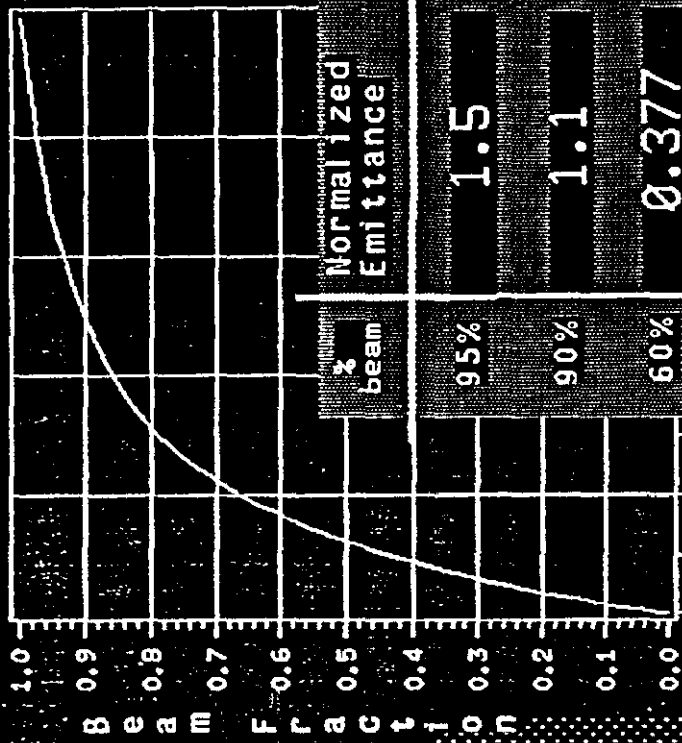
-10.3 Beam Profile 1.891

<x'> = -12.68 +/- 35 mrad

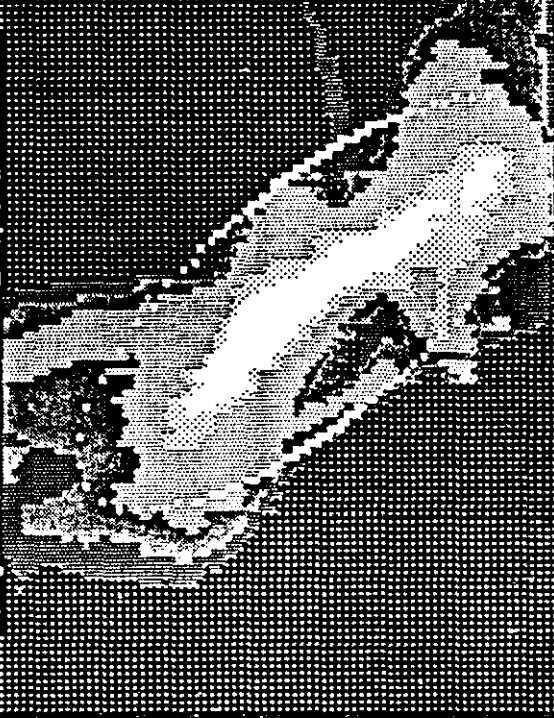
Angle Projection

Toroid 99.6 mA
 Sol. #1 0 Amps
 Sol. #2 0 Amps
 KE 0.0335 MeV

Sat Sep 16 11:43:27 1989



Projection Emittance (pi mm-mrad)



72 mA
 586 A
 728 A

FIG. 7

Save Data

Take Data

New Data

Main Menu

Plot Data

RMS Quantities

Norm' zed Emit. 1.47 pi mm-mrad
 Alpha 0.439
 Beta 0.0343 mm/mrad
 Gamma 34.7 mrad/mm

<x> = -2.979 +/- 1.22 mm

-10.18 2.015

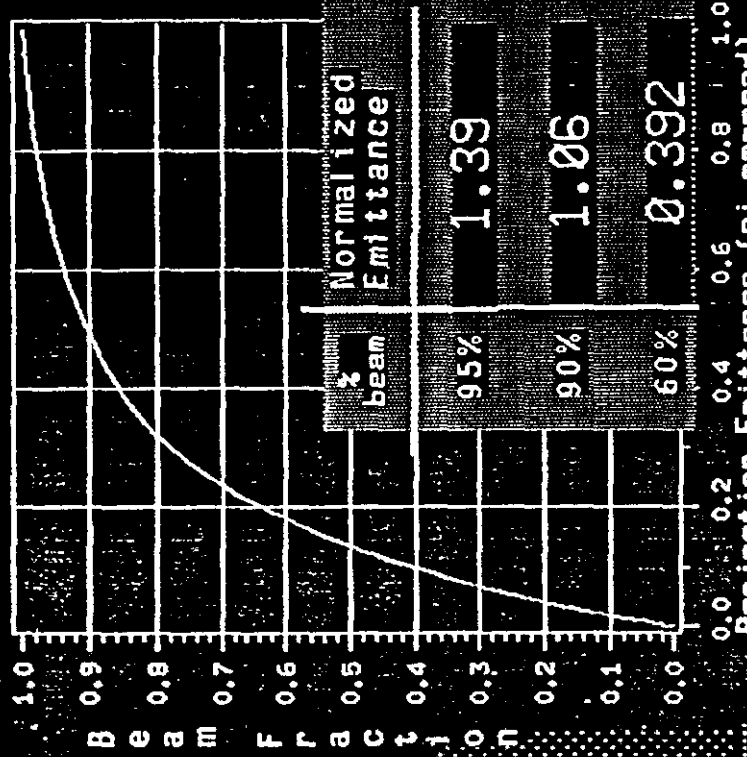
Beam Profile

<x'> = -11.04 +/- 38.8 mrad

Angle Projection

Toroid 99.6 mA
 Sol. #1 0 Amps
 Sol. #2 0 Amps
 KE 0.0335 MeV

Sat Sep 16 11:46:15 1989



72 MA
 586 A
 744 A

FIG. 8

Save Data

Take Data

New Data

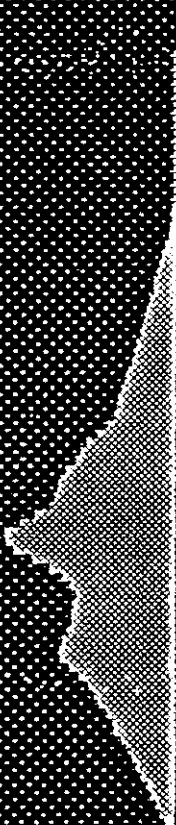
Main Menu

Plot Data

RMS Quantities

Norm'zed Emitt. 2.53 pi mm-mrad
 Alpha 1.05
 Beta 0.27 mm/mrad
 Gamma 7.74 mrad/mm

$\langle x \rangle = -6.714 \pm 4.5$ mm



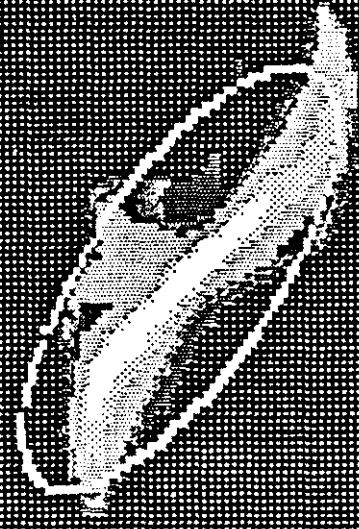
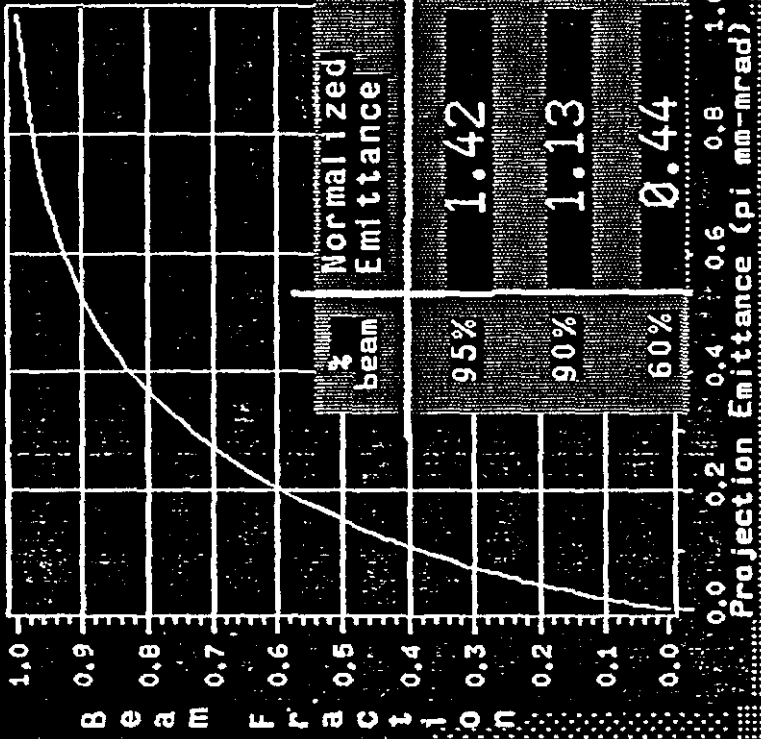
-20.15 -25.12 +/- 24.1 10.33

$\langle x \rangle = -25.12 \pm 24.1$ mrad



Toroid 99.6 mA
 Sol. #1 0 Amps
 Sol. #2 0 Amps
 KE 0.0335 MeV

Sat Sep 16 16:19:09 1989



57 mA
 548 A
 350 A

FIG 9

Save Data

Take Data

New Data

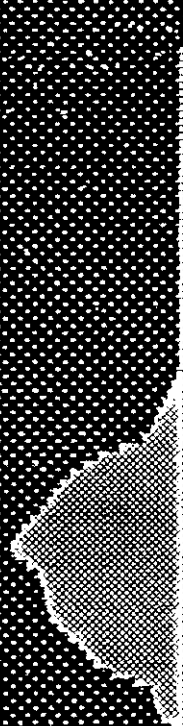
Main Menu

Plot Data

RMS Quantities

Norm' zed Emitt. 3.04 pi mm-mrad
 Alpha 0.82
 Beta 0.183 mm/mrad
 Gamma 9.15 mrad/mm

$\langle x \rangle = -3.159 \pm 4.06$ mm



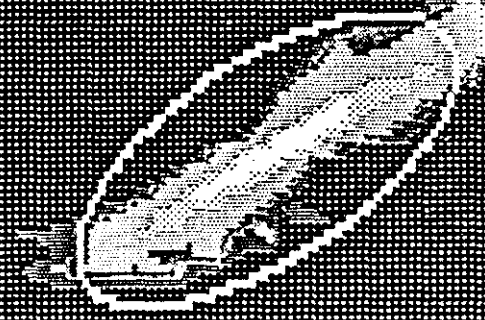
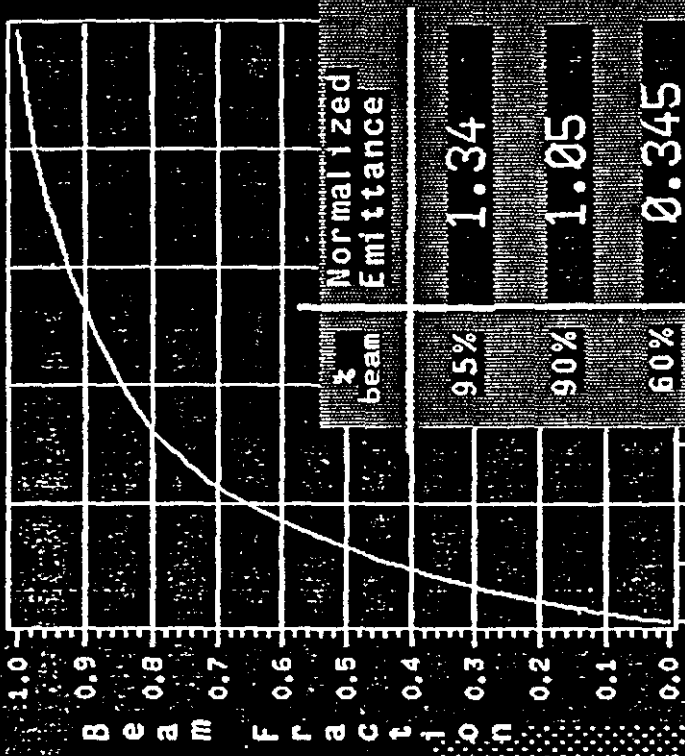
-19.77 20.87

$\langle x' \rangle = -19.85 \pm 28.7$ mrad



Toroid 99.6 mA
 Sol. #1 0 Amps
 Sol. #2 0 Amps
 KE 0.0335 MeV

Sun Sep 17 11:34:55 1989



50 mA
 609 A
 650 A

FIG. 10

STMR 03 = 6.515 A

Normalized Acceptance of RFQ
 vs Vane-Voltage factor for
 various currents. (Matched beam assumed)

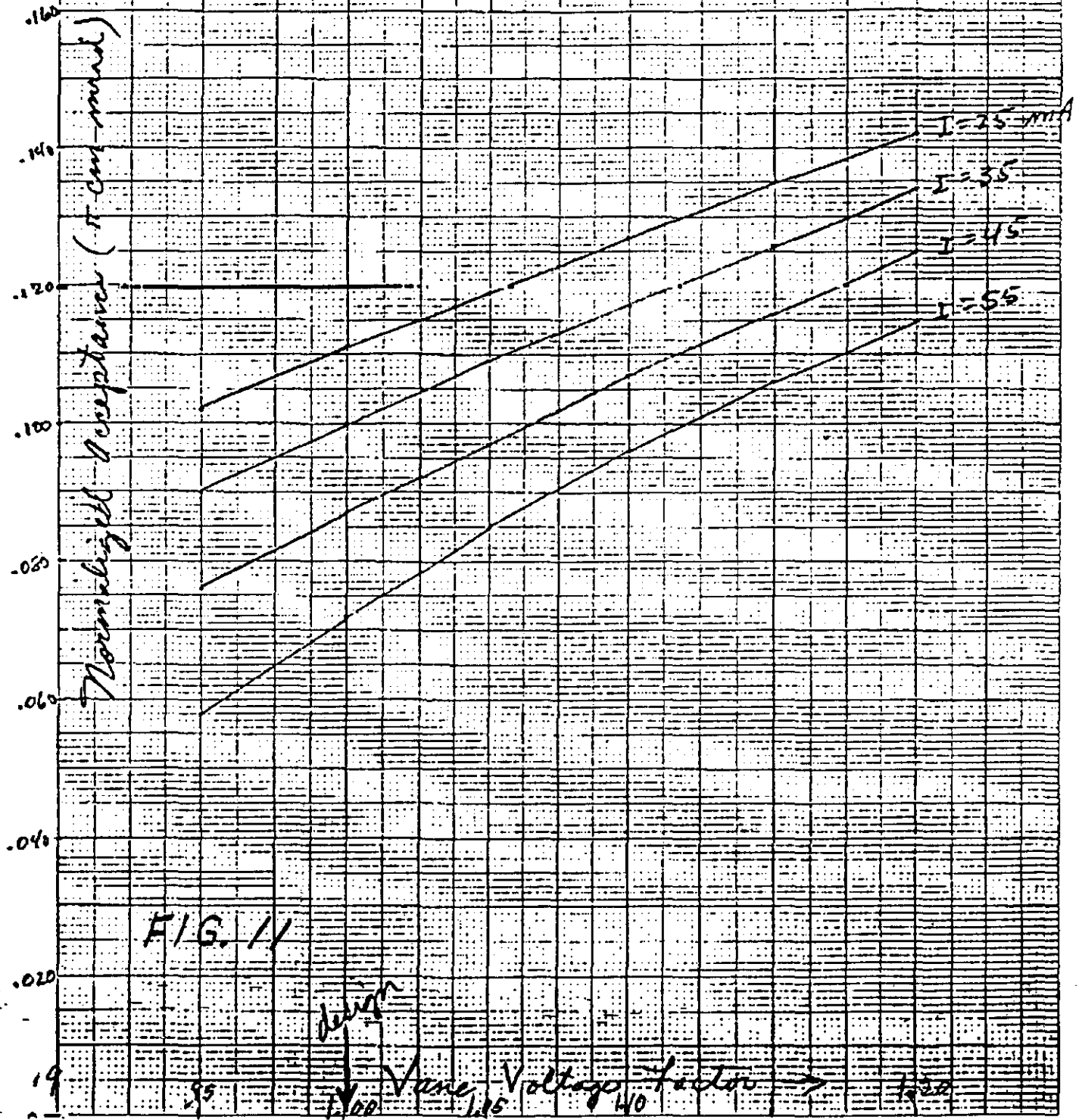


FIG. 11

design

Vane-Voltage factor →

46 1320

No. 2 KEUFEL & ESSEN CO. NEW JERSEY

A.4 The Injection Line and Matching at Injection

The 2 MeV beamline consists of all the components from the end of the RFQ injector to the pulsed kicker that brings the beam onto the central orbit of the synchrotron. This report is limited to the beam optics and beam dynamics arising from the design; electrical, mechanical and vacuum considerations are omitted. A list of the optical elements comprising the line and the distances along the beam axis to the downstream end of each element from the end of the RFQ¹ are given in Table I. The lengths given are those used in the optics calculations; because they are measured along the beam trajectory they differ from the layout coordinates because of the bends.

Table I: Injection Line Components

Element	Length [cm]	Cum. Length [m]
end of RFQ		0.000
D1 drift	29.30	0.293
Q1 quadrupole	10.60	0.399
D2 drift	20.00	0.599
Q2 quadrupole	10.60	0.705
D3 drift	20.00	0.905
Q3 quadrupole	10.60	1.011
D4 drift	29.33	1.304
RF debuncher	16.00	1.464
D5 drift	50.30	1.967
Q4 quadrupole	10.60	2.073
D6 drift	20.00	2.273
Q5 quadrupole	10.60	2.379
D7 drift	20.00	2.579
Q6 quadrupole	10.60	2.685
D8 drift	31.50	3.000
Q7 quad	15.60	3.156
D9 drift	35.20	3.508
BH 180° horiz. gradient bend	255.35	6.062
D10 drift	29.85	6.360
Q8 quadrupole	15.60	6.516
D11 drift	35.88	6.875
BV1 -25° vert. bend	31.07	7.186
D12 drift	86.75	8.053
BV2 20° vert. bend	25.40	8.307
D13 drift	36.84	8.676
KV 5° vert. kicker	40.66	9.082

The functions of the injection line are transport and matching of the beam from injector to synchrotron. Matching the coordinates of the longitudinal phaseplane (phase, energy) is the principal concern because the synchrotron is limited in momentum acceptance but generous in transverse acceptance compared to the RFQ emittances. A little more specifically, and in order of importance, the tasks for the 2 MeV line are

1. efficient transport of beam from RFQ to synchrotron
2. reduction of momentum spread of the tightly bunched beam from the RFQ
3. matching dispersion function of beamline to dispersion of synchrotron
4. matching transverse beam envelope to lattice functions of synchrotron

The importance of efficient beam transport is primarily to provide the beam for the desired intensity of operation without placing unnecessary demand on the RFQ and ion source. The injector will provide better beam quality and more reliable operation if beam current out of the RFQ is not pushed. Experience indicates that it is reasonable to expect routine operation at ~ 20 mA. Although this is somewhat below the design level, it nonetheless corresponds to beam intensity in excess of 10^{11} for losses $< 25\%$.

The greatest inefficiency in injection results from the wide energy spread of the beam leaving the RFQ ($\sim \pm 20 - 30$ keV) and the increase in that spread resulting from spacecharge forces as the beam moves along the transport line. The effect of space charge is particularly strong in the part of the line between the RFQ and the debuncher over which the beam is tightly bunched initially ($\sim \pm 15^\circ - 20^\circ$) but spreads to $\pm 180^\circ$. It was a design choice to place the debuncher far enough downstream to achieve this $\pm 180^\circ$ spread to reduce the sensitivity of the buncher operation to phase error induced by beam loading and to reduce the importance of optimum phase setting. A negative aspect of this choice is that a significant fraction of the momentum distribution, perhaps one third, lies outside of the effective phase range for the debuncher; this beam is not brought within the momentum acceptance of the synchrotron. Also, commissioning and diagnosis of buncher operation is complicated by the fact that one will not have distinct bunch signals to measure performance.

The dispersion in the synchrotron is large (~ 9 m), and the momentum spread of the 2 MeV beam ($\sim 0.75\%$) is considerably greater than the design momentum aperture. It is not obvious what allowance must be made for the transverse phasespace in the horizontal aperture because the emittance from the RFQ is rather small, but one expects the emittance in the synchrotron to be dominated by spacecharge induced blowup. A reasonable guess would be that the emittance will be about the same in both planes and will fill the vertical aperture at injection. In this rather pessimistic estimate the aperture left for momentum is $\pm 0.25\%$. However, beam width from dispersion will reduce the horizontal tune spread just as beam width from radial betatron oscillation does. Therefore, even without a detailed study one can surmise that the allowance for betatron amplitude can be less in the horizontal plane. To know how much less would require careful study, but an arbitrary optimistic

guess of one cm for betatron amplitudes corresponds to a momentum aperture $\approx \pm 0.39\%$. In either case dispersion matching is important to maximize the horizontal acceptance for the off-momentum particles. Fortunately, this match is not a function of beam current so that continuous monitoring and adjustment for changes in beam current are not required. So long as the quadrupole following the 180° bend is not varied, the match is guaranteed by the 180° bend and the ring lattice. According to simulation results from AccSys², it should be possible to adiabatically capture $\gtrsim 6 \times 10^{11}$ protons in the absence of other losses. This intensity requires that the debuncher be correctly tuned; some part of the failure to approach this intensity may result from inadequate debuncher performance or adjustment. There has been no systematic investigation of the debuncher; if empirical tuning on phase and gradient do not result in anticipated momentum distribution, more fundamental studies will be wanted. Such studies should initially be made at low beam current to reduce the effects of beam loading of the debuncher and to permit measurements on distinct bunches downstream.

On the other hand, exact transverse matching is not especially important because the transverse emittances will blowup considerably in the synchrotron because of spacecharge forces. The beam will spread transversely until spacecharge tuneshift is reduced to what the guidefield quality permits. At high current the beam will either fill the physical aperture or a dynamic aperture depending on chromaticity, stopband width, and other effects of nonlinear guidefield. Only for low current operation is performance likely to show sensitivity to details of the injection match. To a first approximation any beamline settings which result in clean transport of the beam to the central orbit of the synchrotron should result in similar conditions there.

The calculation of parameters for both longitudinal and transverse matching is uncomplicated at zero beam current. The solution for $I = 0$ establishes the correct dispersion matching and a starting point for non-zero beam current. To account for spacecharge forces one can employ either envelope or multiparticle codes. The readily available programs which include spacecharge³ seem to have one or another limitation which makes them less completely satisfactory — individually and even in combination. Some of the limitations are clearly susceptible to straightforward program improvements. Improved calculations could clarify the dependence of beamline parameters on beam current and give additional information on the momentum distribution of the beam. More credible than the results of even a good calculation would be an empirical tuning study which works from a well-understood low current tune to a successful tune at the operating current in several intermediate steps of beam current. Such a study would be facilitated by additional profile monitors and could be managed most easily in an installation/commissioning stage in which the line would be more accessible. The difficulty (impossibility?) of verifying position and size of beam waists within the 180° bend is a significant obstacle to rational beam tuning. However, because of the tolerance of the synchrotron injection to transverse mismatch, tuning based simply on minimization of losses in the line should be satisfactory operationally.

Probably the most important uncertainty in calculations of injection line optics is the absence of good information on the beam parameters at the end of the RFQ. Calculations

by AccSys⁴ show that the parameters should be sensitive to the output current, but there are no measurements on the Loma Linda RFQ as it has been operated with the synchrotron. Various unexplained features of the RFQ operation including its preference for higher injection energy and higher input power as well as its unexpectedly low beam transmission lower the credibility of the simulation predictions of beam properties. Table II lists the predictions of AccSys simulations for output 0 mA and 34 mA. The beam parameters used by the designers of the injection line⁵ are the 34 mA values. The conditions to be matched at the injection point in the synchrotron are also given.

Table II: Matching Requirements

Calculated Beam Parameters at End of RFQ				
Beam Property		$I_{\text{beam}} = 0 \text{ mA}$	$I_{\text{beam}} = 34 \text{ mA}$	Units
Kinetic energy	T	2.00	2.00	MeV
Horizontal emittance ^a	ϵ_x	5.88	7.85	$\pi \text{ mm mrad}$
Vertical emittance ^a	ϵ_y	5.88	7.35	$\pi \text{ mm mrad}$
Longitudinal emittance ^a	ϵ_φ	n. a.	580.5	$\pi \text{ keV deg}$
Horiz. beam envelope param.	α_x	-1.34	-3.56	
	β_x	0.143	0.346	m
Vert. beam envelope param.	α_y	1.48	3.49	
	β_y	0.167	0.415	m
Long. beam envelope param.	α_φ	0.032	0.210	
	β_φ	0.390	0.624	deg/keV
Matching Conditions at Injection Point in Synchrotron				
Lattice Property		Value		Units
Horiz. Courant-Snyder func.	α_x	0.00		
	β_x	4.86		m
Vert. Courant-Snyder func.	α_y	0.00		
	β_y	1.88		m
Horiz. dispersion func.	x_p	8.98		m
Vert. dispersion func.	y_p	0.00		m
Horiz. acceptance ^b	a_x	418.	$\pi \text{ mm mrad}$	
Vert. acceptance	a_y	159.	$\pi \text{ mm mrad}$	
Momentum acceptance ^c		0.94		%
^a 100 % for equivalent uniform beam ^b $\Delta p = 0$ ^c at $\epsilon_x = 0$				

For infinitesimal beam current the transverse optics and dispersion match are decoupled from the longitudinal distribution and momentum spread. The line can be designed in this regime using a first order optics program with fitting.⁶ The basic pattern is a quadrupole

triplet mounted as close to the end of the RFQ as possible to focus the beam to waists in both planes in the vicinity of the center of debuncher followed by another triplet to recollect the beam. The dispersion match is obtained from a 180° horizontal bend. The bend has a gradient to produce a vertical waist near its center. The bend is flanked by quads focusing in the horizontal plane to make a horizontal waist in the magnet also. The slope of the dispersion function is matched to zero by the quad following the bend. After the bend is a -25°, 20°, 5° vertical dogleg consisting of a pair of septa and a pulsed kicker. Because there are no intervening quads, there is no vertical dispersion introduced; the effect on the optics is only the small amount of edge focusing.

Table III contains two sets of results for the 2 MeV line parameters. The element spacing is the result of first order calculation⁷ as reported by McCrory.⁸ The first order calculation for zero current has been redone for this report using the zero-current values for the beam parameters of the RFQ given in Table II in place of the 34 mA values used originally. The Table also gives the gradients calculated by McCrory for 34 mA operation with an envelope code. Multiparticle tracking⁹ shows that for beam currents greater than 20 mA or so the bunches have sheared to ~ 180° phase spread at the debuncher. Therefore it is permissible and convenient to proceed downstream of that point with a two-dimensional envelope code, *i. e.* one that applies to dc beam. It is evident by inspection that the two solutions differ substantially; even some polarities differ.

Table III: Beamline Quad Settings [A]

Quad	Beam Current		
	0 mA ^a	34 mA ^b	18 mA ^c
Q1	7.478	9.724	n. a.
Q2	-8.891	-9.896	n. a.
Q3	8.736	7.427	7.494
Q4	4.162	0.970	5.075
Q5	-4.723	1.029	-3.182
Q6	2.706	-4.458	5.018
Q7	0.620	2.698	2.589
Q8	1.070	1.070	1.174

^a calc. by TRANSPORT
^b calc. by TRACE 2D
^c Operational, 26 July 89

For operational purposes it would be useful to have a family of solutions in which the distinguishing parameter is the beam current. Such a set would provide valuable guidance on how to adjust the line for different conditions and on what to expect on the profile monitors. Because the initial conditions are themselves current dependent, there need to be simulations or measurements (or both!) on the RFQ at the several current levels. With this information in hand there is a rather convenient calculation which uses a single program to calculate the

entire line. At least for moderate currents the transverse envelope code TRACE 2D can be used with the effect of debunching approximated by a BUNCHER/DEBUNCHER element immediately following the RFQ arranged to reduce the spacecharge force continuously over the section of the line from RFQ exit to debuncher. A multiparticle code can be used as a check at several current levels to ensure that the approximation in using the two-dimensional calculation is adequate, but it is very tedious to employ a multiparticle code to find the gradients needed for matching. As mentioned before, all solutions should have the same gradient for the final quadrupole to preserve the dispersion match.

For all that has been said above the synchrotron has been characterized only by the values of the lattice functions (Courant-Snyder functions and dispersion function) on the central orbit. However, both machine experiments and magnetic measurements have shown that the guide field at injection is non-ideal and in particular that there is a large sextupole component. Fig. 1 shows the field gradient *vs.* radial position in the dipole at injection field and the corresponding tune difference for particles off the central orbit. The indicated spread in tune of $\sim \pm 0.1$ is large enough that it may be an important contributor to the observed limitation of momentum aperture. The fact that the lattice functions and tunes depend on momentum and that tunes may also depend on betatron amplitudes might result in a pathological condition with unexpected sensitivity to the transverse match. All that can be done in the injection line to ameliorate the effects of imperfection of the guidefield is to optimize debuncher performance to get maximum beam near the central momentum and watch steering to avoid unnecessary betatron amplitudes. Even if it is decided to improve the dipole field it is quite possible that debuncher tuning will be an effective and efficient route to early intensity gains.

References

1. E. McCrory, memo: Loma Linda 2 MeV Beam Transport Design (29 April 89)
2. C. W. Owen, quoting AccSys results in LL - 263 (October 87)
3. K. Crandall, TRACE 2D and TRACE 3D
D. A. Swenson *et al.*, PARMILA
4. C. Curtis, quoting K. Crandall (AccSys) in LL - 203 (28 May 87)
5. A. Malensek and E. McCrory, priv. comm.
6. K. Brown and D. Carey, TRANSPORT
7. A. Malensek, priv. comm.
8. E. McCrory, memo *sup. cit.*
9. E. McCrory, priv. comm., confirmed by author

From D. HARDING.

Deviation from uniform gradient LDL102 at 207 Amp

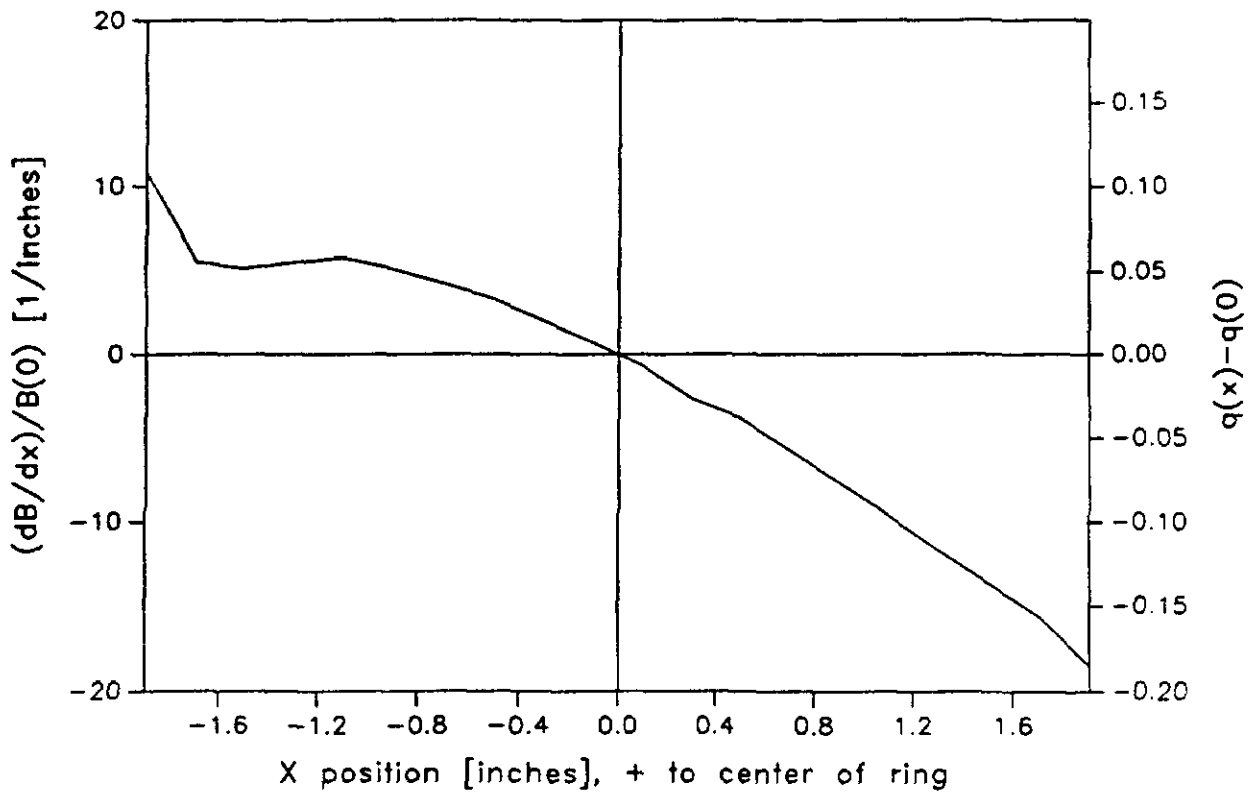


Figure 1: Gradient and Expected Tune Shift from Dipole Field Error

B.1 BEAM OBSERVATIONS AT INJECTION

P. MARTIN

This section reviews the experiences during commissioning at Fermilab of the Loma Linda Medical Accelerator, with respect to observations of the beam behavior at low energy. The dipole current conditions at injection for much of the commissioning were such that the current at injection was held constant, with remanent fields that were uncontrolled. Injecting into a dc level allows adiabatic capture of the injected beam; adiabatic capture should be most efficient, in principle, in the absence of other effects. The power supply had no invert capability, so the current simply decayed until it fell below the set value, at which time the supply responded and brought it back up to the desired value. The uncontrolled undershoot was about 25 A. Modifications were made to allow controlling the undershoot value and duration (Figure 1). The power supply would still undershoot the desired level, however, and then overshoot the injection level, with the amount of overshoot proportional to the difference between the undershoot and injection levels. In spite of these difficulties, undershoots in the range of 100 A led to improved momentum acceptance at injection, although this failed to translate into improved intensity to flattop. This was not pursued in great detail, however, as the focus shifted to injecting on the fly, but the experiences clearly demonstrated the significance of remanent fields in the magnets. A curiosity of the behavior observed was that the beam intensity also depended on how much time was spent at the undershoot level vs. how much at the injection level, prior to injection; i.e. there were apparently some time dependences to the remanent fields, or some subtle power supply related effects.

Injecting on the fly, i.e. injecting while the dipole current has a substantial dI/dt , became the operational mode after investigations of that method led to a 50% increase in the amount of beam accelerated to flattop. Injecting on the fly has the advantage of spending less time at low energy, where the vacuum lifetime is worse. More important is the added benefit of the eddy-current induced sextupole cancelling the large chromaticity at injection. It also avoids the overshoot with the present power supply. The optimum conditions (dI/dt) for injecting on the fly have not been determined conclusively. For higher dI/dt , the bucket width shrinks, (since the rf voltage cannot be raised arbitrarily high due to the small momentum acceptance of the ring). The notch in the beam caused by the 250 nsec falltime of the injection kicker is also important; if the falltime can be shortened, a lower dI/dt may be desirable (to provide a smaller synchronous phase and hence larger bucket width to accept the increased time spread of the beam). There were also problems related to the limited parabola rate of the main dipole power supply, which prevented reaching the maximum dI/dt , simply because the minimum current cannot go negative, and there were limitations with the clock system in use at Fermilab. This entire question of optimization with the clock system in use at Fermilab. This entire question of optimization of the injection conditions must be addressed at Loma Linda with the final power supplies and clock systems.

The tunes and chromaticities, both horizontal and vertical, were measured at injection and higher energies. The measurements were not completely straightforward, especially during the ramp (see the discussion under Diagnostics and Beam measurements). The tunes were measured, within errors, to be as predicted ($\nu_x \approx .6$, $\nu_y \approx 1.3$) just from the focusing from the dipoles, i.e. without having to power any of the separate quadrupole elements. Powering RSSQ3 and RSSQ4 to small currents at injection generally was found to increase the intensity slightly. The chromaticities had the same shape, as a function of current, but were roughly 50% larger than predicted (Figure 2). The predictions were based upon magnetic measurements taken under significantly different conditions with respect to the undershoot level than was the case for the beam measurements, however.

The ring is equipped with four dipole correction magnets for each plane, located at the four long straight sections. During commissioning at Fermilab, these correctors were powered by PEI power supplies which were not well matched to the loads, and ripple was a serious problem. The current/voltage capability of these supplies was 200 A at 100 V. Filters were added to the four horizontal trims (and to the three quadrupoles that were powered by identical supplies). The power supplies were controlled by Motorola MVME 133A-20 "ramp-cpu" cards which allowed specifying the current as a function of time referenced to various timing events related to the main dipole ramp, e.g. start of ramp or start of flattop. The output current could also be scaled to the main dipole instantaneous or flattop current, if desired. Although the supplies were bipolar, switching the polarity required manually operating a reversing switch. Further, the filters used polarized capacitors which implied that switching polarity ultimately meant reversing the leads at the magnet. The trim dipoles were used to explore the aperture of the machine, with limited success, at various times during the commissioning period. The exercise of using three-bumps to determine the aperture limits were very tedious, as the three dipole curves had to be changed and loaded sequentially. Changes to the control system allow quickly changing a single time slot of each of three elements in a three-bump, in the appropriate ratio, would make this procedure vastly easier.

The horizontal aperture at injection appeared to be substantially smaller than the expected ± 43 mm. Consequently, the beam was injected to the radial inside by about 10 mm, and then moved back to the center over the ensuing 100 msec, during which time the beam should have shrunk by at least 25% due to the 50% increase in $\beta\gamma$. When injecting into a dc current (adiabatic capture), the limiting aperture appeared to be in the vicinity of LS4. A series of scans was done, in which single dipoles (not three-bumps) were excited, and the positions around the ring were recorded that resulted in substantial beam loss; most positions around the ring showed both positive and negative excursions, but LS4 never went positive, possibly indicating an obstruction to the radial outside (Figure 3). More recently, however, while injecting on the fly, it has been noted that there

is a substantial beam loss on the first turn. Namely, the LS2 toroid, which shows injected beam only 1/4 turn from the injection point, and then circulating beam after the injection kicker is discharged, shows a $\approx 40\%$ decrease in intensity in the time between 1/4 and 1-1/4 turns (Figure 4). The intensity remains approximately constant over the following turns on the time scale of interest. Using the BPM Fast Sum signals, (and stopping the beam after the first turn by turning on the dipole at LS1, just before the injection septum, very hard) it appeared that the intensity was roughly constant up to SS2, then dropped by 30% between SS2 and LS3, and then was roughly flat again. Later investigations showed the drop between LS3 and SS3, however. A plate which collimates the beam horizontally (and in momentum spread, due to the 9m dispersion) was mounted on the back of the multiwire profile monitor downstream of the 180 degree bend. The multiwire by itself reduced the beam intensity, through attenuation, by about 10%; the addition of the collimator reduced the beam by a factor of 3, i.e. it was eliminating all beam beyond about $.4\sigma$, assuming a Gaussian distributed beam. When the multiwire and collimator were placed in the beam the 40% loss in the first few turns was reduced to a 25% loss; this would indicate that there were beam losses in both the vertical and horizontal planes. (Had the losses been only in the vertical, the loss would have remained at 40%; had they been only horizontal, they should have been reduced to essentially zero). The beam pipe was opened up to look for obstacles in both LS3 and LS4, but nothing was found.

The large dispersion (9.6 m) in the ring should imply that the horizontal beam size is determined primarily by the momentum spread of the beam. For example¹, a momentum spread of the beam of $\pm 3.7 \times 10^{-3}$ implies a width due to the momentum spread of $9.6 \text{ m} \times \pm 3.7 \times 10^{-3} = \pm 35 \text{ mm}$. A good field aperture of 43 mm then leads to a transverse width $X_{\beta} = \sqrt{(43)^2 - (35)^2} = 25 \text{ mm}$. However, measurements of coasting, rf-captured beam at injection show that the momentum spread of the beam is only 4.4 keV, or $\Delta p/p = 1.1 \times 10^{-3}$, so the width due to the momentum spread is only 10.6 mm; taking the good field aperture to be 43 mm minus the 10 mm radial offset at injection, the transverse width is $X_{\beta} = \sqrt{(33)^2 - (10.6)^2} = 31 \text{ mm}$. A beam size of 25 (31) mm implies a transverse emittance (95% normalized) of 6.8 (10.4) $\pi \text{ mm-mrad}$ at a lattice location whose β is 6 m.

Other indications that the momentum acceptance of the machine was limited include the observations that (i) lowering the rf voltage at the end of adiabatic capture from 75V to 50V led to a 10% increase in the beam intensity; (ii) injecting into a fixed rf voltage whose bucket height is larger than the acceptance of the machine allowed a direct measurement (Figure 5) of the momentum acceptance for that rf frequency (radial offset) -- that the measurement yielded the 4.4 keV number quoted above.

Summary of Transmission

We conclude with a summary of the typical beam efficiency at various times in the injection and acceleration sequence. The toroid after the 180 degree bend is taken as 100%. (These data were taken on September 6, 1989; they are typical of earlier measurements.)

Location/Time	Current	Intensity	Step-wise Efficiency	Cumulative Efficiency
180 Bend	13 mA	8.1×10^{10}	---	---
1/4 Turn	14 mA	8.8×10^{10}	100%	100%
a few turns	8 mA	5.0×10^{10}	57%	57%
200 μ sec	5.7 mA	3.6×10^{10}	72%	41%
2 msec	3.1 mA	1.9×10^{10}	53%	22%
Flattop	---	1.6×10^{10}	84%	18%

The toroid after the 180 degree bend actually reads lower than the one in the ring at LS2, indicating a calibration problem. The loss in the first few turns has already been discussed above; here, we are excluding the loss due to the kicker falltime--the numbers indicate the peak reading. The 200 μ sec loss is almost entirely due to the kicker falltime. The 200 μ sec time represents the peak of the intensity signal when the LS2 toroid signal is filtered with a 3 kHz filter to average over the rf cycle, removing the bunch structure (Figure 6). The 2 msec loss occurs as the beam which is not captured in the bucket is lost; it has two components, one which disappears in about 700 μ sec, the remainder in about 1.2 msec. (If the rf is turned off, and beam injected at the same rate of dI/dt , the beam disappears in about 700 μ sec in an approximately linearly fashion.) The remaining losses, during acceleration, primarily after .4 sec, are not understood. When the RFQ was operated at its peak gradient, the beam around the 180 degree bend exceeded 20 mA, and the beam to flattop was as high as 2.5×10^{10} . Another comment should be made related to the above data. There have been occasions when the intensity to flattop is bistable, i.e. is one of two values in a seemingly random pattern. The ratio between the two has varied between 90% and 60%; under those circumstances, the beam around the 180 degree bend appears to have been constant, but the amount of beam after 1/4 turn was varying, and all subsequent numbers along with it. Thus, some variation in an element in the injection line or first 1/4 of the ring was able to have a very significant effect on beam intensity. This may be a clue to what is limiting the intensity in general.

One last comment on strange behavior: it was observed that when the slow extraction feedback system was gated on, feeding back on noise, at injection (adiabatic capture mode), the amount of captured beam was increased by roughly 10%.

Recommendations.

- (1) The aperture must be explored systematically (three-bumps) once the machine is installed at Loma Linda with the final power supplies.

The exploration may want to be done at a number of energies. Software changes would make this task easier. Injection aperture may need to be studied as a function of dI/dt at injection.

- (2) The beam loss on the first turn should be studied as a function of: (i) injecting on the fly vs. injecting into a dc current; and (ii) using dipoles (three-bumps) to minimize loss.
- (3) The optimum dI/dt for injection has to be studied, once the final power supplies are in use. The optimization must include varying the undershoot level as well as dI/dt itself.

Reference

1. Note by L. Teng, "Beam Emittances at Various Energies", Nov. 24, 1987.

B.2 SPACE CHARGE EFFECTS AT INJECTION

D. FINLEY

The Loma Linda Medical Accelerator proton beam experiences defocussing forces which result in tune spreads. Edwards and Syphers (1988 Cornell Summer School, AIP Conference Proceedings 184) have provided a recent discussion of this space charge effect. They relate the resulting tune spread $\Delta\nu$ to accelerator and beam parameters by:

$$\Delta\nu = \frac{3 \pi N r_o R}{(\beta\gamma) \gamma \epsilon_N}$$

in which

N is the number of particles per unit length,
 r_o is the classical proton radius (1.535×10^{-18} m),
 R is the radius of the accelerator,
 β and γ are relativistic factors, and
 ϵ_N is a normalized emittance.

It is convenient to express this in terms of the total number of particles by using $n = 2 \pi R N$ and to replace ϵ_N by:

$$\epsilon_N = (\gamma\beta) A^2 \pi / \beta_L$$

where A is the betatron amplitude and the amplitude lattice function is β_L . Then:

$$\Delta\nu = \frac{3 n r_o \beta_L}{2 (\beta\gamma)^2 \gamma A^2 \pi}$$

At Mid-L in the Loma Linda Medical Accelerator the vertical $\beta_L = 1.88$ meters. If the good field region is taken to be 5 cm, $A = 0.025$ m. For an injection kinetic energy of 2 MeV, one obtains the relativistic factors as:

$$\gamma = E/m = (2 \text{ MeV} + 938 \text{ MeV}) / 938 \text{ MeV} = 1.0021$$

and

$$(\gamma\beta)^2 = \gamma^2 - 1 = 0.00427.$$

A given upper limit on the tune spread ($\Delta\nu$) gives an upper limit on the total number of particles (n). For example,

with $\Delta\nu = 0.150$ one obtains $n = 29 \times 10^{10}$.

Another example using lower (and perhaps more relevant) intensity is:

for 2×10^{10} the space charge tune spread is $\Delta\nu = 0.010$.

Should the tune spreads from space charge be expected to impose real limits on the operation? In addressing this question, the minimum considerations should include: the base machine tunes, additional expected sources of tune spread, and the relative importance of low order resonances.

The design tunes are $[\nu_h, \nu_v] = [0.60, 1.30]$ which puts the horizontal on the 5th ($5\nu_h = 3$) order resonance. However, the base tune can be changed by powering the quadrupole circuit. For 2500 Amps in the main power supply, 50 Amps in the quadrupole circuit lowers the horizontal tune by 0.08 and raises the vertical tune by 0.05. At injection, this quadrupole circuit can, of course, cause larger changes in tune; however one may assume the range of operationally available tunes is determined by the higher energy. In this case, figure A shows the effect of using a bipolar quadrupole circuit. Resonances up to 5th order are shown along with the space charge tune spread appropriate for injecting 2 and 5×10^{10} . Relocating the base tunes to the point labeled P could avoid all resonances up to 5th order for the lower intensity if space charge were the only source of tune spread. However, the higher intensity of 5×10^{10} cannot avoid all the resonances up to 5th order with the single quadrupole circuit. In particular the $-2\nu_h + 3\nu_v = 5$ cannot be avoided.

Another source of tune spread is due to the combination of chromaticity and momentum spread. The relationship is:

$$\Delta\nu = \xi (\Delta p / p)$$

The calculated natural chromaticities are:

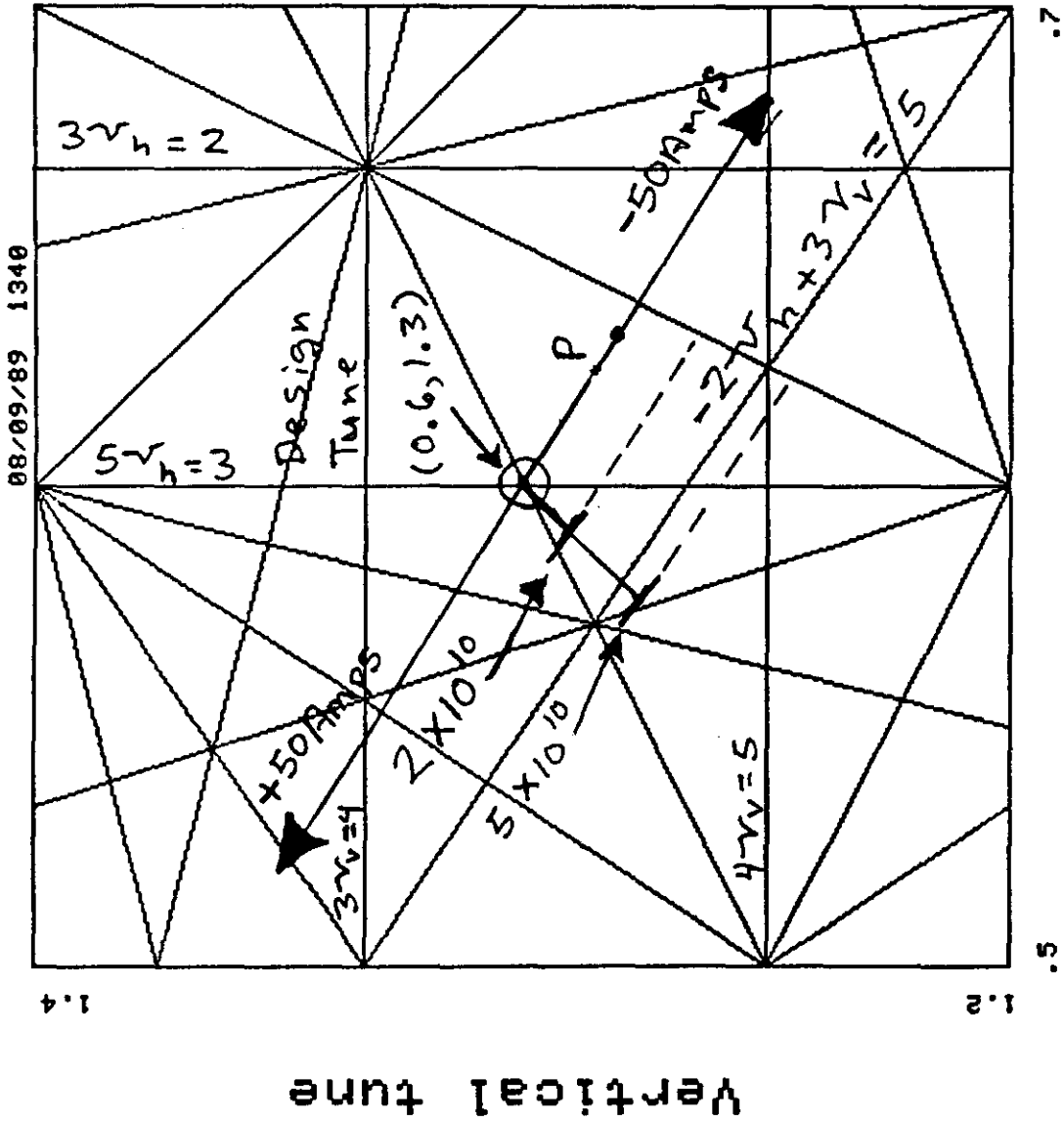
$$[\xi_h, \xi_v] = [0.61, 1.25].$$

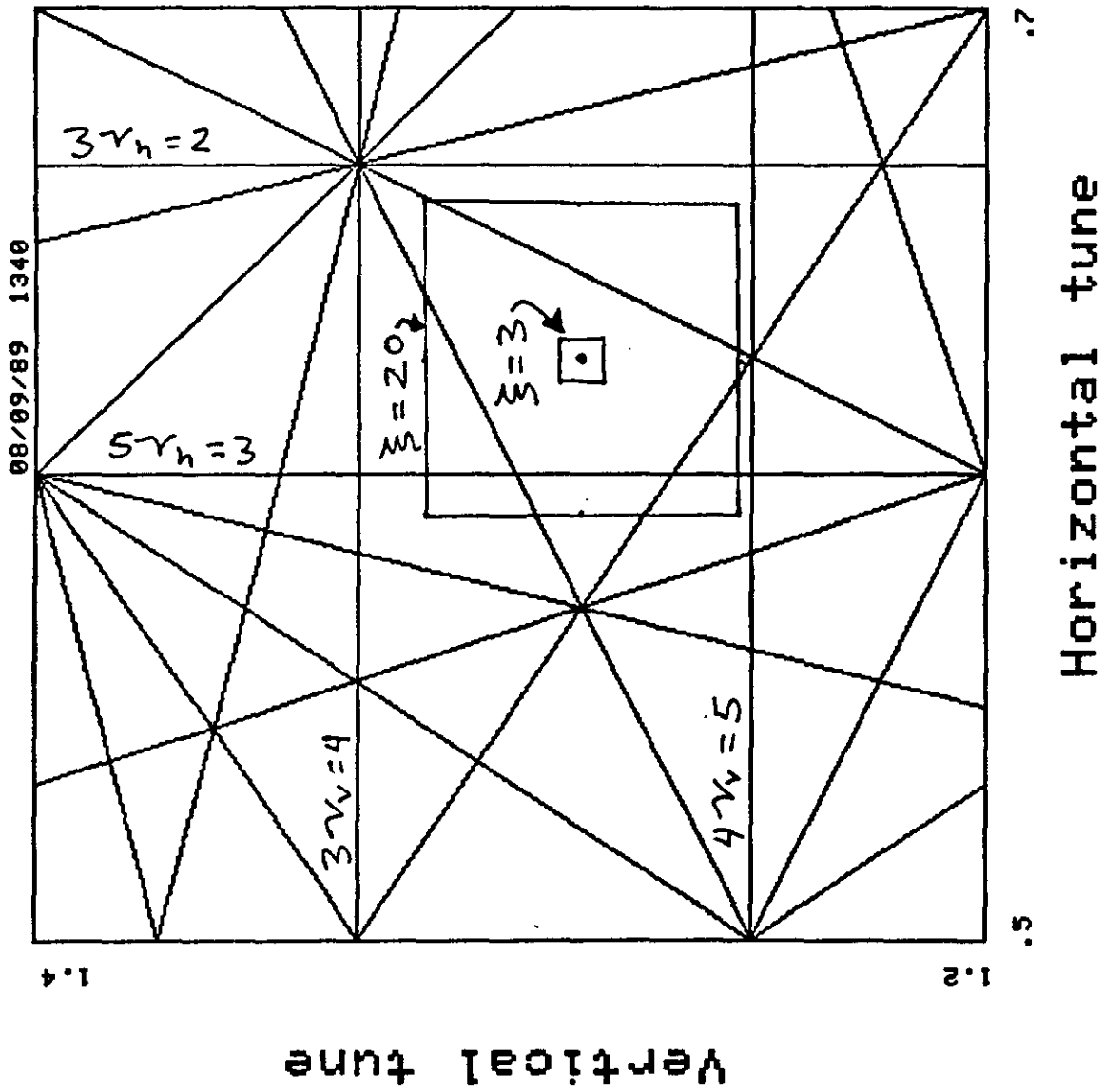
Combined with a full width at half maximum (FWHM) momentum spread of 3.3×10^{-3} , this gives a tune spread of:

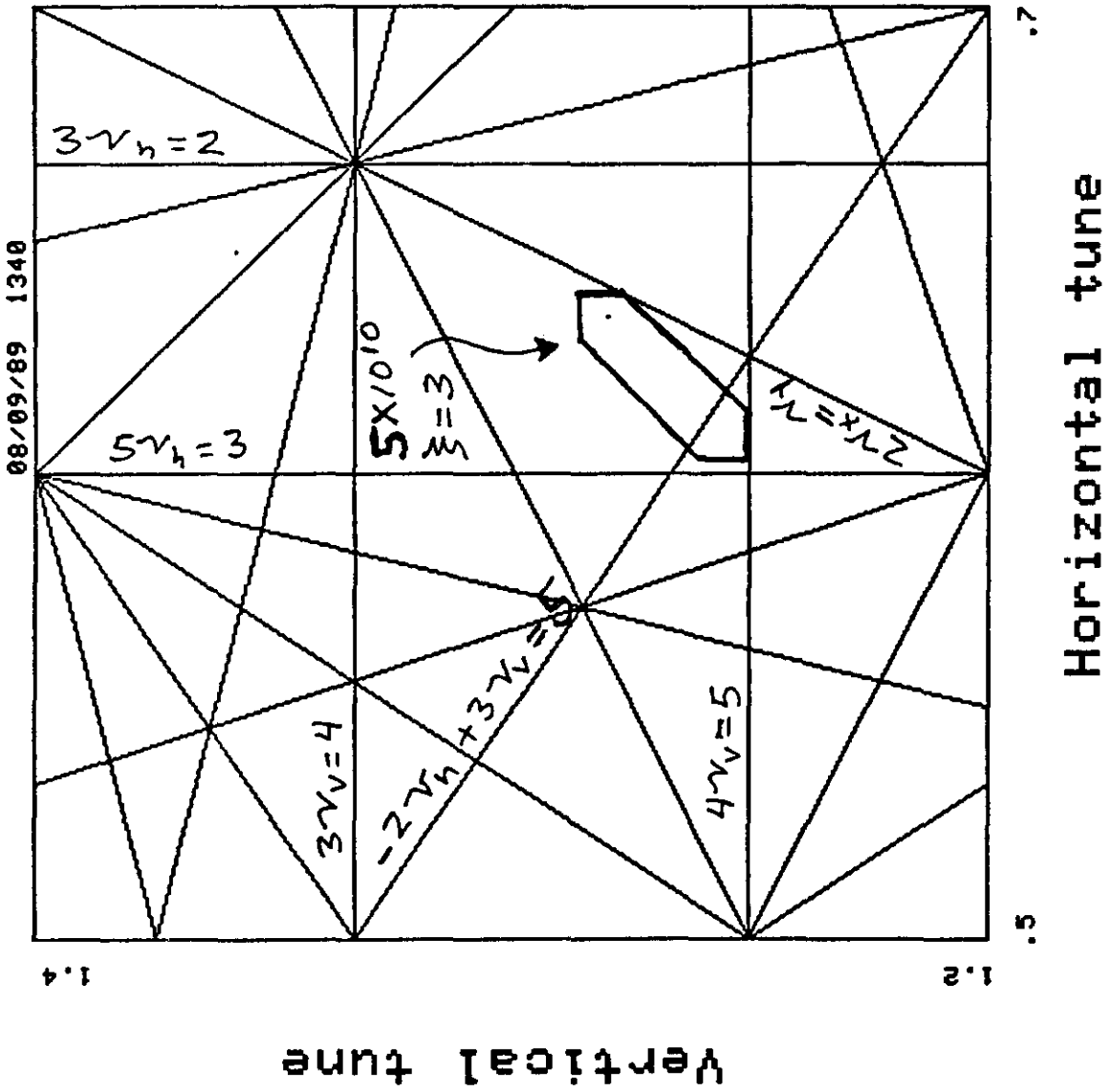
$$[\Delta\nu_h, \Delta\nu_v] = [0.002, 0.004] \text{ FWHM.}$$

However, if the chromaticity were a few times larger, this contribution to tune spread would overwhelm that due to space charge. For example, a chromaticity of 3 would give a FWHM $\Delta\nu$ of 0.010, which corresponds to the space charge tune spread for an intensity of 2×10^{10} . If the chromaticity were as large as 20, then the FWHM tune spread would approach 0.07; such a value of chromaticity causes the space charge tune spread to become negligible by comparison. These two cases are shown in figure B. The larger chromaticity clearly cannot avoid putting beam on the low order resonances. Indeed avoiding the 3rd's ($3\nu_v = 4$ or $3\nu_h = 2$) and the 4th ($4\nu_v = 5$) will require some care.

Figure C shows the result of combining the tune spreads from a chromaticity of 3 with an intensity of 5×10^{10} , and using a single bipolar quadrupole circuit to adjust the base tunes. If one again ignores the $-2\nu_h + 3\nu_v = 5$ resonance, these accelerator and beam parameters provide a tune spread which is bounded by 5th ($5\nu_h = 3$), 4th ($4\nu_v = 5$) and 3rd ($2\nu_h = \nu_v$) order resonances.







B.3 LOMA LINDA COHERENT INSTABILITY SURVEY

A. BOGACZ

Longitudinal Stability

The microwave instability, which provides the lowest threshold, will dominate the low energy region corresponding to the injection at 70 MeV ($\gamma = 1.004$). Although the transverse beam size is quite large (95% beam radius of 2×10^{-2} m) the lowest energy is dominated by the space charge effects (capacitive longitudinal coupling impedance $|Z/n|_{s-c} = 4 \times 10^3$ Ohm). Going to higher energies the broad-band impedance induced by the bellows $|Z/n|_{b-b} = 7 \times 10^2$ Ohm (TBCI simulation) will become comparable to the space charge contribution. Assuming beam intensity of 5×10^{10} ppb a new estimate of $|Z/n|$ including the broad-band part will reset Dp/p constraint at 3×10^{-3} , while the allowed value of Dp/p with the space charge forces only is 2×10^{-3} . Some reduction of the longitudinal impedance e.g. a compensation by an induction part generated by a helical transmission line may be considered.

Transverse Stability

The resistive wall instability driven by the wake fields due to the Lambertson magnet lamination and resistive vacuum chamber walls dominates the coherent betatron motion in the low frequency region. Assuming the beam intensity of 5×10^{10} ppb the characteristic growth-time of the instability is $t = 5 \times 10^{-2}$ sec. For lower energies the incoherent space-charge force produces enough betatron tune spread (Laslett effect) to suppress the instability through Landau damping. Above the cross over energy of 180 MeV some decohering mechanism is required e.g. an amplitude dependent betatron tune induced by small octupole field component.

The slow head-tail instability driven by the wake fields induced by the kicker magnets dominates the coherent betatron motion in the high frequency region. The transverse impedance calculation (MAFIA simulation) allows a simple estimate of the characteristic instability growth-time for various modes as a function of chromaticity (Sacherer's model). For the beam intensity of 5×10^{10} ppb and the chromaticity of $\xi = 15$ the offending $l=1$ mode is characterized by the growth-time of $t = 5 \times 10^{-3}$ sec. Finally, one should study whether some additional octupole field component would provide enough betatron tune spread to suppress the instability through Landau damping (using more realistic "air bag" model).

B.4 TRANSVERSE DYNAMICS DURING ACCELERATION

S.Y. HSUEH

The goal of controlling the transverse dynamics of the beam during acceleration is met when the beam can be accelerated without significant loss of particles and when the final transverse emittance of the beam is satisfactory.

Transverse problems may well be feared. The operating point of the machine ($Q_x=0.600$, $Q_y=1.317$) is half way between the $Q_y=4/3$ resonance and the $2Q_y-Q_x=2$ resonance. This leaves 0.016 on either side in Q_y space. Horizontally there is 0.032 to the $2Q_y-Q_x=2$ line. If the half-width at the base of the beam momentum is 0.2%, then we can expect to be able to tolerate a horizontal chromaticity of 16 and a vertical chromaticity of 8. The natural chromaticities are 0.61 and 1.25.

The shape of the magnetic field in the eight dipoles is not flat and it varies dramatically with excitation current. Figure 10-1 shows the field shape after removing the quadrupole component in one magnet (LDL002) for 10 currents from injection through extraction along with the fit of the next three orders of polynomial. Figure 10-3 shows the change in sextupole, octupole, and decapole component of the magnet as a function of current. Table 10-1 gives the chromaticity on the central orbit calculated from the fit of x^2 term for each measured current. Any deviation of the closed orbit from the central orbit would change the chromaticity. Table 10-2 gives the measured chromaticity on flat-tops of different currents. The agreement between magnetic and beam measurements is good.

The problem is largest at injection. Here, too, is the relevance of the measurements to the machine performance most questionable. The recent history of the magnet current is most important at low currents and is also poorly matched between the measurement cycle and the machine operating cycle. A reproducible ramp which falls below the injection current during the recovery phase is crucial. The existing sextupole magnet could be used to compensate for the undesired sextupole fields at injection. It would take a flexible curve generator to correct the sextupole all the way through acceleration. To fully tailor the field would require octupole and decapole magnets as well, each with an independently ramped power supply.

As the dipoles ramp the changing field induces longitudinal eddy currents in the vacuum pipe. The eddy currents in turn produce an additional normal sextupole field (Lee Teng 10/21/87, Fred Mills). We expect the chromaticity change due to this sextupole to be proportional to $(dI/dt)/I$. As dI/dt increases during the initial parabola, the

chromaticity rises then falls. During the steady ramp ($dI/dt = \text{constant}$) the chromaticity decreases further. If we write the current as $I=b+ct$, the chromaticity is proportional to $2ct/(b+ct)$. The peak chromaticity comes at $t=\sqrt{b/c}$ and is proportional to $\sqrt{c/b}$. dI/dt at that time is $2\sqrt{bc}$. With $b = 212$ Amp and a dI/dt of 2500 Amp/sec, the steady ramp is reached just at the peak if the d^2I/dt^2 in the parabola is 14700 Amp/sec/sec. A lesser d^2I/dt^2 or a greater ramp rate will extend the parabola beyond the chromaticity peak. Table 10-x gives the calculated peak chromaticity change and the time after the start of the parabola for which it occurs for various values of d^2I/dt^2 .

On-the-fly measurement of chromaticity is hard, but we (S. Hseuh) have measured the tune at the same time in the ramp for two different radial offset feedback settings. This gives the tune at two momenta and thus the chromaticity. The results are listed in Table 10-y.

Table 10-a
Measured chromaticity on flat-tops of different currents

Current	Q-x	Q-y	eta	xi-x	xi-y	
212 Amp			-24+-2	10+-2		
500 Amp			-18	9.0		
1000		.603	1.317	2.02	-12.7	8.6
1500		.594	1.320	2.11	-14.1	7.1
2000		.603	1.317	2.199	-12.1	10.8
2500		.602	1.317	2.32	-22.2	14.6

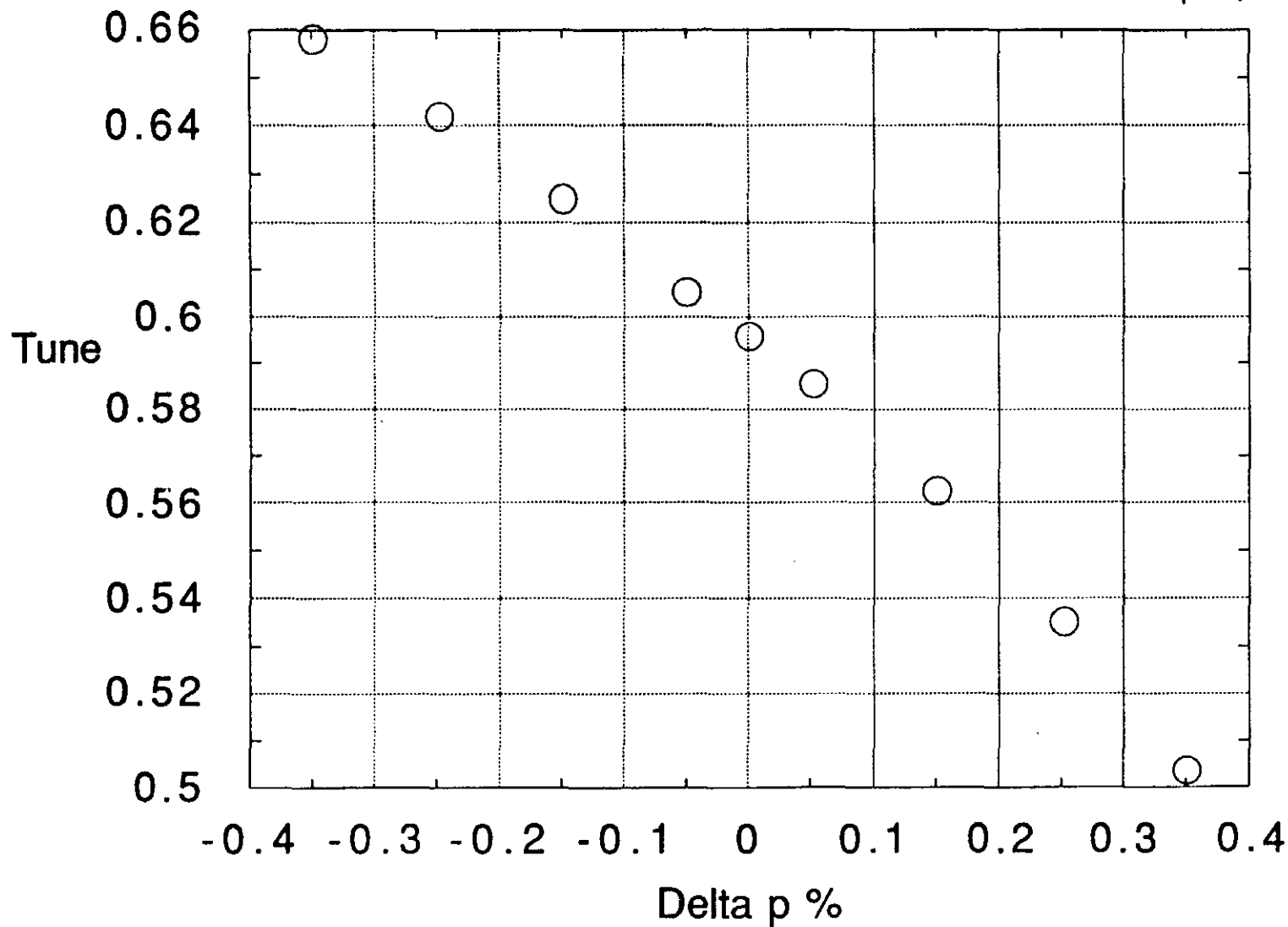
Table 10-x
Calculated maximum chromaticity change due to beam pipe eddy currents and the time relative to start of parabola of the peak. The initial current is 212 Amp.

d^2I/dt^2		chromaticity	peak time
8000	17.64	units 0.225	sec
10000	19.72	Units 0.207	sec
12000	21.61	Units 0.186	sec
14000	23.34	Units 0.174	sec

Amp/sec/sec

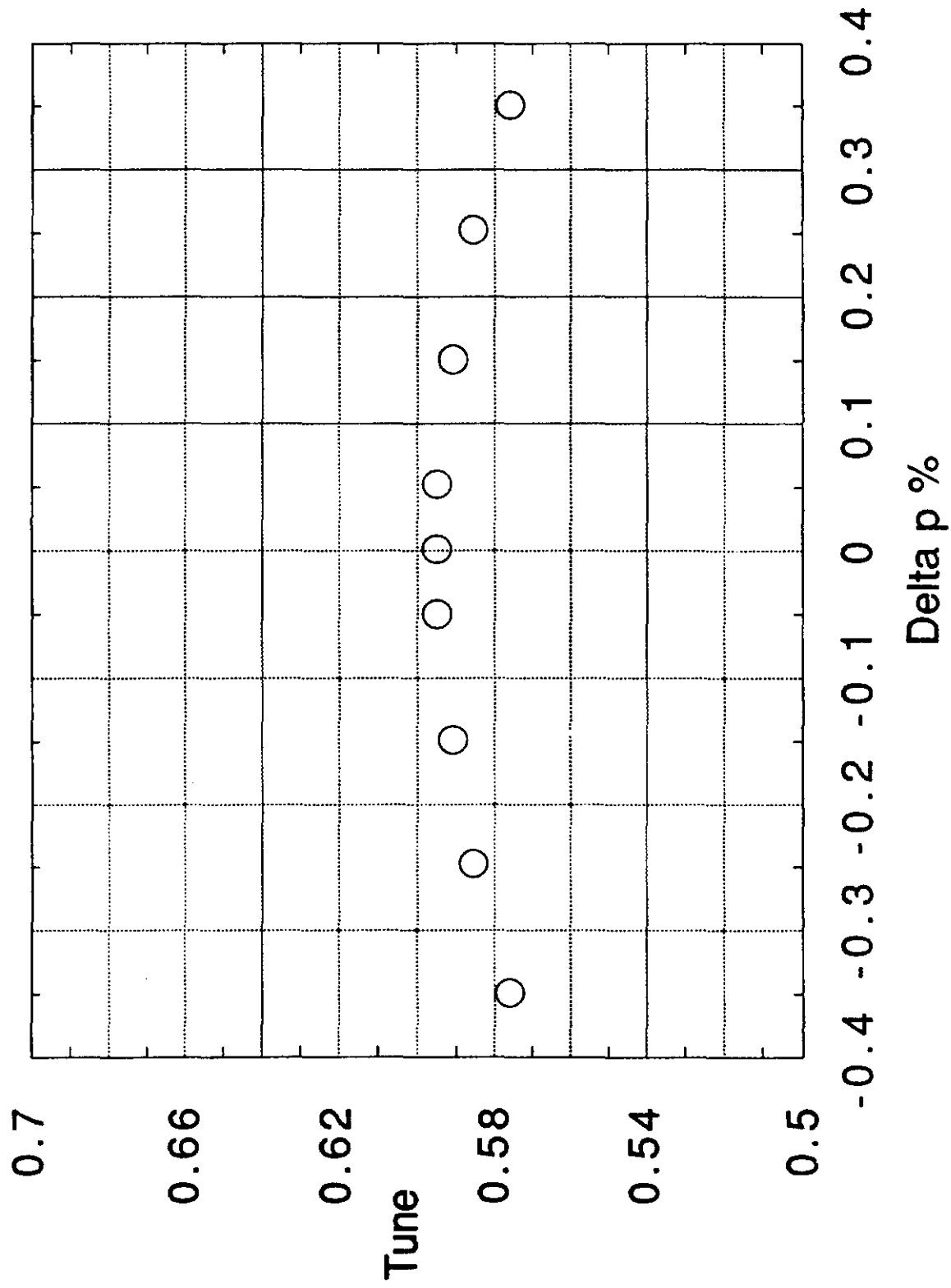
Tune v's Momentum
Sextupole harmonics only

*fr. M. Harrison
by product of Y. Chao's ext.
tracking prog.
from Mag. Meas. evaluated 250 MeV
14 July 89*

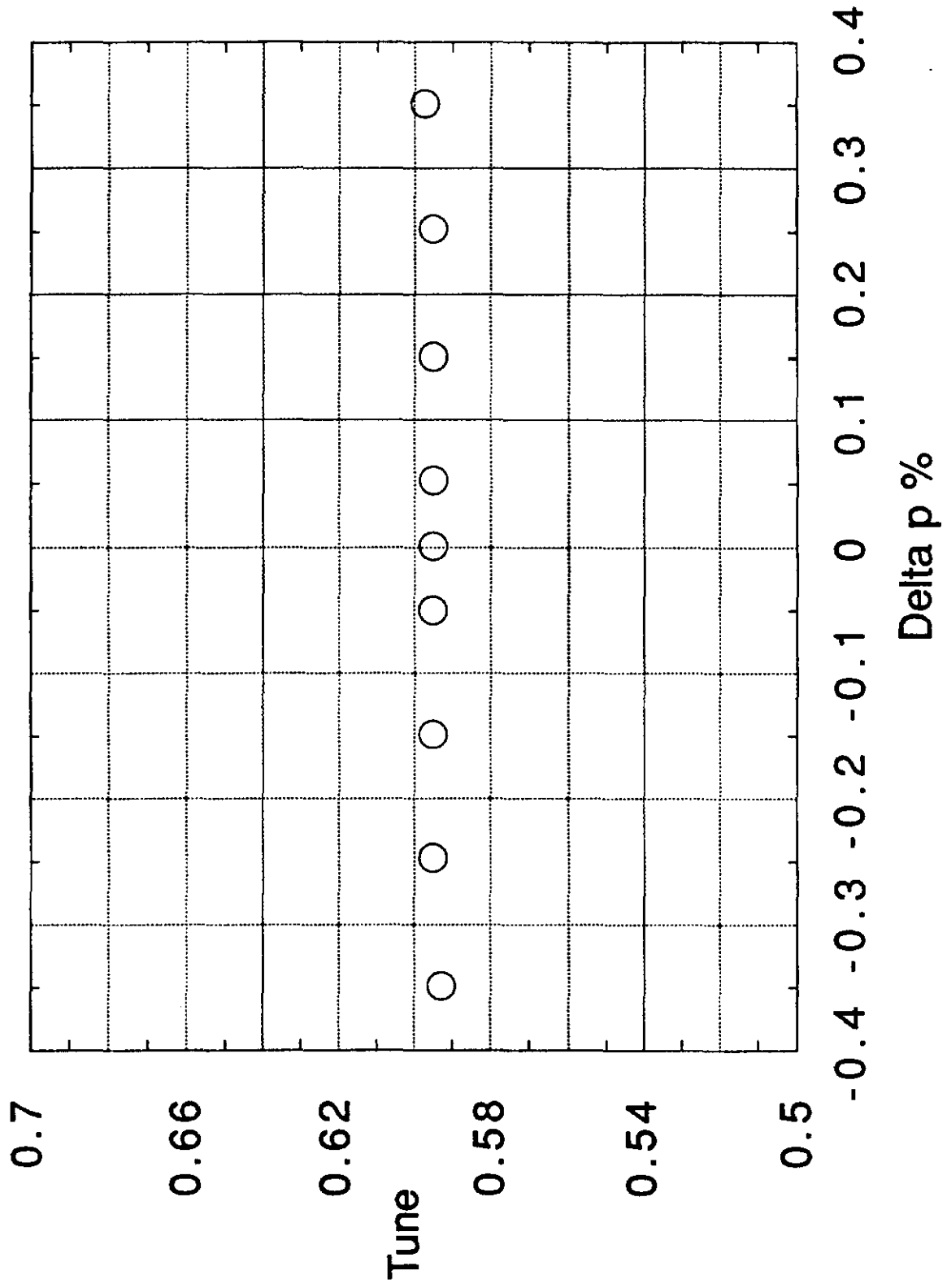


Tune v's Momentum

Octopole harmonics only



Tune v's Momentum
Decapole harmonics only



B.5 BEAM LIFETIME DUE TO GAS SCATTERING

V. VISNJIC

It is assumed that the gas scattering consists mostly of multiple Coulomb scattering. The contribution of the nuclear collisions in the energy range of interest is presumed to be less than the uncertainties in estimating the Coulomb scattering which are mostly due to uncertainties in the gas composition.

The basic formula in computing the beam lifetime due to multi Coulomb scattering are:

$$\text{Lifetime} = \frac{W_a}{D} \tau \quad (1)$$

$$W_a = \frac{a^2}{\beta} \sim \frac{(4.5\text{cm})^2}{2m} = 1.01 \times 10^{-3} m \quad (2)$$

$$\text{and} \quad D = \beta \frac{d\langle\theta^2\rangle}{dt} \quad (3)$$

In the above formula θ is the scattering angle which depends on the beam energy and the radiation length as follows:

$$\frac{d\langle\theta^2\rangle}{dt} = \frac{168.75 \times 10^8}{T[\text{MeV}]^2} \frac{\beta_{\text{Lorentz}}}{L_{\text{rad}}[\text{m}]} \quad (4)$$

I have computed the radiation lengths for H₂, H₂O, OH, CO, and N₂ molecules to be the following:

Molecule	L _{rad}
H ₂	$\frac{5.8 \times 10^8}{P[\text{torr}]} \text{ cm}$
H ₂ O	$\frac{3.8 \times 10^{-7}}{P[\text{torr}]} \text{ cm}$
HO	$\frac{3.9 \times 10^7}{P[\text{torr}]} \text{ cm}$
CO	$\frac{2.7 \times 10^7}{P[\text{torr}]} \text{ cm}$
N ₂	$\frac{2.6 \times 10^6}{P[\text{torr}]} \text{ cm}$

The measurements give the total pressure (in the better part of the pipe) of 3×10^{-8} torr which, together with the scanning results, gives the partial pressures of 69.4%, 18.4%, 6.1% and 6.1% for H_2 , H_2O , HO and CO/N_2 , respectively.

Putting all this together, we get the following result for $d\langle\theta^2\rangle/dt$

$$\frac{d\langle\theta^2\rangle}{dt} = 4.6 \times 10^{-4} \frac{\beta_{\text{Lorentz}}}{T[\text{MeV}]^2} \quad (5)$$

and finally,

$$\text{Lifetime} = 1.1 \frac{T[\text{MeV}]^2}{\beta_{\text{Lorentz}}} \tau \text{ msec.} \quad (6)$$

τ is actually a time dependent quantity representing the time variation of the lifetime. Asymptotically $\tau \sim 0.7$ and we get the following estimates of lifetimes:

$$1^* T = 2 \text{ MeV}, \beta = 0.06 \\ \text{Lifetime} \sim 51.1 \text{ msec}$$

$$2^* T = 250 \text{ MeV}, \beta = 0.61 \\ \text{Lifetime} \sim 80 \text{ sec}$$

C.1 RF CAPTURE

F.E. MILLS

The accelerator is furnished with a broadband amplifier and cavity furnishing up to 300 V for acceleration over the frequency range 0.9-9 MHz. At this two MEV injection energy this provides a phase oscillation frequency (per turn) of $\nu_s = 5.5 \times 10^{-3}$, or a frequency of about 4.5 kHz. The low value $\gamma_t = 0.6$ causes y to vary slowly with energy and γ/E and hence ν_s , to be approximately constant during acceleration. The matching parameter for small oscillation $Y = \Delta P/P/\Delta\phi = \nu_s/h\gamma$ is about 2.2×10^{-3} at injection. The stationary bucket height and area are $16Y$ and $*2Y$, p so the RF system makes a bucket of momentum width $*4.4 \times 10^{-3}$. this corresponds closely with the clear radial space $*40$ mm, which with the dispersion of $9m$ gives $\Delta P/P = *4.4 \times 10^{-3}$. Then the RF system should be able to capture a beam of $16Y/2T \approx .6\%$ total width. Upon subsequent acceleration the stable phase shifts by -15° so the bucket area will be reduced by about 25%, with attendant beam loss. The phase oscillation frequency is sufficiently high that capture and other processes are adiabatic on millisecond time scales, much shorter than beam lifetime.

Injection on a ramped magnetic field should provide similar capture capability, and provide the benefits of reduced losses to scattering, and chromaticity compensation by eddy currents induced in the vacuum chamber.

C.2 Acceleration: Longitudinal Dynamics, RF Requirements,
Performance, and Noise in Feedback Loops.

James L. Crisp

The basic function of the RF system is to accelerate the beam from the 2 MeV energy at the output of the RF Quad to the extraction energy, between 70 and 250 MeV, within 1/2 second. In addition, the RF system has the responsibility of controlling the energy of the beam to match the synchronous value determined by the field of the main bending magnets. This will keep the beam centered in the aperture.

The 20.053 meter circumference and unity harmonic number results in a synchronous frequency which increases from .974 to 9.174 Mhz. For a linear ramp in momentum, the energy gain per turn can be calculated as shown below.

$$\frac{\Delta E}{\text{turn}} = \frac{1}{f_{\text{rot}}} \frac{dE}{dt} = \frac{\text{circ}}{\beta c} \beta \frac{dP}{dt} = \frac{20.053}{c} \frac{(729.14e6 - 61.295e6)}{.5}$$

$$\approx 90 \text{ eV/turn}$$

The RF cavity, or more appropriately the accelerating gap, uses ferrite rings in parallel with a 50 ohm load to provide a broadband 50 ohm impedance to the power amplifier. The 1 kilowatt power amplifier can produce about 320 volts and 6 amps at the accelerating gap. Because the average beam current ranges from 1.6 to 14.7 milliamps per 1010 protons, beam loading will be small. The synchronous phase will be about 16.3°.

The equations that provide the bucket area and half height are provided here. The moving bucket factors, $\alpha(\phi_s)$ and $\beta(\phi_s)$, can be found in appendix D of reference 1.

$$\text{Area} = \alpha(\phi_s) \frac{16R}{h^2 c} \sqrt{\frac{hVE}{2\pi|\eta|}} \quad [\text{eV-sec}]$$

$$\Delta P = \beta(\phi_s) \frac{2}{h} \sqrt{\frac{hVE}{2\pi|\eta|}} \quad [\text{eV/c}] \quad (1/2 \text{ height})$$

$$\alpha(16.3^\circ) = .5389, \text{ moving bucket factor}$$

$$\beta(16.3^\circ) = .7738, \text{ moving bucket factor}$$

$$\eta = \left(\frac{1}{\gamma_t^2} - \frac{1}{\gamma^2} \right) \quad (\gamma = E/E_0)$$

$$\gamma_t = .5832, \text{ gamma at transition}$$

$$c = 2.998 \times 10^8 \text{ m/s, speed of light}$$

$$h = 1, \text{ harmonic number}$$

$$R = 20.053/2\pi, \text{ machine radius}$$

$$V = 320 \text{ volts, peak RF voltage}$$

$$E = \text{total energy}$$

With the accelerating rate of 90 eV/sec and peak voltage of 320 volts, the bucket area becomes .014 eV-sec and the bucket half height becomes .23 MeV/c. For a constant bucket area, the required voltage goes as the square of $\alpha(\phi_s)$. With $\alpha(0^\circ) = 1$, the voltage required for a bucket area of .014 eV-sec at injection or extraction becomes $320(.5389)^2 = 93$ volts.

The momentum spread of the beam can be converted to a physical width by scaling it with a_p , the dispersion. The dispersion can be found with the approximation $a_p \approx R/\gamma t^2 = 9.38$ meters. The beam width caused by it's momentum spread is greatest near injection, where the momentum is 61.3 MeV/c, and is calculated below for a full bucket.

$$\Delta R = a_p \frac{\Delta P}{P} = 9.38 \frac{.23}{61.3} = \pm 35 \text{ millimeters}$$

Thus the 1 kilowatt power amplifier provides a bucket with a momentum spread, or beam size, that reasonably matches the ± 50 mm good field aperture of the accelerator.

At Fermilab, the bending magnet power supply limited the rise time of the bending field to about 1 second. The RF voltage used was 208 volts which provided a bucket area of about .013 ev-sec during acceleration. The bunch areas and heights were calculated from their length according to figures 6 and 7 of reference 2. Table 1 lists the results. The areas represent 90 to 100% of the beam. The length was obtained from an oscilloscope photograph thus the percentage of beam is only a visual estimate. Between 0 and 1 second the beam was accelerated from 2 MeV to 230 MeV. Extraction began at 2 seconds and ended at 3 seconds.

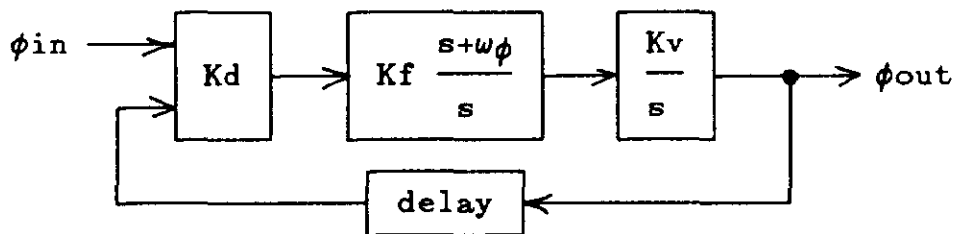
Table 1

time sec	P MeV/c	sync phs deg	rf volt	bkt area eV-s	bkt ht $\Delta p/p$	bkt % nsec	bnch lng nsec	bnch area eV-s	bnch ht %
.025	64	14.4	47	.0061	.1504	683.8	512.0	.0045	.133
.1	96	27.8	99	.0054	.1118	358.0	309.0	.0048	.107
.2	166	14.1	191	.0125	.1179	268.2	152.0	.0059	.086
.3	235	13.3	202	.0132	.0867	194.3	109.0	.0061	.062
.4	304	13.3	202	.0133	.0670	153.0	84.5	.0060	.048
.5	374	13.3	202	.0133	.0546	127.5	67.9	.0056	.038
.6	443	12.9	208	.0137	.0472	111.2	65.1	.0068	.035
.7	512	12.9	208	.0137	.0410	99.1	66.2	.0085	.034
.8	582	12.5	214	.0142	.0370	90.8	64.5	.0097	.032
.9	651	12.2	219	.0146	.0338	84.4	62.9	.0107	.030
1.0	695	1.7	221	.0212	.0376	101.5	58.1	.0110	.028
1.25	695	0	221	.0228	.0385	112.4	66.3	.0128	.029
1.5	695	0	221	.0228	.0385	112.4	69.6	.0139	.030
1.75	695	0	221	.0228	.0385	112.4	71.1	.0143	.031
2.0	695	0	221	.0228	.0385	112.4	62.5	.0117	.028
2.5	695	0	221	.0228	.0385	112.4	48.6	.0075	.022

A block diagram of the low level rf system is provided in figure 1. The system consists basically of two loops, the phase loop and the radial position loop. During injection, the phase loop locks the VCO to a reference oscillator until the beam is captured into the rf buckets. Once the beam bunches begin to form, the loop can be switched over to a beam derived signal. The radial position loop controls the phase of the rf cavity with respect to the beam. By shifting the phase, the beam can be either accelerated or decelerated with respect to the synchronous particle, thereby controlling the radial position.

Because frequency is the derivative of phase, both loops can be considered as controlling the frequency. The system could be constructed with only one loop but this requires the use of a differentiator circuit which suffers from noise at the higher frequencies. In addition to these, there is a third loop which servos the gap voltage to the voltage program.

Ignoring the path through the accelerator, the phase lock loop can be analyzed using the block diagram below. The delay block represents a cable delay used to compensate for the sum of the cable delays between the beam detector and ϕ_{in} and from ϕ_{out} to the accelerating gap. This will make the phase difference from beam detector to cavity gap independent of frequency. The delay required at Fermilab was about 450 nsec. Closed loop stability requires the phase shift of the open loop to be less than 180° for gains larger than unity. The $1/s$ term, which represents the integration that converts the frequency output of the VCO to phase, contributes 90° to this. At 278 KHz the 450 nsec delay will contribute another 45° , leaving a 45° phase margin for the loop. The closed loop bandwidth then is limited to be less than 278 KHz. Currently the bandwidth of the phase loop is only about 10 KHz. A larger bandwidth in this loop would reduce the effect of frequency program errors as well as noise on the system. It would not, however, affect the transient response of the beam.



The characteristic equation describing the phase loop is shown below. For the Loma Linda system the measured constants result in $2\pi\omega_n = 8.9$ KHz and $\zeta = .46$. The measured step response is compared to the calculated response in figure 2.

$$\frac{\phi_{out}}{\phi_{in}} = \frac{f_{out}}{f_{in}} = \frac{K_d K_f K_v s + K_d K_f K_v \omega_\phi}{s^2 + K_d K_f K_v s + K_d K_f K_v \omega_\phi} = \frac{2\zeta\omega_n s + \omega_n^2}{s^2 + 2\zeta\omega_n s + \omega_n^2}$$

K_d = phase detector gain, volts/rad

$K_f \frac{s+\omega\phi}{s}$ = compensation filter

K_v = VCO gain, rad/sec-volt

In order to understand the radial loop, the equations for synchrotron motion need to be introduced. They are greatly simplified by assuming the RF voltage is a linear function of phase. Using ϕ , R , and Ω to represent the differences between the beam phase, radius, and frequency and their synchronous values, the equations are presented below.

$$\frac{d}{dt} \phi = aR + \Omega \quad a = \frac{\omega\eta}{\beta^2\alpha_p}$$

$$\frac{d}{dt} R = b\phi \quad b = eVf_0 \cos\phi_s \frac{\alpha_p}{E}$$

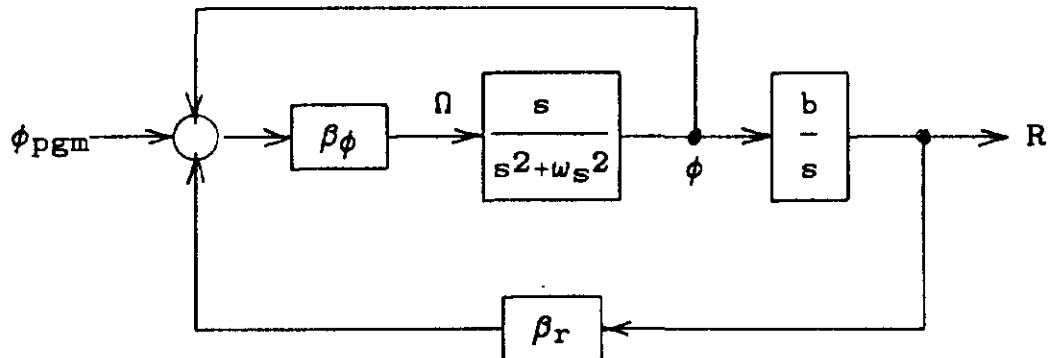
Stability requires that a and b have opposite sign. The value of a ranges from $3.0e8$ at 2 MeV to $3.9e7$ at 230 MeV and b ranges from .46 to 16. Laplace transforms can be applied to the above system of equations to obtain their solution as well as their impulse response as shown below.

$$\frac{\phi(s)}{\Omega(s)} = \frac{s}{s^2 + \omega_s^2} \quad (\Omega(s) = 1) \quad \phi(t) = \cos\omega_s t$$

$$\frac{R(s)}{\Omega(s)} = \frac{b}{s^2 + \omega_s^2} \quad R(t) = \frac{b}{\omega_s} \sin\omega_s t$$

Thus we see the radial response of the system to an impulse in frequency is an undamped sine wave whose frequency of oscillation, or synchrotron frequency, is $\omega_s = \sqrt{aB}$. It is interesting to note that the radius is just the integral of the phase scaled with b .

The phase error, ϕ , is equivalent to the phase difference at the input to the phase detector of the low level system. Employing this approximation a simple block diagram can be assembled as shown below.



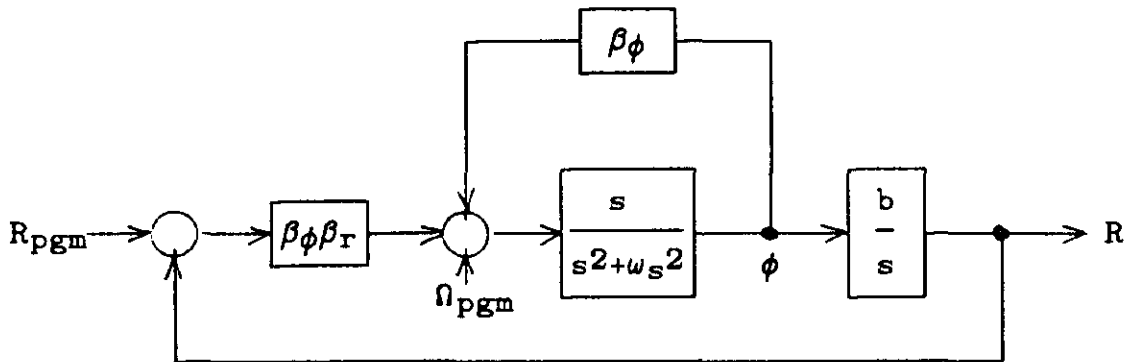
$$\beta_{\phi} = K_d K_f K_v$$

K_d = phase detector gain, volt/rad
 K_f = phase loop filter
 K_v = vco gain, rad/sec-volt

$$\beta_r = G_d G_f G_{\phi}$$

G_d = radial position gain, volt/meter
 G_f = radial loop filter
 G_{ϕ} = phase shifter gain, rad/volt

Manipulating the blocks, a more appropriate diagram can be formed as shown below along with the associated characteristic equation.



$$\frac{R(s)}{R_{pgm}(s)} = \frac{\beta_{\phi} \beta_r b}{s^2 + \beta_{\phi} s + \omega_s^2 + \beta_{\phi} \beta_r b}$$

$$\text{for } \beta_{\phi} = k_{\phi} \frac{s + \omega_{\phi}}{s} \quad \text{and} \quad \beta_r = k_r \frac{s + \omega_r}{s}$$

$$\frac{R(s)}{R_{pgm}(s)} = \frac{k_{\phi} k_r b s^2 + k_{\phi} k_r b (\omega_{\phi} + \omega_r) s + k_{\phi} k_r b \omega_{\phi} \omega_r}{s^4 + k_{\phi} s^3 + (k_{\phi} k_r b + k_{\phi} \omega_{\phi} + \omega_s^2) s^2 + k_{\phi} k_r b (\omega_{\phi} + \omega_r) s + k_{\phi} k_r b \omega_{\phi} \omega_r}$$

A comparison of the measured and calculated step response at 230 MeV is shown in figure 3. The measured quantities are; $b = 15.7$, $\omega_s = 2\pi 3.9$ KHz, $k_{\phi} = 5.1e4$, $\omega_{\phi} = 2\pi 9.7$ KHz, $k_r = 181$, and $\omega_r = 2\pi 1.6$ KHz.

The bandwidth of the radial loop is limited by the available rf voltage not by stability. With the variables used above, the maximum radial position rate of change is about 3.5 mm/msec for a 1 mm step input. This would result in a 12° synchronous phase shift. Since the required phase shift is proportional to the rate of change of position, a 120° phase shift would be required if the radial loop were 10 times faster. Although the feedback system would remain stable, the beam would be lost for lack of accelerating voltage.

In the previous discussion it was adequate to consider the bunch as a single particle. A more accurate model allows it to consist of a large number of particles all undergoing synchrotron

oscillations independently but contained within a longitudinal phase space area. Because the accelerating voltage has a sinusoidal dependance on phase, the oscillation or synchrotron frequency will decrease with amplitude. If the bunch is not matched to the bucket, this effect will cause the bunch to filament and eventually occupy a larger area.

Mismatch can be caused by such things as changes in the accelerating voltage or errors in the low level system. The amount of growth caused by a mismatch will depend on both its amplitude and duration. Noise in the RF system can cause beam dilution to occur.

References:

- 1) C. Bovet, R. Gouiran, I. Gumowski, K.H. Reich, "A Selection of Formulae and Data Useful for the Design of A.G. Synchrotrons", CERN/MPS-SI/Int. DL/70/4, April 1970.
- 2) S. Ohnuma, "The Beam and the Bucket", Fermilab TM-1381, TM-1381A, January 1986.
- 3) H.G. Hereward, "Open and Closed-Loop Properties of an R.F. Accelerated Beam", PS/4497.
- 4) F.E. Mills, "RF Feedback Loops for the LLMA", Fermilab LL-300, July 1988.
- 5) S. Hansen, A. Hofmann, E. Peschardt, F. Sacherer, W. Schnell, "Longitudinal Bunch Dilution due to RF Noise", IEEE Trans. Nuc. Sci., Vol. NS-24 No. 3, June 1977.

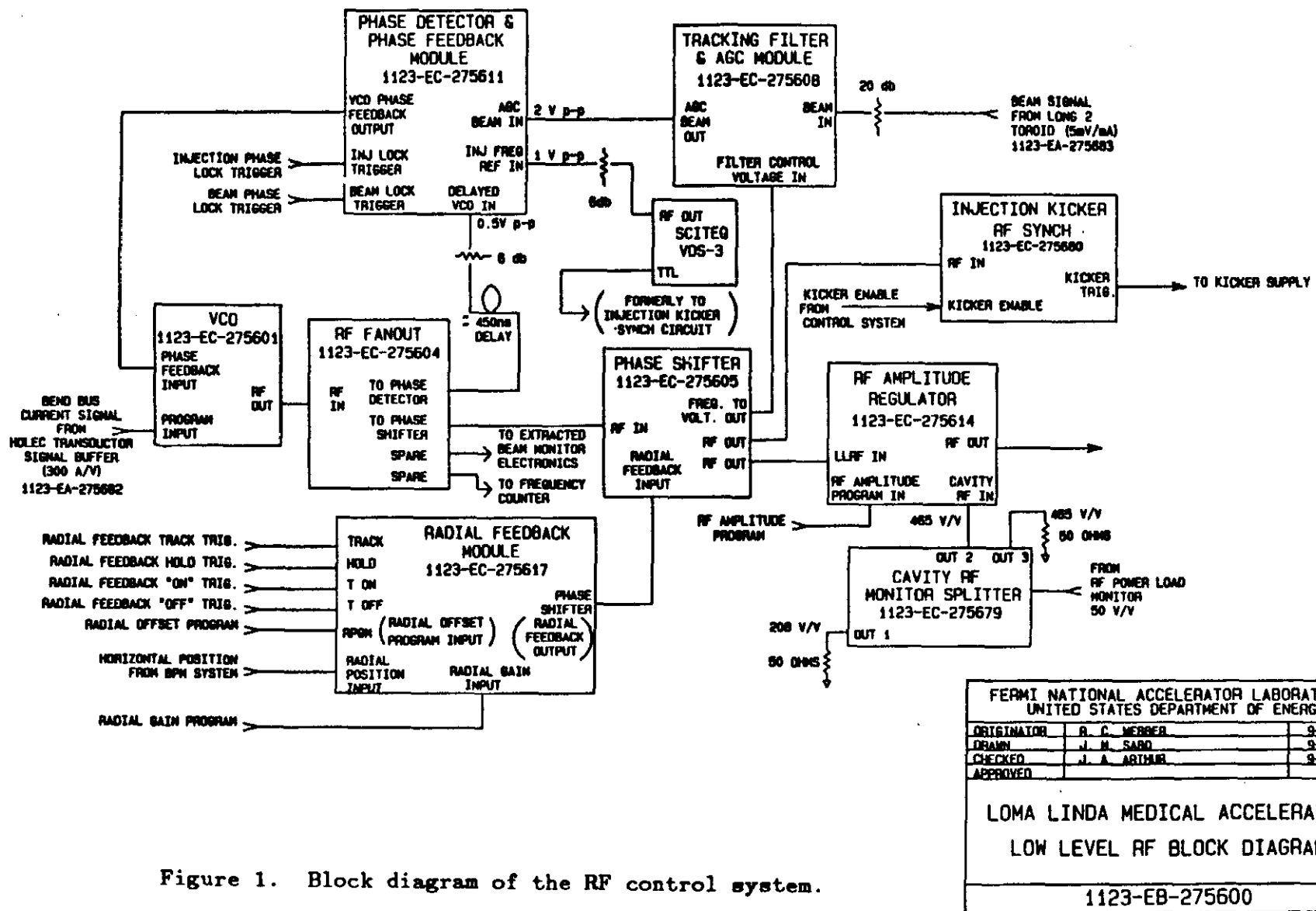


Figure 1. Block diagram of the RF control system.

FERMI NATIONAL ACCELERATOR LABORATORY UNITED STATES DEPARTMENT OF ENERGY		
ORIGINATOR	R. C. MERRER	9-13-89
DRAWN	J. M. SARD	9-13-89
CHECKED	J. A. ARTHUR	9-13-89
APPROVED		
LOMA LINDA MEDICAL ACCELERATOR LOW LEVEL RF BLOCK DIAGRAM		
1123-EB-275600		

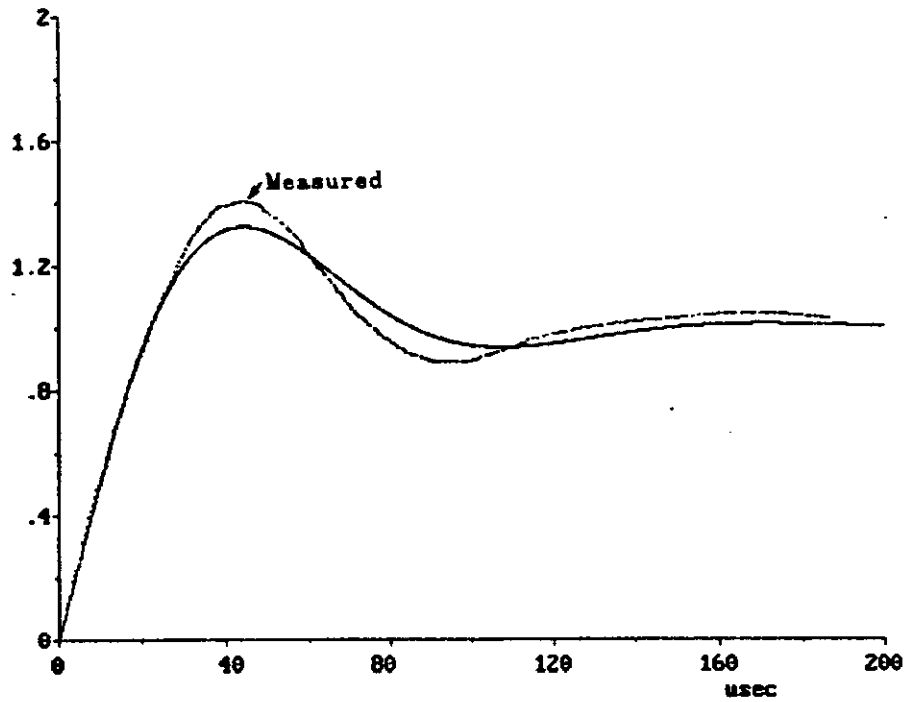


Figure 2. Measured and calculated step response of the RF control system phase loop.

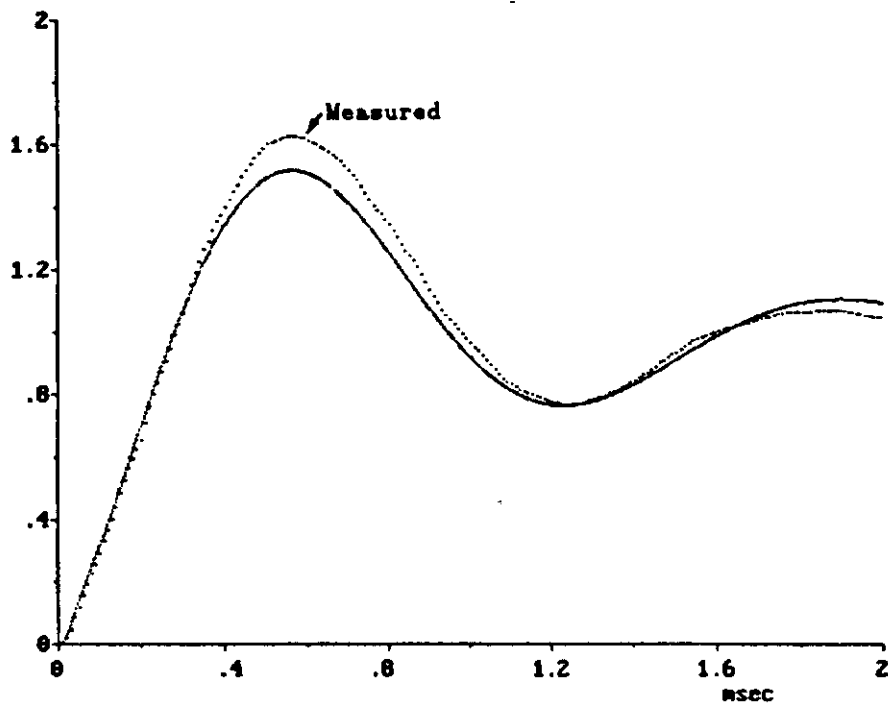


Figure 3. Measured and calculated step response of the RF control system radial position loop.

I. Principle

The beam is extracted by horizontal half-integer resonant extraction. The unperturbed motion is described by

$$\frac{x}{\sqrt{\beta}} = r \cos(\phi + \frac{1}{2}\theta) \quad (\text{E-1})$$

$$\frac{\alpha x + \beta x'}{\sqrt{\beta}} = -r \sin(\phi + \frac{1}{2}\theta),$$

where $\theta = \int \frac{ds}{v\beta}$, and $\theta = 0$ at the electric septum.

In terms of r and ϕ ,

$$\begin{aligned} \frac{dr}{d\theta} &= 0 \\ \frac{d\phi}{d\theta} &= \nu - \frac{1}{2}. \end{aligned} \quad (\text{E-2})$$

There are four quads symmetrically placed around the ring. See figure E.1. They are used to depress the horizontal tune from 0.6 toward 0.5. A octupole is used to create a stable region in the phase space. Define

$$\begin{aligned} \bar{Q} &= \frac{1}{2\pi} \int \frac{1}{4} \beta \frac{B'}{B\rho} ds = \frac{1}{2} \Delta\nu \text{ where } \Delta\nu \text{ is the tune change, } \bar{Q} < 0. \\ \bar{E} &= \frac{1}{2\pi} \int \frac{1}{96} \beta^2 \frac{B'''}{B\rho} ds. \end{aligned}$$

The equation of motion becomes

$$\begin{aligned} \frac{d\phi}{d\theta} &= (\nu - \frac{1}{2}) + 2\bar{Q} + 6r^2\bar{E} \\ \frac{dr}{d\theta} &= 0. \end{aligned} \quad (\text{E-3})$$

The first harmonic of the four quads around the ring provides the driving term. Define

$$Qe^{i\psi} = \frac{1}{\pi} \int \frac{1}{4} \beta \frac{B'}{B\rho} e^{i\frac{s}{C}} ds, \text{ where } Q \text{ is the half width of the stopband, and } Q > 0.$$

The equation of motion becomes

$$\begin{aligned}\frac{d\phi}{d\theta} &= \left(\nu - \frac{1}{2}\right) + 2\bar{Q} + 6r^2\bar{E} + Q\cos(2\phi + \psi) \\ \frac{dr}{d\theta} &= Qr\sin(2\phi + \psi).\end{aligned}\tag{E-4}$$

The figure E.2 shows the tune after quads are excited.

Notice that four fold symmetry implies that all four quads are located at the same beta function. We get

$$\bar{Q} = \frac{\beta}{8\pi} \sum_{i=1}^4 \left(\frac{B'}{B\rho}\right)_i,\tag{E-5}$$

$$Qe^{i\psi} = \frac{\beta}{4\pi} e^{i\theta_0} \left\langle \left(\frac{B'}{B\rho}\right)_4 - \left(\frac{B'}{B\rho}\right)_2 + i \left[\left(\frac{B'}{B\rho}\right)_1 - \left(\frac{B'}{B\rho}\right)_3 \right] \right\rangle,$$

where θ_0 is the angle between quad 4 and electric septum.

The design uses all four quads to depress the tune. The quad 2 and 4 are used to produce the stopband. The quad ramps are represented qualitatively in the figure E.3.

Since quad 1 and 3 have the same ramp, we get

$$Q = \frac{\beta}{4\pi} \left\langle \left(\frac{B'}{B\rho}\right)_4 - \left(\frac{B'}{B\rho}\right)_2 \right\rangle, \text{ and } \psi = \theta_0 = 0.83115\pi.\tag{E-6}$$

The phase space is plotted in figure E.4 in terms of variables

$$\begin{aligned}R^2 &= \frac{6\bar{E}}{Q} r^2, \\ \delta &= \frac{1}{Q} \left(\nu - \frac{1}{2} + 2\bar{Q}\right) = 1 + b^2.\end{aligned}$$

. The seperatrix are two overlapping circles. The overlapped region is the stable region. Its area is

$$2(\delta \tan^{-1} \sqrt{\delta - 1} - \sqrt{\delta - 1}).\tag{E-7}$$

The motion on the out streaming seperatrix is described by

$$\frac{b \tan\left(\phi + \frac{\nu}{2}\right) + R \sec\left(\phi + \frac{\nu}{2}\right) - 1}{b \tan\left(\phi_0 + \frac{\nu}{2}\right) + R_0 \sec\left(\phi_0 + \frac{\nu}{2}\right) - 1} = e^{-4\pi b Q n},\tag{E-8}$$

where n is the number of turns after the initial condition ϕ_0 and R_0 at the electric septum .

II. Design

II.a Quad and octupole ramp

The electric septum is placed at 30mm from the closed orbit. The resonance causes the horizontal betatron amplitude to grow to 30mm at the electric septum. Two turns later the amplitude grows more to cross the electric septum. We want the phase of the beam particles to be zero ($\phi=0$) at the electric septum in order that around the ring $x<30$ mm. The electric septum kicks the particles by 1.5 mrad which transforms into a gap at the Lambertson septum. Since the electric septum is 10mm wide, the last two-turn growth can not be greater than 10 mm. The design fixed the last two-turn growth to be 10 mm at the end of the extraction ($b=0$).

The third condition requires that initially the stable region in the phase space equals the beam emittance, i.e.

$$2(\delta \tan^{-1} \sqrt{\delta - 1} - \sqrt{\delta - 1}) = -\frac{6\bar{E}}{Q} \epsilon, \quad (\text{E-9})$$

where ϵ is the beam emittance. We assume it is 10π mm-mmrad.

Given the above three conditions, we can calculate the extraction ramp for the quads and octupole using equations E-1, E-8, and E-9. We assume $\beta=4.98$ m and $\alpha=0.15$ at the electric septum. We get

$$\begin{aligned} Q &= 0.03408 & \rightarrow & 0.04035 \\ \bar{Q} &= -0.02983 & \rightarrow & -0.02983 \\ \bar{E} &= -18.39 & \rightarrow & -10.23. \end{aligned}$$

II.b Propagation from electric septum to Lambertson

Two turns before extraction the extracted beam is right on the edge of the electric septum ($x=30$ mm). We also want the extracted beam to be on the edge of the Lambertson. See figure E.5. Since $\phi=0$ at the electric septum, the betatron motion turns the beam toward the center. At the Lambertson $x=20$ mm. During extraction the closed orbit have to be bumped to 30 mm at the electric septum and 20 mm at the Lambertson. There are four trim dipoles around the ring to achieve this. See figure E.1.

III. Extraction Simulation

The particle dynamics at high field (250 Mev) have been investigated using a tracking program. The program consists of two complementary parts; one is a multi-particle multi-turn tracking program which mimics the time evolution of a particle distribution in phase space in the machine. From this we obtain the extraction efficiency, extracted beam phase space distributions, and information on aperture demands. The other piece of the program is a single particle tracking routine from which we can get machine parameters such as chromaticity, dispersion, together with dynamical quantities such as closed orbit, tune, and tune spread.

The program incorporates all the optical elements and dynamical variables relevant to the extraction process into the tracking environment. It includes the effect of the individual main magnet multipole fields up to the decapole component obtained from the magnet measurement data, including the designed edge focussing. Each magnet has been independently measured as a function of energy, the program assigns these multipole fields corresponding to the position of the magnet as installed in the ring. All trim dipoles, octopole, and ramped quadrupoles are included. The program operates only in the horizontal plane, no vertical tracking is done. A 3-vector ($x, x', dP/P$) is assigned to each particle generated in a tri-gaussian distribution of specified mean and standard deviation. No synchrotron oscillations are included since the number of turns the particle spends in the unstable region of phase space is small compared to the synchrotron frequency, hence tune modulation at large amplitudes is irrelevant to the process. Particle distributions are produced at both the electrostatic septum location (L3) and the magnetic septum (L4). Phase space distributions can be obtained at any time during the extraction cycle, special distributions showing the final 3 turns prior to exiting the machine are given at both L3, and L4. Physical apertures at these locations are examined on a turn-by-turn basis and phase space distributions of the particles lost at either place are also available. Tune information is obtained by a Fourier analysis of the particle motion over 512 turns.

IV. Extraction losses and Machine aperture

IV.a Linear Optics

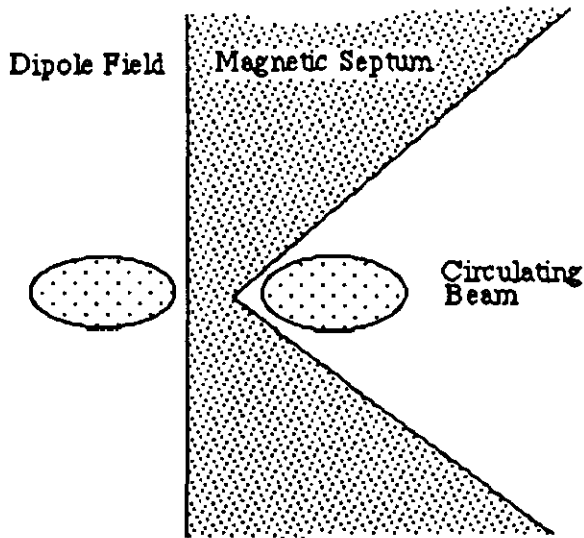
The first step in evaluating the extraction system involves using the linear machine i.e. incorporating no dipole field harmonics, and assessing the aperture needs in a perfect world. The simulation was performed using 400 particles and the quadrupole ramps were adjusted to achieve a beam spill over 20 ms. This spill length is sufficiently long (20000 turns) that the extraction dynamics will be established and phase space distributions are not sensitive to the spill length. The machine energy was set to be 250 Mev; although this is a somewhat arbitrary choice it does reflect the worst case dipole harmonics as the magnets start to go into saturation. Starting with the unperturbed machine lattice ($\nu_x=0.61, \nu_y=1.31$) the horizontal tune is adjusted close to the half integer resonance by ramping the extraction quadrupoles over a 3 ms time span, the extraction octopole is also turned on during this time. The beam is extracted by then enlarging the half-integer stopband by ramping Q2 negative and Q4 positive while keeping the machine tunes constant.

The electrostatic septum was positioned with a displacement of 39 mm with respect to the central orbit and produced a radial kick of 1.5 mrad which corresponds to a

separation between the circulating and extracted beams of ~ 4 mm at the the Lambertson location in L4. A 1.5 mrad kick at 250 Mev requires a voltage gradient of 26 kV/cm or a total voltage of 40 kV across the septum gap of 15 mm. The Lambertson magnet horizontal position was then adjusted to be aligned with the beam separation. This defined the required offset to be ~ 36 mm to the magnetic septum, and the outside of the extraction channel at 55 mm. These offsets were chosen to agree with the approximate radial positions of the various elements in the ring. Provided the electrostatic and magnetic septa are aligned with respect to each other then the absolute value of the septa offsets are arbitrary. The beam position was adjusted to be ~ 10 mm offset with respect to the central closed orbit at the L3 and L4 regions, though again this is somewhat arbitrary and reflects the choice of quadrupole ramp settings and extracted beam phase space rather than any fundamental aspect of the machine performance. The initial particle distributions have an rms spread of ± 4 mm in position and ± 0.2 mrad in angle which corresponds to a beam which occupies ± 2.0 cm in aperture at the injection energy of 2 Mev. A radial position offset corresponding to a momentum offset 0.15% was used to agree the present extraction settings. The simulated quadrupole currents require an average setting of 35A with Q2 and Q4 ramping by 60A from this value, to be compared to the experimentally determined results of an average setting of 60A with a 40A ramping needed to extract all the beam. The optimum octopole setting was found to be 6A in the simulation similar to the operational value.

Results of the extraction simulation are shown in figure E.6 which gives the phase space distributions of the particles at the Lambertson septum for the last 3 turns prior to the beam entering the extraction line. The 2-turn particle increase in amplitude is ~ 14 mm for the most extreme particles and has been adjusted to this value to utilize 12 mm of the electrostatic septum aperture. The gap between the circulating and extracted beams is ~ 4.5 mm as would be expected. The phase space distributions are suitably well behaved and assuming an effective thickness of 4 mm for the magnetic septum then the expected extraction efficiency would be $\sim 98\%$ since no beam would hit the magnetic septum. A detailed phase space of the extracted beam at both septa locations is shown in figure E.7. The radial beam size is similar at both locations demonstrating that the design apertures in these regions (15 mm and 19 mm) are well matched to the beam dimensions, the beam divergence at the start of the extraction channel has a full width at the base of ~ 2 mrad. Since the simulation program only executes in the horizontal plane then we must make an assessment of whether an effective magnetic septum thickness of 4 mm, as used in the program, is appropriate in calculating the extraction efficiency.

Schematically the beam position looks like :



Beam Positions at the Extraction Channel

The required beam separation for no particles lost is given by the vertical size of the beam, the magnet pole face angle, and the 'notch' thickness. The vertical beam size will vary as the beam intensity due to space charge blow-up at injection, a worst case scenario where the beam fills the aperture at injection (± 2.0 cm) would result in a ± 5 mm beam at 250 Mev where we have scaled by $(\beta\gamma)^{1/2}$. At lower flattop energies the vertical size would also be bigger. The septum 'notch' has a thickness of 1.5 mm with an alignment tolerance of 0.5 mm for an effective septum of 2 mm. The 'notch' half angle (ϕ) is 36 deg . The other factor to be considered is the relative vertical alignment of the beam with respect to the magnet. The required horizontal beam separation is then given by

$$\Delta_x = (\text{vertical half height})/\tan(90 - \phi) + \text{septum thickness} + \text{closed orbit error}$$

hence

$$\Delta_x = 5/\tan 64 + 2.0 + 1.0 = 5.44 \text{ mm}$$

The difference between this estimate of the necessary beam separation and that used in the simulation program is the estimate of a ± 1 mm vertical closed orbit error of the beam with respect to the 'notch', which was not present in the perfectly aligned simulation program. This estimate is based on typical closed orbit measurements made on the machine at flattop. This estimate of necessary beam separation would imply an electrostatic voltage requirement of ~ 50 kV on the extraction septum at 250 Mev.

Another factor to be considered in the issue of beam separation at the entrance to the extraction channel is the overall beam focussing in that region and the finite length of the magnetic septum. Particles at large amplitudes tend to be focussed towards the center of the machine. This can be seen in figure E.1. where both the circulating and extracted beam exhibit a net -2.5 mrad horizontal angle. The correction dipole system is capable of adjusting beam positions but not both position and angle simultaneously in this

area. This angle would imply an out-to-in radial motion of ~ 1 mm along the 50 cm length of the septum which would not be capable of correction by the trim dipoles. The solution is simply to align the septum along the phase space trajectory of the large amplitude particles rather than parallel to the nominal closed orbit. This adjustment requires moving the downstream end of the magnet while leaving the upstream end fixed. Although the size of this effect is small it is significant compared to the beam separation created by the electrostatic septum i.e. 9 kV effect voltage on the electrostatic septum.

In conclusion then from the aperture requirements based on the linear machine optics, the septa apertures are well matched and sufficient to allow good extraction efficiency. The extracted beam phase space is well behaved and the settings needed to extract the beam agree quite well with those obtained empirically on the machine. For high intensity operation when space charge emittance growth is expected then an electrostatic voltage requirement of ~ 50 kV is likely at 250 MeV output energy. Vertical position control at the magnetic septum is critical. An 'in-situ' horizontal alignment of the magnetic septum along the extraction trajectory will be necessary to maximise the available aperture and achieve best extraction efficiency. Any increase in vertical beam emittance would result in lower extraction efficiency.

IV.b Non-linear effects

Non-linear phase space behavior will occur due to higher order magnetic multipoles arising from the inevitable field errors in the as-built magnets. Each of the 8 dipoles in the ring has been measured for harmonic content (up to decapole) at various field excitation levels from injection (1 kG) to 250 Mev (15 kG). These field measurements have been incorporated into the tracking program. The extraction dynamics are potentially more sensitive to these field imperfections since large particle amplitudes are inherent to this process and multipole contributions involve higher exponents of the particle amplitude in the strength of their contributions.

The effect of these multipole fields is demonstrated in figure E 8, which contains the tune ν 's momentum information obtained by turning on the individual multipole components in the dipole magnets one at a time. It is reassuring to note that the decapole and octopole terms show a relatively small effect across a $\pm 0.4\%$ momentum range which corresponds to a position change of ± 30 mm in the dipole aperture. The sextupole term is not so negligible with the simulation predicting a horizontal chromaticity of -20 units arising from the dipole fields, this agrees well with the measured value of -22 units. The inclusion of the edge focussing from the dipoles has changed the base tune of the machine from the design value from 0.61 to 0.595, a relatively small change. The effect of these dipole fields on the extraction process is shown in figure E 9; the phase space distribution at the extraction channel. In this run the chromaticity of the machine was adjusted with the ring sextupole to -2.0 units i.e. the dipole sextupole field component was compensated. The phase space distribution of the extracted beam should be compared to that of the linear simulation shown in figure E 1. It is clear that the octopole and decapole terms have only a limited effect and produce a slight phase space rotation for particles at the largest amplitudes together with a 3 mm increase in the turn-by-turn step size. Figure E 10. demonstrates what happens when the chromaticity is uncorrected: there is now a significant phase space rotation for the large amplitude particles and the extracted beam size is larger than the available aperture causing $\sim 13\%$ of the beam to be lost. This is due to the increased tune spread across the beam requiring increased quadrupole driving terms to sweep the resonance across the full beam. The increase in driving terms also results in a increased step size which in turn pushes the large amplitude particles outside the available aperture. We have not attempted to compensate for this effect by attempting to bring the beam closer to resonance before initiating extraction and hence reducing the necessary driving terms, lowering the octopole field would also reduce the maximum step size. Since there is no appreciable dilution of the phase space volume arising from non-linear fields it is likely that suitable extraction settings can be found which would operate efficiently for large chromaticities.

A non-linear effect which we have not included in the calculation is that due to the fringe fields of the magnetic septum. This problem is potentially serious due to the large bend angle in this magnet and hence the correspondingly large fringe fields. Since no magnetic measurements were made of the fringe fields in the field-free region no qualitative statements can be made. Measurements on similar devices used elsewhere at Fermilab would lead us to expect highly non-linear behavior close to the 'notch' region where the field integral could be of the order of 1-2 kG-in for the kind of magnet design used in this machine. The effect of these fields could be significant for the large amplitude particles though one would not expect to observe much of an effect on the beam circulating on the central orbit. Since the beam only spends a few turns at the large amplitudes where these fields are at their highest the most likely effect would be to induce orbit coupling which would manifest itself as a shift in the vertical beam position. Vertical emittance growth of the extracted beam is unlikely since (hopefully) only the last 5 or so turns could be expected to be passing through this non-linear region which in all but the most extreme cases in

insufficient time to fully diffuse the beam in tune space. An intermediate case between these two scenarios is a strongly coupled regime where the vertical beam position of the extracted particles is a function of their horizontal offset. Under this hypothesis the vertical phase space will be distorted. A particle at the extreme horizontal amplitude in the extracted phase space passes ~6 mm closer to the 'notch' just prior to leaving the machine than one which barely makes it across the electrostatic septum. The particle passing close to the 'notch' experiences a vertical kick 2 turns before exiting the machine and ends up with a significant vertical displacement. It is exceedingly difficult to make any direct measurements on these small amounts of circulating beam at the edge of the phase space. The best way to observe this effect is by measuring the beam profiles in the extraction line and reconstructing both the horizontal and vertical beam phase space profile at the entrance to the start of the extraction channel. A vertical beam offset and a vertical phase space distortion would not change the extraction efficiency, growth in the vertical emittance would however strongly influence the extraction efficiency since for a fixed beam separation the aperture tolerances are quite restrictive.

Since the extraction efficiency is very sensitive to vertical beam emittance it is worth postulating whether any other potential mechanism is available to cause this effect. One such method could involve the vertical beam resonance at $\nu_y=1.33$. The natural vertical tune is close to this value and as the horizontal tune is lowered to approach the extraction condition then the vertical tune will rise and cross this resonance. The resonance is expected to be relatively weak since the skew sextupole driving harmonics in the dipoles are small (septum fringe fields?) but the beam does spend a significant time at flattop which would enhance any potential effect. This effect can be studied experimentally by placing the beam on the resonance but without turning on the extraction system and measuring the vertical emittance.

In conclusion, the effects of field nonlinearities in the dipole magnets are small and should not prevent good extraction efficiency. Large chromaticities modify the extracted phase space but should not cause beam losses if the quadrupole circuits are retuned. Extraction efficiencies will be strongly influenced by the vertical beam size, vertical emittance growth can arise from the non-linear fringe fields in the magnetic septum coupling the large horizontal amplitudes into the vertical plane, or from the effect of the vertical resonance at 1.33. Experimental observations should allow these effects to be identified.

V. Experimental Observations

Figure E.11 shows a beam intensity trace of an acceleration cycle together with the extracted beam intensity recorded in a Faraday cup in the extraction 'cave' located ~ 20 m downstream of the extraction point. The beam extraction cycle starts at 1.5 s and takes 0.5 s. There is no spill feedback turned on; the quadrupole curves are dead reckoned. The beam intensity is a bunch length sensitive signal which is only calibrated correctly at the point indicated in the cycle and shows an intensity just before flattop of 2.1×10^{10} protons. The integrated signal from the Faraday cup shows 1.3×10^{10} extracted beam. Assuming no beam losses during the intervening time then this would imply an extraction efficiency of 62%. This assumption of no beam loss is obviously not correct as can be seen by the fact that the intensity trace is declining during flattop when the bunch length is constant, the question is obviously how much beam is lost prior to the extraction time. If one takes the other extreme case by assuming that the intensity signal is correct during flattop then the circulating beam intensity at 1.5 s is 1.45×10^{10} which would imply that the extraction efficiency is 90%. The correct answer lies somewhere inbetween these two

extremes and will not be known until the final intensity monitor is installed, we are also assuming that all the beam is transported from the machine to the 'cave'. In any event the gross features of the extraction dynamics have been demonstrated to work, and particles will circulate in a well defined fashion at betatron amplitudes in excess of 40 mm as predicted in the simulation. The fact that the extraction efficiency is lower than one would estimate could still be due to slight septum misalignments at either L3 or L4. At these intensities the vertical beam emittance should not be causing any aperture problems. The mechanism causing the beam loss prior to extraction has not been identified but is obviously not caused by physical aperture limitations in the ring hence some dynamic mechanism is suspected. This effect could easily be causing vertical emittance growth which would result in lower extraction efficiencies. A measurement of the extracted beam emittances should be available soon which will be able to clarify this behavior.

In conclusion from the experimental observations one can say that the extraction system has been demonstrated to work though the absolute efficiency is not known within the range of 60->90%. The beam loss mechanism at flattop must be identified before continuing much further. A measurement of the extracted beam emittances should be made as soon as possible.

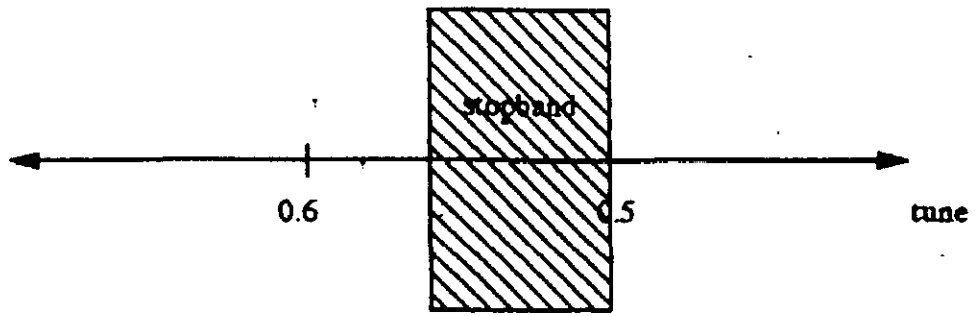


Figure E.2 Tune diagram

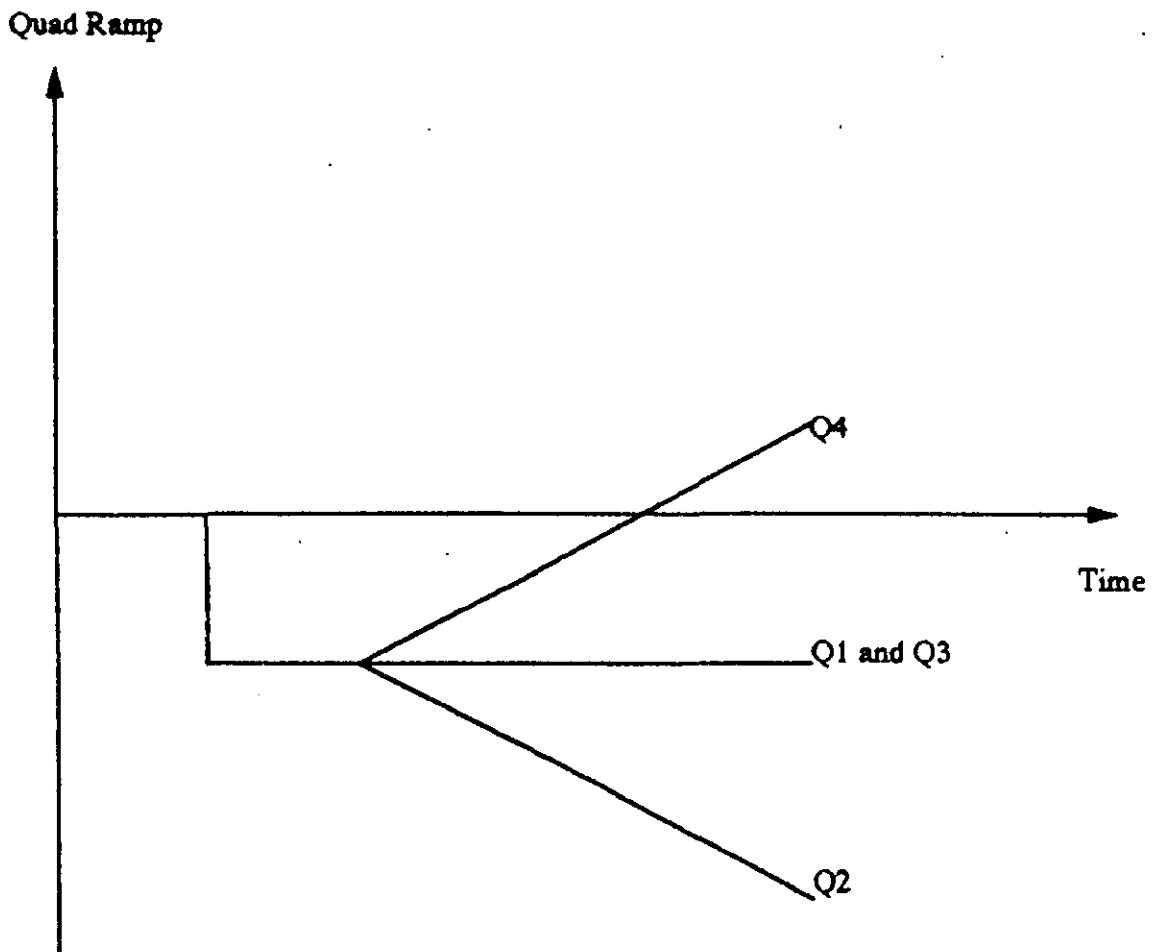


Figure E.3 Quad Ramps

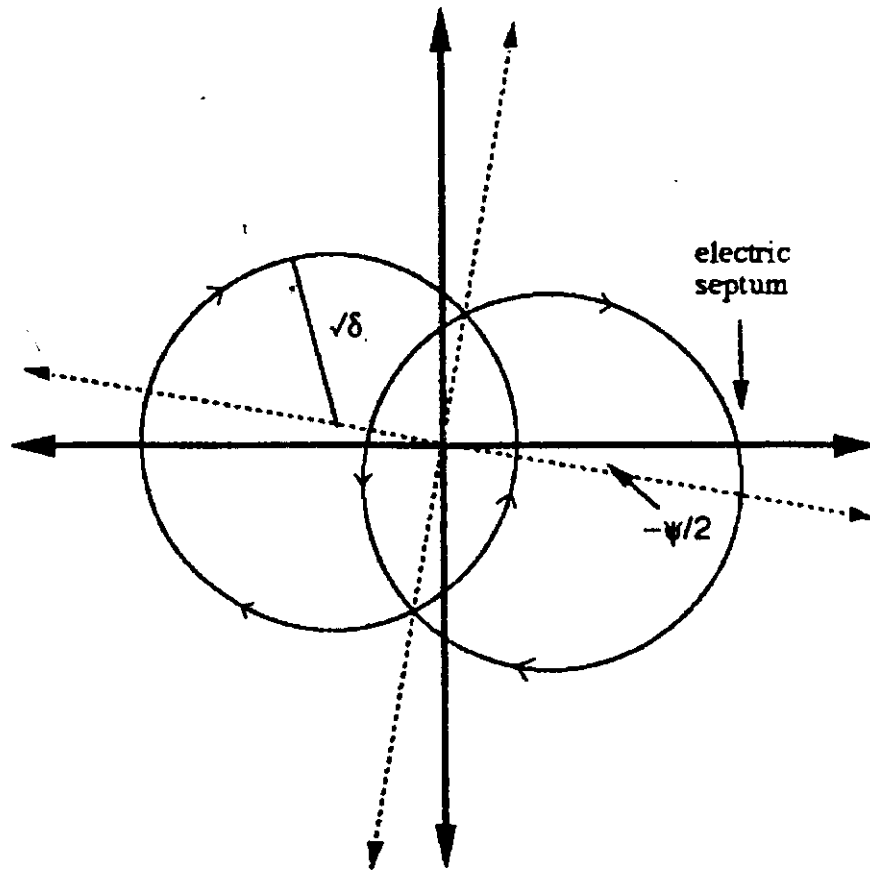


Figure E.4 Phase space trajectories



circulating beam



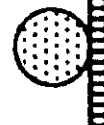
extracted beam

20 mm



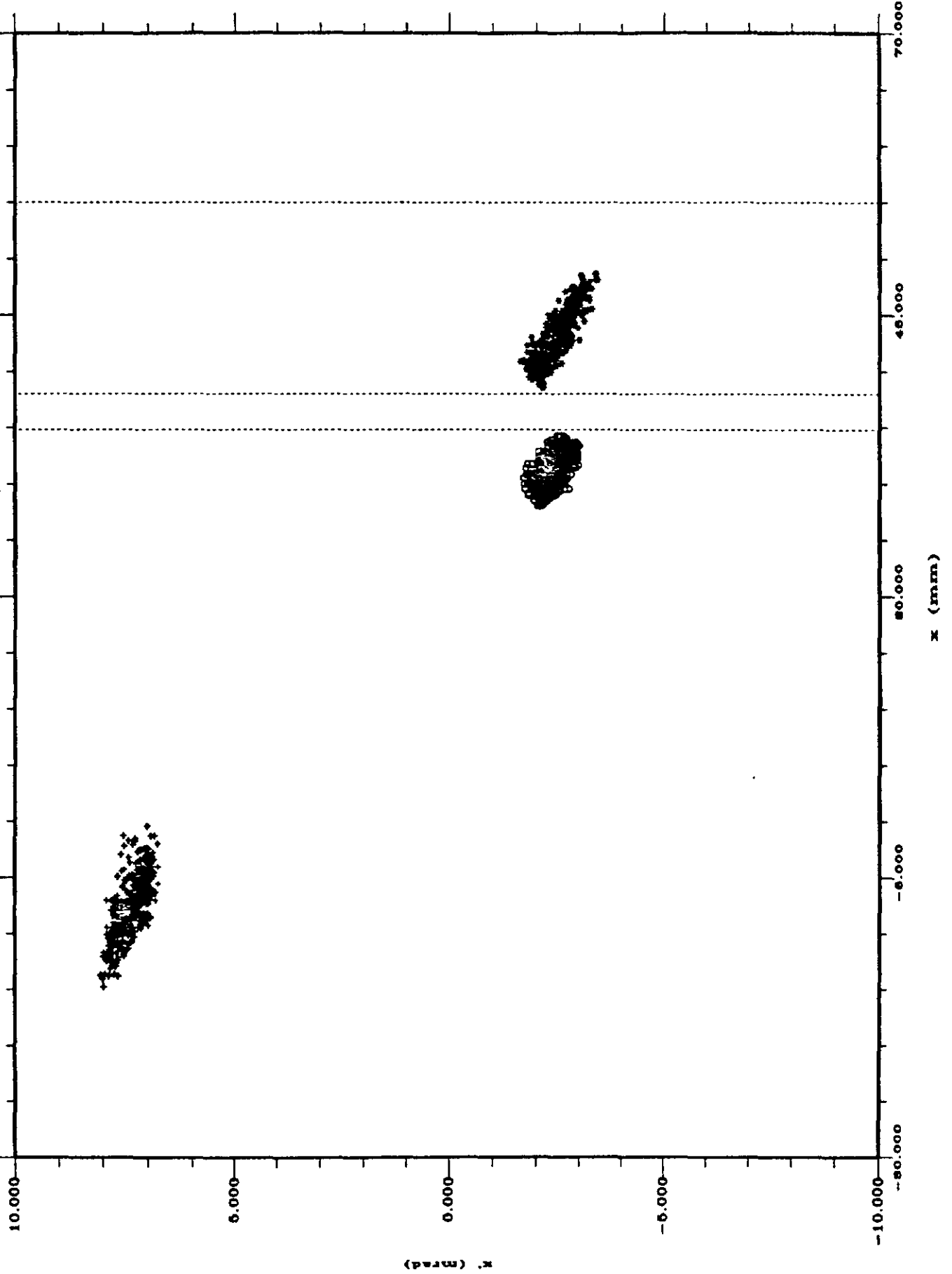
Lambertson

30 mm



Electric Septum

FAST SPILL RAMPS
Extracted at L4 (L4 dist.)
400 particles



FAST SPILL RAMPS

L3 septum
400 particles

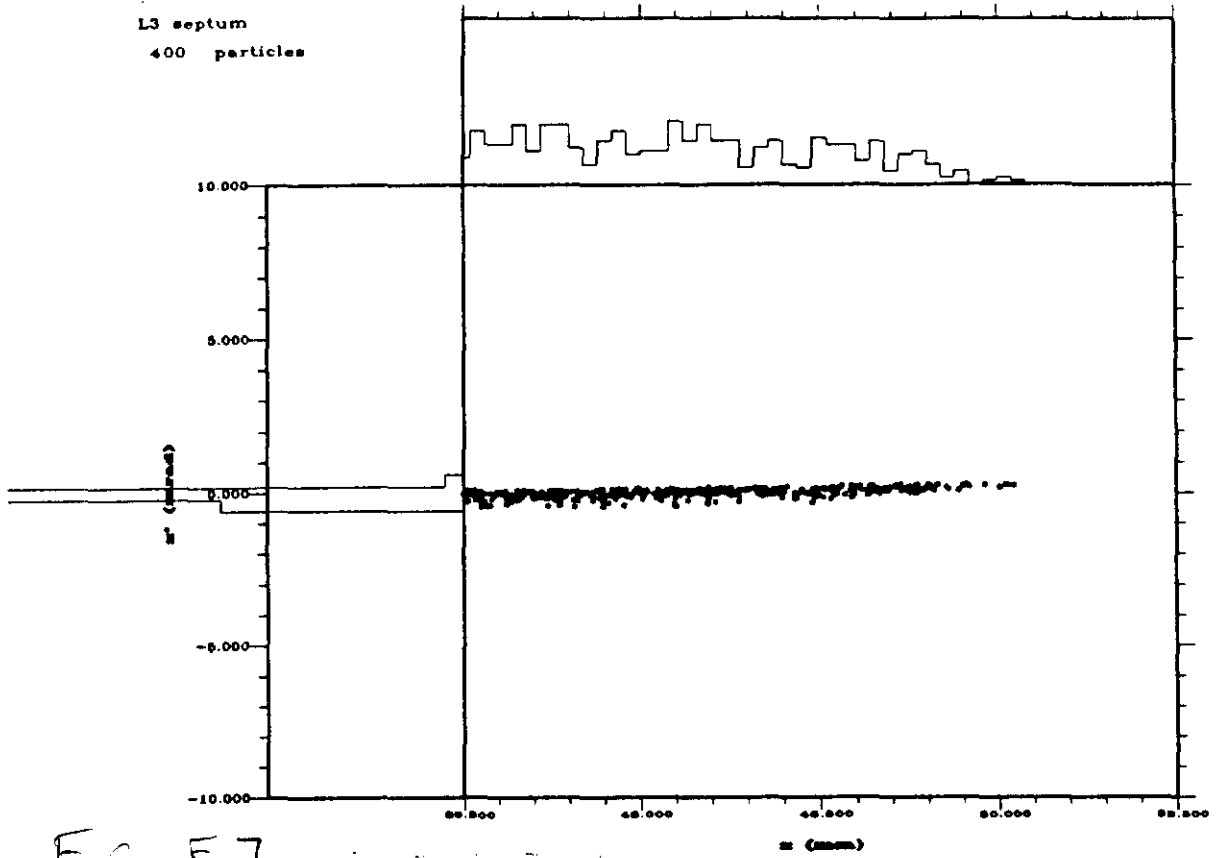
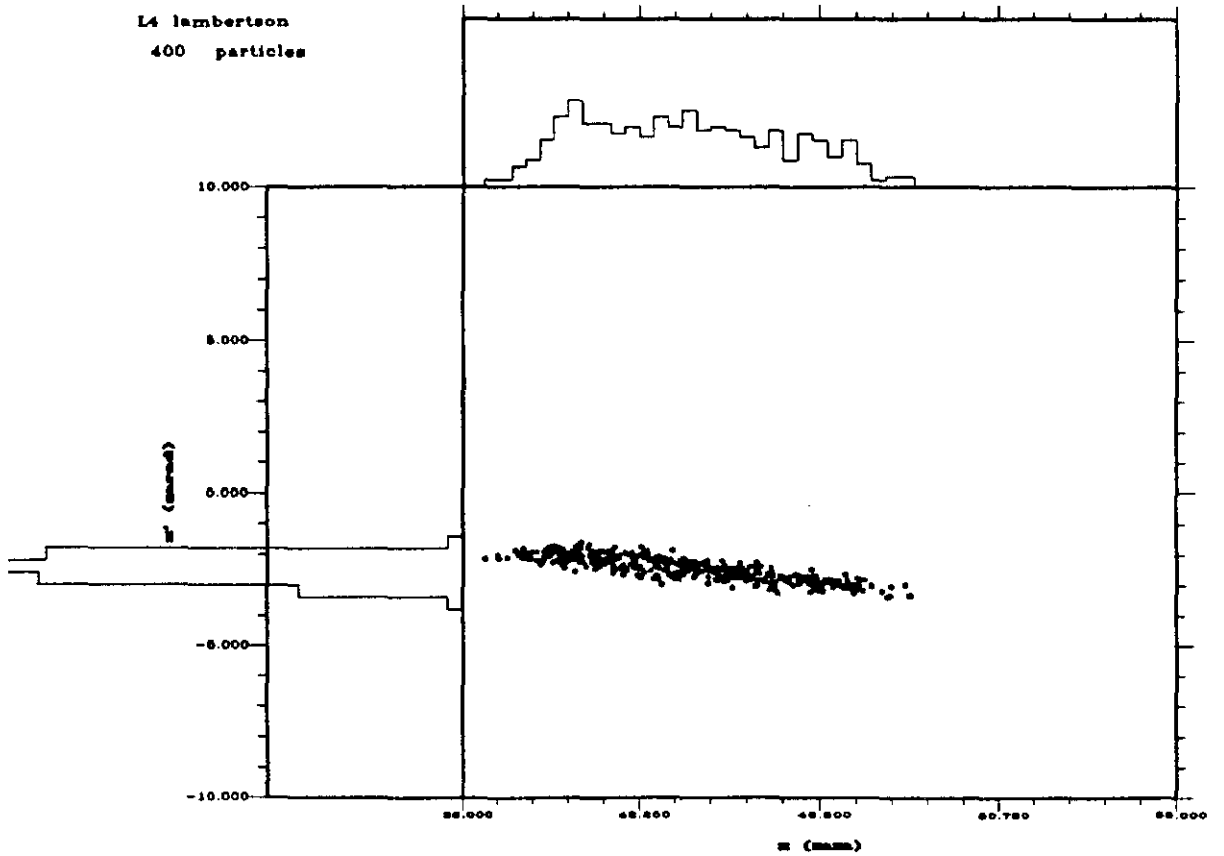


FIG E7

FAST SPILL RAMPS

L4 lambertson
400 particles



Tune v's Momentum
Sextupole harmonics only

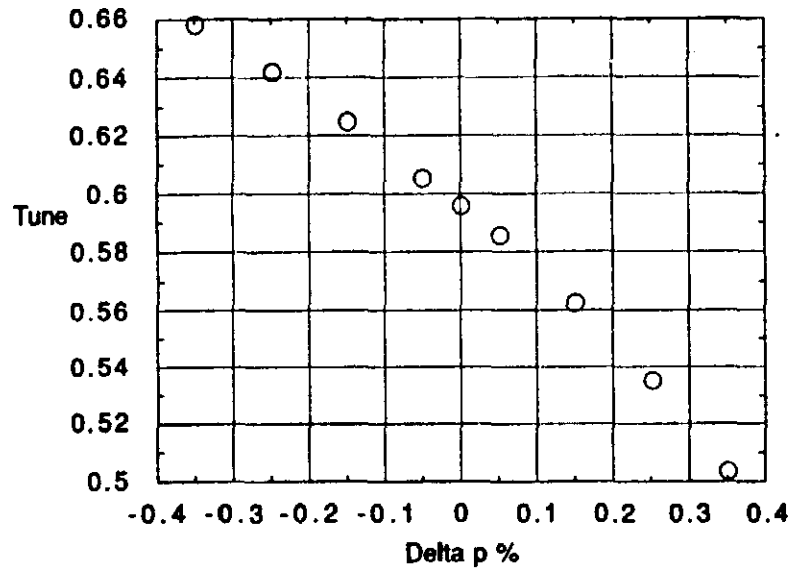
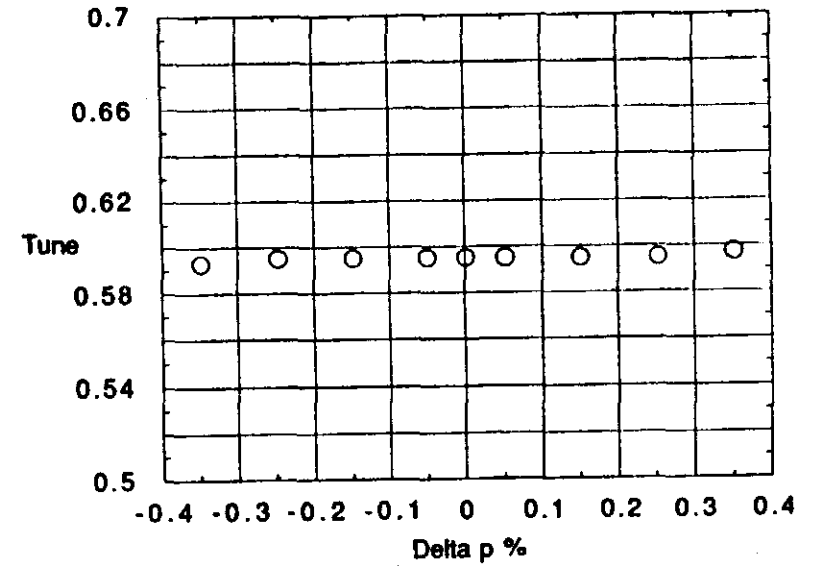
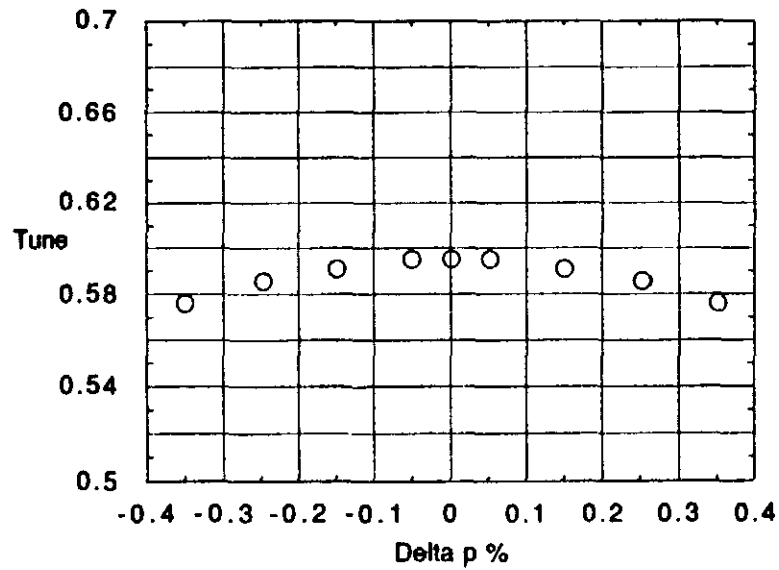


Figure 8 Tune v's Momentum

Tune v's Momentum
Decapole harmonics only



Tune v's Momentum
Octopole harmonics only



FAST SPILL RAMPS
All particles at L4
400 particles

FIG E-9

CHROMATICITY CORRECTION

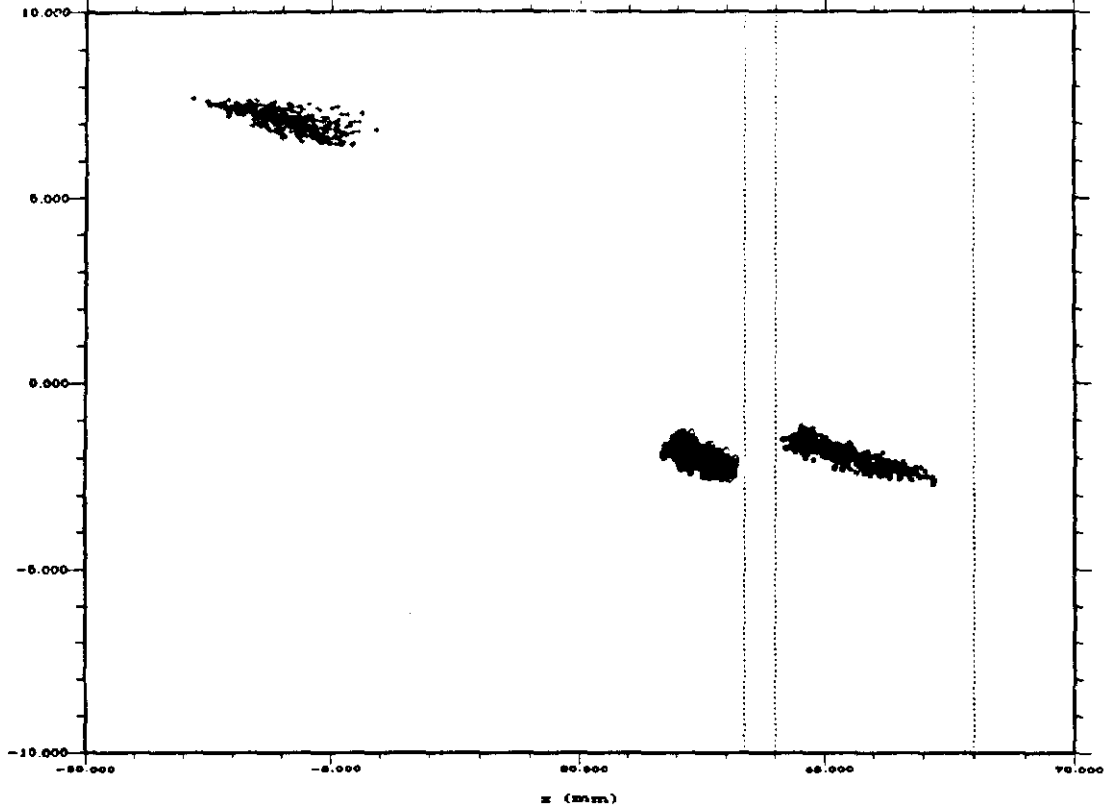
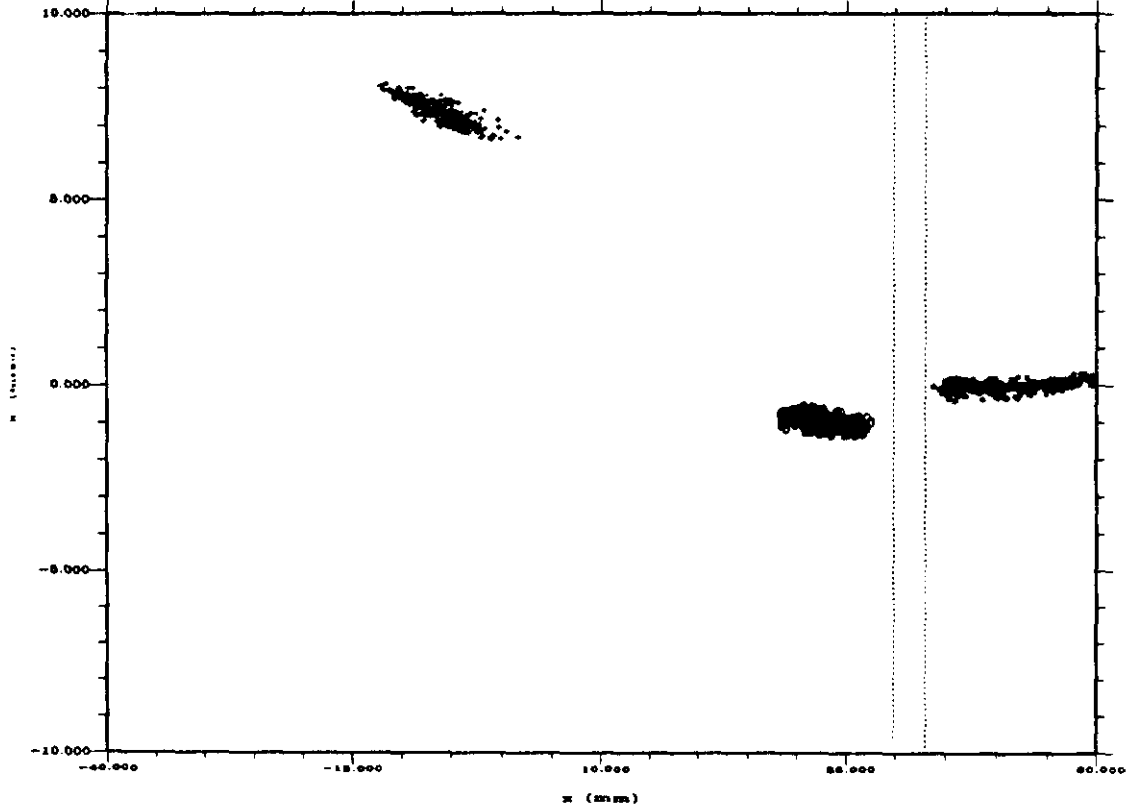


FIG E-10 NO CHROMATICITY CORRECTION

FAST SPILL RAMPS
Extracted at L4 (L4 dist.)
346 particles



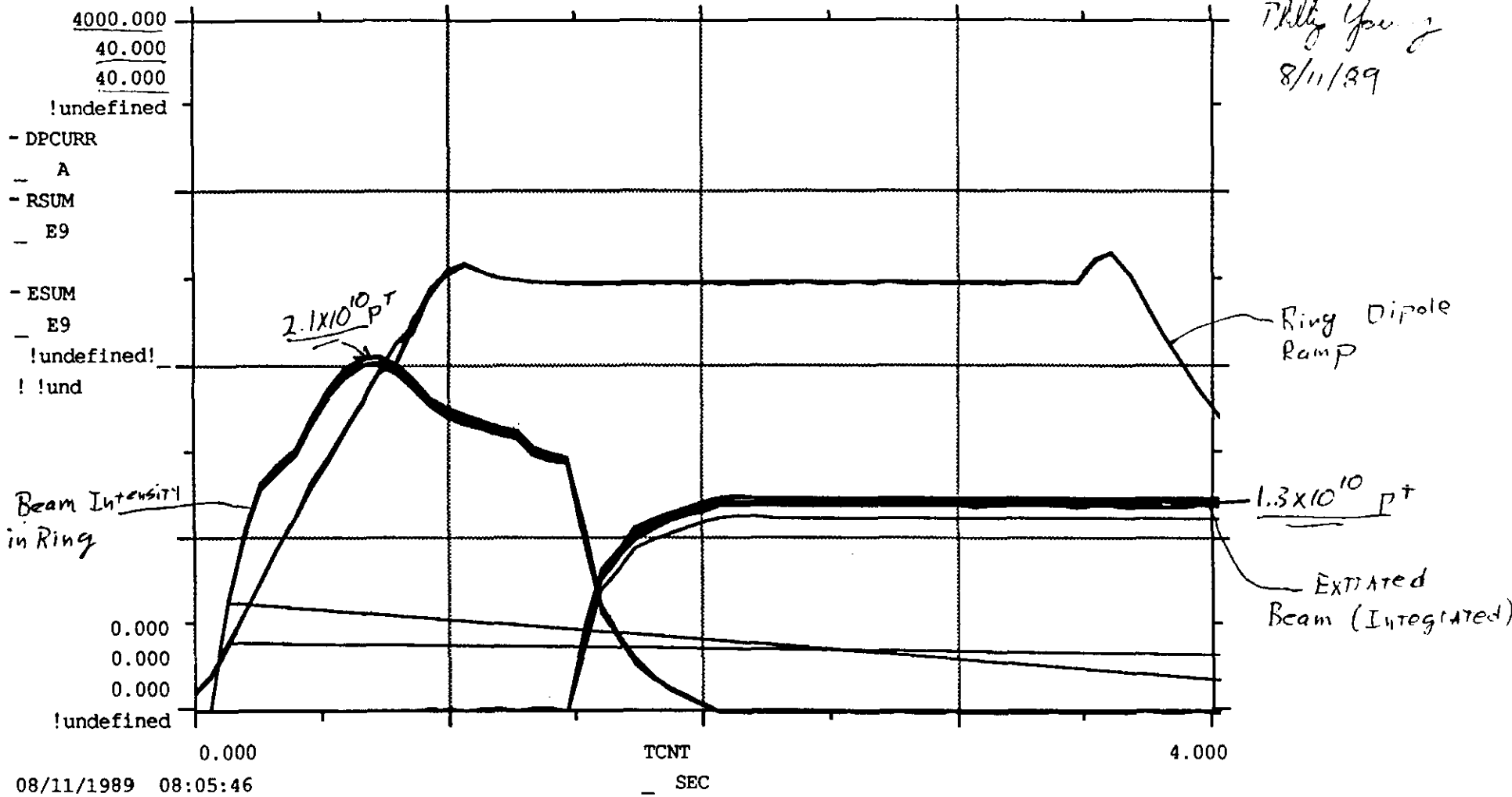


FIG E.11
 BEAM INTENSITY AND EXTRACTED BEAM
 DURING THE RAMP

D.2 Beam spill control and feedback systems.

James L. Crisp

The simple model used to understand extracted beam regulation assumes the beam has uniform density in tune space. As the tune decreases linearly with quadrupole field, or current, that portion of beam crossing the half integer resonance is extracted from the machine. This would make the extracted beam intensity proportional to dI/dt in the quadrupole as well as the density of beam in tune space. The tune spread and width of the resonance are of course complicated functions with many variables. In practice, assuming a linear relation between beam spill and quadrupole current has been found more accurate.

The fundamental limit to bandwidth of the extraction regulator is the beam response to a step change in quadrupole field. Approximately 20 turns, or 2 usec, are required before beam begins to spill out. The simplest type of feedback loop would have a 20 db/decade open loop roll off which would have an associated 90° phase shift. An integrator could be used to obtain this. To maintain a 45° phase margin, considering the 2 usec delay, the open loop gain must be less than unity at a bandwidth of $45/(360*2 \text{ usec}) = 62.5 \text{ Khz}$. The closed loop bandwidth then becomes 62.5 Khz. The loop could of course be made more complex but the performance improvement would not justify the effort. The advantage in implementing this large bandwidth is that errors, or spill variations, are reduced by the open loop gain. Spill variations caused by 60 Hz power supply ripple would be reduced by about a factor of one thousand.

The next problem to be considered is the shielding effect of the beam pipe. The iron core trim quadrupoles located at the short straight sections are mounted outside of the beam position detectors. The detector wall is constructed from .125 inch thick stainless steel and is roughly rectangular with dimensions 3.25 x 5.72 inches. A round conducting pipe would act like a low pass filter with a corner frequency as given below.

$$f_0 = \frac{n\rho}{\pi\mu a\omega}$$

μ - permitivity, $4\pi e-7$

a - radius of pipe, meters

ω - wall thickness, meters

ρ - resistivity, $9e-7$ ohm-meter for stainless steel

n - 1 for dipole, 2 for quadrupole

Assuming the detector can be approximated with a 6 inch diameter .125 inch wall stainless steel pipe, the corner frequency becomes 1880 Hz. In addition to this roll off, the iron core itself will introduce another pole. This compares with the estimated 220 Hz roll off of the dipole field due to the stainless beam pipe in the main dipole magnets.

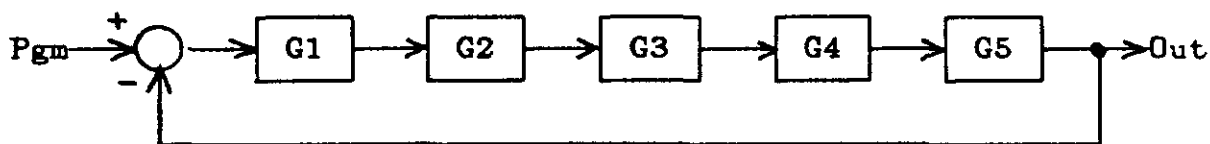
In order to realize a broad bandwidth system it was necessary to use an air core quadrupole mounted on a ceramic beam tube. The air core quad is driven with a, small, current regulated, ± 20 amp, ± 100 volt supply having a 40 KHz bandwidth, a Tecron 7560. It is more cost efficient to use an iron core trim quad to control the larger, slow variations in spill however. The iron core quad is driven with a current regulated shunt transistor supply built by Fermilab which has a two pole roll off at 250 Hz but can produce up to 200 amps at 20 volts.

The iron core quad has 24 turns per pole, is 3 inches long, and has an impedance of .048 ohms in series with 3.2 mH. The air core quad has 45 turns per pole, is 6 inches long, and has an impedance of .35 ohms in series with 1.5 mH, including the cable into the enclosure. The inductance of the quadrupoles and the maximum supply voltages will limit the amount of current available at the higher frequencies.

This dual system parallels the ones used in the Main ring and Tevatron fairly closely. In those systems the fast loop is known as the "bucker", it bucks out fast ripple in the spill, and the slow one is called "QXR", for quadrupole extraction regulator. The bandwidth limits due to quadrupole step response, about 400 usec, are much more severe in those machines however.

With an intensity of $1e10$ protons, the average extracted beam current becomes $1.6e-10$ amps if it is spilled out over a 10 second period. The formidable task of measuring this quantity with the required accuracy and bandwidth was accomplished using a photomultiplier tube and plastic scintillator. A gas scintillator was tried without success. The problems were apparently the signal to noise ratio and the saturation level of the tube. Once these problems are overcome the gas scintillator is the better detection method as it offers a smaller cross section to the beam.

A simple block diagram is shown below for the buckler system. With the constants below, stability will limit the bandwidth to about 30 KHz. The open loop gain will stay constant to 37 Hz, then decrease at 20 db/dec to reach unity gain at 30 KHz. The closed loop response will stay constant at unity gain to 30 KHz, then decrease at 20 db/dec.



Block diagram used for both the buckler and QXR systems

$G1 = Kf$	$Kf = \text{variable, nominally } 5$
$G2 = Kp \frac{\omega_p}{s + \omega_p}$	power supply, $Kp = 12.5, \omega_p = 40\text{Khz}$
$G3 = \frac{1}{R} \frac{\omega_l}{s + \omega_l}$	load, $R = .35 \text{ ohms}, \omega_l = 37 \text{ Hz}$
$G4 = Kb e^{-as}$	beam, $Kb = \text{unknown}, a = 2\text{usec}$
$G5 = Kd$	spill detector, $Kd = \text{unknown}$

The Tecron supply has an AC coupled mode with a corner frequency of around 60 Hz. This seems to be about right for the cross over frequency between the QXR and the bucker loops. The 60 Hz corner frequency allows the use of zero for the bucker program. This will provide a 3 msec rise time at the beginning of spill.

The bucker loop is used without a memory system. The QXR loop however uses an IBM AT computer to digitize the beam current in the accelerator and to generate an error signal that drives the special supply for RSS2Q, the iron core trim quad at short straight 2. The computer is used to form a learning or memory system which can reduce repetitive errors. The fast errors that the bucker works on are unlikely to repeat cycle after cycle and thus do not require a learning system. The QXR loop, however, works on slower variations consistent with line voltage changes or temperature drifts in the various devices used in the accelerator. It will also learn out or correct imperfections in the program for the other quads used in extraction. The block diagram used for the bucker can be used for QXR with the redefinition of the blocks as shown below.

$G1 = Kc$	computer transfer function
$G2 = Ks \frac{\omega_s^2}{(s + \omega_s)^2}$	power supply, $Ks = 20 \text{ A/V}, \omega_s = 250 \text{ Hz}$
$G3 = \frac{\omega_p}{s + \omega_p}$	beam pipe, $\omega_p = 1880 \text{ Hz}$
$G4 = Kb$	beam, $Kb = \text{unknown}$
$G5 = Kd$	intensity monitor, $Kd = 1V/2.8e9$

The QXR loop digitizes the accelerator beam current as determined with the position detector, or BPM, sum signal. The BPM sum signal has a 10 Khz bandwidth and is sampled at a 2 Khz rate. The 2 Khz sampling rate was selected as it provides a reasonable memory requirement for the IBM AT, a comfortable oversampling rate,

and is obtainable with inexpensive A/D boards readily available. Oversampling provides a margin against nonlinear sampling effects such as aliasing and improves accuracy. In addition, the display of the sampled spill provides a more useful diagnostic. A 1 KHz single pole filter prior to the A/D converter and after the D/A converter are used to reduce aliasing.

The sampling code is written in assembly language and makes use of the 80287 numerical coprocessor. The calling program, however, is coded in the C language. The program is outlined below.

- 1) wait for interrupt while processing keyboard input, (in C)
- 2) Initialize pgm and dpgm on the first sample, (in assembler)


```

      pgm      = adc
      dpgm     = pgm/np
      
```

each 2 Khz sample, read adc and output to dac

```

      ain[i]  = adc
      err[i]  = ain[i] - pgm
      dac     = prp*err[i] + mem[i]
      pgm     = pgm - dpgm
      
```
- 3) after extraction, update memory, (for all i), (in C)


```

      mem[i] = ret*mem[i] + lrn*err[i+psft]
      
```
- 4) apply neighbor gain, or filtering, (for all i), (in C)


```

      mem[i] = ng*(mem[i+1] + mem[i-1]) + (1-ng)*mem[i]
      
```
- 5) correct gain and limit to ± 2048 , (in C)


```

      mem[i] = (1-ng)*mem[i];
      
```
- 6) plot ain, err, or mem arrays as requested, and return to wait for interrupt, (in C)

variables

```

float arrays, np elements
    ain      input array, beam current
    err      error
    mem      memory
double precision
    pgm      desired beam current
    dpgm     desired beam current change per sample
    prp      proportional gain
    ret      retention rate
    lrn      learning rate
    ng       neighbor gain
integers
    adc      A/D reading
    dac      D/A output
    psft     phase shift
    np       number of samples
  
```

Single precision floating point arrays are required for ain, err, and mem in order to avoid overflow errors. The learning algorithm uses a phase shift term, psft, so that the error signal can be shifted in time to correct for delays through the system, such as the delay through the power supply. The variable "lrn" adjusts the amount of error added to memory and the variable "ret" adjusts the amount of memory retained. The effects of these algorithms on one memory array element versus number of cycles can be understood by tracking the value for a few steps as shown below for a constant error input.

$$\begin{aligned} \text{mem}(m) &= \text{ret} * \text{mem}(m-1) + \text{err} \\ \text{mem}(1) &= \text{err} \\ \text{mem}(2) &= \text{ret} * \text{err} + \text{err} \\ \text{mem}(3) &= \text{ret}^2 * \text{err} + \text{ret} * \text{err} + \text{err} \end{aligned}$$

for $\text{ret} \neq 1$

$$\frac{\text{mem}(m)}{\text{err}} = \sum_{n=0}^{m-1} \text{ret}^n = \frac{1 - \text{ret}^m}{1 - \text{ret}}$$

for $\text{ret} = 1$

$$\frac{\text{mem}(m)}{\text{err}} = m$$

for $\text{ret} < 1$

$$\frac{\text{mem}(m)}{\text{err}} \approx \frac{1}{1 - \text{ret}} \left[1 - \exp^{-m(1 - \text{ret})} \right]$$

It should be noted that if "ret" is greater than one, the memory values will grow without bound. If it is less than one, the memory values will converge to a finite value, and if it is equal to one it will be proportional to m. If "ret" is less than one then the system will act like a low pass filter with time constant $\tau = 1/(1 - \text{ret})$ in cycles.

Neighbor gain is a simple way to smooth the memory array each time the cycle is completed. In order to understand its effect on the feedback loop, the algorithm was applied to a random series of numbers and a fourier transform was applied to the the output sequence. The result is that it could be approximated with a simple low pass filter with the bandwidth shown below for a 2 Khz sample rate.

ng	BW
.99	4 hz
.968	14
.9	40
.684	98
.5	146

Typical operating values for the QXR program are provided below.

prp	16	
ret	.95	$\tau = 20$ cycles
lrn	8	
ng	.95	BW = 20 Hz

The A/D and D/A are both on a Data Translation DT2811 board. The board also has 8 digital inputs and 8 digital outputs as well as an external interrupt and clock. The A/D has 16 single ended input channels which can be switched into the sample and hold that drives a single 12 bit A/D converter with a 20 usec acquisition time. There are two independent 12 bit D/A converters having a 7 usec settling time on the board for output. The D/A is configured for 0 to +5 volts input and the A/D for ± 5 volts.

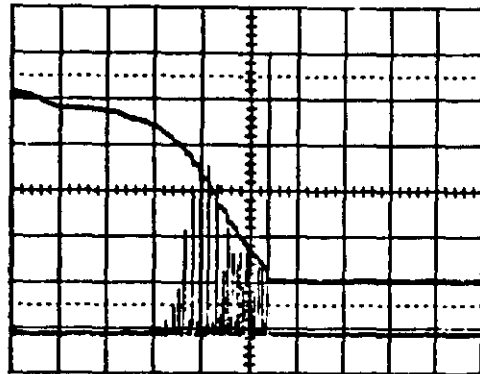
The accuracy of the system with 12 bit resolution is greatly improved with oversampling. The largest intensity for the 12 bit A/D would be 4096. With a sampling rate of 2 KHz and beam spill lasting 10 seconds, the desired beam current would change by only .2 counts per sample. However, the 250 Hz bandwidth of the QXR power supply has the effect of averaging 8 of these samples together to form the correction. Although the sampling errors of $\pm 1/2$ count are large compared to the desired regulation, the mean value of the samples should follow the true beam current with sufficient accuracy.

The calculations in the sampling loop are performed with the 80287. Internal to the 80287 all numbers are stored in an 80 bit floating point format. In particular, the values for pgm, dpgm, and prp are kept in registers throughout the extraction period. Thus the accuracy of the pgm value, which tracks the desired beam current, is more than sufficient.

Figure 1 compares the beam current and spill intensity for 3 conditions, both loops off, QXR loop on, and QXR and the bucker loops on. Variations in spill intensity are reduced by a factor of 30.

References:

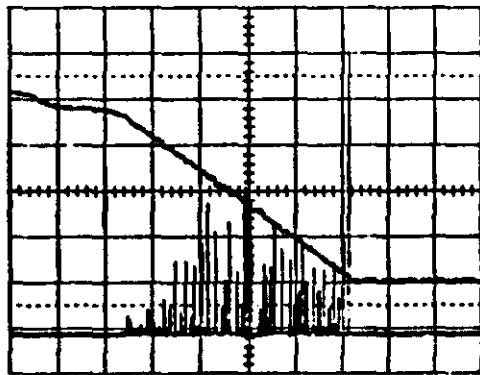
- 1) Chapman, L., Finley, D. A., Harrison, M., Merz, W., Tevatron Extraction Microcomputer, IEEE Trans. Nuc. Sci., Vol. NS-32, No. 5, October 1985.
- 2) Chapman, L., Finley, D. A., Harrison, M., Merz, W., Pfeffer, H., Operation of the Tevatron Extraction System., IEEE Tran. Nuc. Sci., Vol. NS-32, No. 5, October 1985.



QXR and Bucker off

BPM Σ

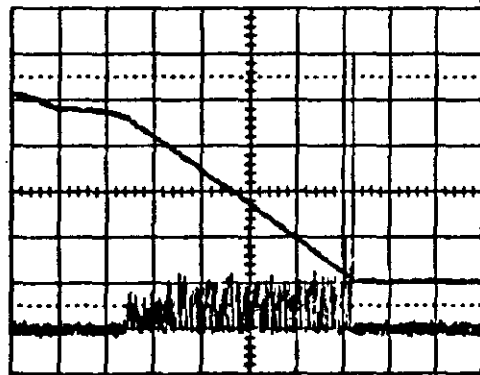
spill 2V/div



QXR on, Bucker off

BPM Σ

spill 2V/div



QXR and Bucker on

BPM Σ

spill 200mV/div

Figure 1. Beam current and spill during extraction. Spill signal obtained from photomultiplier tube with plastic scintillator. Note factor of 30 reduction in spill modulation. (BPM Σ $1.4e9/div$, $.2sec/div$)

E.1 POWER SUPPLY REQUIREMENTS AND PERFORMANCE IMPLICATIONS

A.T. VISSER

- (1) All power supplies operate from either a 208-v source (3 phase, grounded wye, with 3 ph + g wired to power supply) or a 480V source (3 phase, grounded wye, with 3 ph + G wired to supply), except type D is supplied from a 400 Hz converter.
- (2) All supplies contain two types of regulators selectable through the power supply control system. These regulators are:
 - (a) Constant Voltage (CV)
 - (b) Constant Current (CC)

The CC regulator incorporates the CV regulator as an internal voltage feedback loop.

- (c) Settling time for closed-loop response is specified to be 50 msec for all power supplies.
- (d) Warmup time is specified as 30 minutes for all power supplies

Summary of Specifications Specifications for Power-Supply Types

Supply Type	A	B	C	D	E
HZ	60	60	60	400	60
AC volts in	208	208	208	208	208
KW out	2	7.5	22.5	12	255
Max amps out	200	250	750	400	3000
Operating range					
voltage (v)	10	30	30	30	85
current (a)	200	250	750	400	3000
Operating Quadrants	I,III	I	I	All	I,IV
By Pass Dev	Thyris.	Diode	Diode	Thyris.	Thyris.
Rep. Period (sec)	1	1	1	1	1
Max Ripple Out (MV)					
Pole-to-Pole	33	500	400	33	700
Common Mode	100	1000	400	100	1000
Min Ripple Freq (Hz)	360	360	360	2400	720

Regulation					
CV, % of No Load	0.1	0.1	0.1	0.1	0.1
CC, % of full load	0.1	.05	2	.03	.01
Closed-Loop Response					
Slew rate (CV or CC)					
Voltage (V/sec)	50	50	360	2000	4000
Current (KA/sec)	1	.5	2	10	6
Transient Overshoot					
CV (V)	.15	.15	.15	.30	1.5
CC (A)	4	2	1	4	5
Dynamic Deviation					
CV (V)	1.5	1	0.8	1.2	10
CC (A)	20	5	10	20	12

- (1) Four (4) type D supplies are fed from one static frequency converter rated 208V, 30, 400 Hz, 115A out at 480 V, 30 60 Hz in.
- (2) Reference: Spec No. 37-10174, SSSL/DC-174, WBS 1.3.3.3 Magnet Power Supplies for Loma Linda Medical Center Proton Therapy Facility

In addition to the above magnet power supplies there are the following special power supplies:

- (1) injection septum power supply
- (2) kicker power supply
- (3) chopper power supply

The specified power supplies for the Loma Linda accelerator, to be supplied by INVERPOWER, were not ready at the time of preliminary accelerator testing at Fermilab. A variety of standard beamline power supplies were therefore borrowed by Loma Linda for temporary use at the accelerator test set up at Fermilab.

One PEI 500 KW power supply tapped at 200V/2500A was used instead of the four (4) type E supplies for the 8 ring magnets. The extraction Lambertson was fed from a PEI 240 KW power supply tapped at 50V/1200A and both dogleg magnets from another PEI 240 KW power supply at 50V/1200A. The quads and other loads were mainly supplied from PEI 20 KW power supplies trapped at 50V/100A. Abbreviated data sheets for the PEI 500, 240, and 20 kW power supplies are attached for reference.

Comparing these data sheets to the Loma Linda supplies shows that the current regulation is about the same. There are however major differences in output ripple voltage. Also, all PEI power supplies operate in one quadrant only. I think however that the output in ripple voltage is the most important difference. All PEI power supplies are 12 phase or 6 phase, SCR controlled, with a free-wheeling diode, unfiltered output, power supplies, fed from a 3-phase, 60 Hz source.

All PEI 20 KW power supplies have 360 Hz and higher harmonics in the DC output voltage. The PEI 500 and 2040 KW power supplies have 720 Hz and higher harmonics in the DC output voltage. A small amount of lower harmonics in the DC output could be present as a result of AC sources imbalances and slight power supply transformer differences.

The amplitude of the principal harmonic in the DC output of the PEI power supplies changes with the DC operating level as shown in Figure 1 for free-wheeling diode operation. The ripple is the highest around 50% DC output. For instance the Main Ring PEI 500 KW power supply requires about $2500A \times 8 \times 4.2 \times 10^{-3} \Omega = 84V$ (40%) DC output during flattop and has about $0.15 \times 220 = 33$ volt 720 Hz ripple amplitude at that point. This results in a 720 Hz ripple current of

$$\frac{33}{2\pi \cdot 720 \times 8 \times 3.96 \times 10^{-3}} = 0.23A \text{ amplitude or about}$$

$$\frac{0.23}{2500} \times 100 = 0.01\%.$$

The true operating ripple current will be larger due to eddy current and hysteresis losses of the magnet steel and vacuum chamber.

Injection takes place at lower current and voltage, and a 720 Hz ripple current of 1% could be present during injection. The Main Ring vacuum chamber and magnet steel will attenuate (they act as a low pass field ripple filter) the field effect of the true magnet current ripple may be a factor of 5? Similar exercises can be made for the quad supplies and other magnets.

The specified power supplies produce about a factor of 100 less (depending on the operating point) ripple voltage.

Accelerator operations with the PEI power supplies is therefore not expected to be as good as with the specified power supplies.

References

- (1) SLL/DC-233, WBS 1.3.2.4.2.1, OSHPD SL-879876-36, Revision 0, January 27, 1988, "Loma Linda University Medical Center Proton Therapy Facility Injection Septum Power Supply Design Report".
- (2) SLL/DC-183 WBS 1.3.2.4.1.9, Revision 0, August 26, 1987, "Loma Linda University Medical Center Proton Therapy Facility Kicker Power Supply Design Report".
- (3) SLL/DC-180, WBS 1.3.2.4.0.2, Revision 0, August 26, 1987, "Loma Linda University Medical Center Proton Therapy Facility Chopper Power Supply Design Report".

E.2 DIAGNOSTICS AND BEAM MEASUREMENT

R.C. WEBBER

Intensity and Longitudinal Parameter Measurements

Beam current and charge measurements are essential to many facets of the accelerator operation. These include diagnosing problems and assessing performance during commissioning, monitoring routine operation, and accounting for accelerated beam during patient treatment.

Ion Source and 30 KeV Transport Line

The intensity of the 30 KeV beam is adequately monitored by two toroidal current transformers, as shown in Figure 13.1. The transformers, of Fermilab design and construction to match the tight space constraints in the beam line, have risetimes of less than one microsecond. Presently, the output beam current signals are transmitted to the control room where they are available for monitoring on an oscilloscope and are connected to an amplifier and sample and hold circuit. The sampled output is available to the control system. The beam current signals presently are not integrated to provide total charge signals. Noise pick-up by these transformers and associated electronics, due to the ion source and pulsed injection devices, should be checked after the machine is re-assembled at Loma Linda to assure signal integrity.

2 MeV Line

Three toroidal beam current transformers, two Pearson model 3100 and one Pearson model 2854, are available for monitoring the beam in the 2 MeV transport line. These are located directly after the RFQ, the debuncher, and the 180° bend magnet respectively. Outputs from these transformers are handled in the same manner as those from the 30 KeV line transformers. The low sensitivity of these devices (.5 volt/amp into 50 Ω) and the 10-30 mA beam currents they measure combine to require that particular attention be paid to minimizing noise pick-up to maintain accuracy.

There are no wideband current monitors in the 2 MeV line to see the 425 Mhz bunch structure.

SYNCHROTRON RING

DC Monitoring and Beam Position System Sum Signals

The synchrotron lacks a dc responding current transformer for measuring beam current. This has made beam intensity and efficiency measurements difficult during machine commissioning. At the hospital, a device for

accurate proton measurement and accounting will be essential. An appropriate dc monitor is presently on order from Bergoz in France. The relevant specifications can be found in Table 13.1. Delivery has been quoted as October, 1989, in time for re-assembly of the machine at Loma Linda. Tests of the adequacy of the magnetic shielding as provided by Bergoz are recommended as soon as the device can be installed in its operating environment with near-by magnets, etc. powered and ramping. Additional shielding may be necessary. Baseline variation of the output signal need not be tolerated at any level significant with respect to beam current being measured, e.g. 100 μ A variation maximum.

The current measurement provided by this device can be normalized to the particle velocity to give a charge measurement using a Fermilab supplied analog normalizer circuit and an analog signal proportional to rf frequency (scaled to $V_{out} = F_{rf}$ (Mhz)) available from the low level rf system.

Dc referenced beam intensity measurements are presently made using one or more of the slow sum signals available from each of the eight beam position electronics modules. These signals are useful for relative intensity measurements. One of these signals, connected into an A/D channel of the control system (RSUM), has been scaled in the database to provide a calibrated intensity reading at 230 Mev energy. These signals rely on bunched beam and are frequency and bunch length sensitive. Output signal bandwidth is dc to about 10 KHz.

The beam position system also provides Fast Sum signals with about 20 Mhz bandwidth. These signals are proportional to the derivative of the beam current integrated with a 13 nsec time constant. They have been used so far only in conjunction with some attempts at momentum spread measurements.

Long 2 Toroid

Calibrated beam current measurements are presently made using a Pearson 2854 toroid transformer installed in the Long 2 straight section of the ring. Associated with and located near the transformer is a circuit providing two amplified outputs and feedback to extend the low frequency time constant of the transformer to about 0.5 seconds. The amplified outputs are calibrated at 5 mV/mA into 50 Ω (25 mV/mA into high impedance). The transformer/amplifier system was measured on the bench before installation to have 40 Mhz frequency response. The environment in the ring likely degrades that response somewhat, but it remains in the range of 20Mhz or higher. One of the two outputs is brought back on heliax cable to the low level rf system to be used as the beam phase reference signal. The other output is brought to the control room area on RG58 and connected to an amplifier/fanout module providing two full bandwidth signals (25 mV/mA into 50 Ω) and one each filtered at 1 Mhz and 3 KHz (25 mV/mA into high impedance). These signals are used for general beam current monitoring, calibrated monitoring of fast current changes (destructive calibrated current measurements), and for bunching and bunch shape measurements.

Signals from this transformer suffer from lack of dc response and from noise pick-up due to the pulsed injection devices and the main dipole ramp. An auto-zero function is incorporated in the amplifier/feedback circuit to establish a dc reference at the start of each machine cycle. A dc monitor will complement, not replace the need for, this device.

Wideband Wall Current Monitor

To this point in the development of the synchrotron, the bandwidth of the Long 2 toroid signal has been sufficient to study beam timing, bunching, and other longitudinal phenomena. A wide-band wall current monitor is not planned for the machine, due to apparent lack of necessity and real lack of free space for non-essential, though useful, devices.

Extraction Line

Extracted beam is presently measured by various devices for different information.

Destructive Monitors

A Faraday cup located in the cave is now used to measure the integrated charge extracted each cycle. The signal to noise of this system is quite adequate for this purpose at present extracted beam intensities of several times 10^9 . The beam dump planned for the hospital is also designed to be electrically isolated so that charge signals may be taken from it. These monitors are totally destructive of the beam.

Semi-destructive Monitors

Several semi-destructive monitors (causing significant scattering of the beam) of the instantaneous extracted beam current are available. These include a plastic scintillator/photodiode combination, an ion chamber, and a gas scintillation detector. To varying degrees, these devices offer the bandwidth and signal to noise (S/N) required for fast regulation of beam spill quality; while suffering from beam scattering, linearity, dynamic range, and calibration problems. For machine commissioning, the plastic scintillator/photodiode combination, with the primary extracted beam directly intercepting the scintillator, has proved to be the most straightforward device to use. The beam scattering caused by any of these devices makes them unsuitable for monitoring beam at the extraction point of the synchrotron during operation at the hospital.

Non-interfering Monitors

An rf current monitor has been built and installed in the extraction line. This device presents an impedance of approximately 400Ω to the passing beam current at the second harmonic of the rf frequency (10.95-

18.34 Mhz for 70-250 Mev). A beam of $1E10$ protons spilled over one second represents an average current of 1.6 nA and an rms current at the second harmonic (assuming sensible bunch length) of approximately the same magnitude. The signal power, $i_p^2 \cdot R$, is then $1E-15$ watts or -120 dbm. Fundamental thermal noise in a 10 KHz bandwidth is -134 dbm. Therefore, a S/N of 34 db (worsened by receiver noise contribution) in a 100 Hz bandwidth (the bandwidth of the receiver electronics) should be expected at an average current of 1.6 nA.

Signals from this device have been observed, but little effort has been expended to evaluate them. Reasons for this include: 1) the difficulty of making spill regulation work well even with the relatively noise-free signals from the photodiode, 2) the unsuitability of the receiver output for application in a feedback loop due to its logarithmic amplitude scaling and its 100 Hz bandwidth limitation, 3) the expected fundamental S/N limitation of the rf monitor at the bandwidth needed for spill regulation (14 db at 10 KHz).

Observation

Short of development of a more sensitive rf current monitor, the hospital will have to rely on signals from semi-destructive monitors to regulate spill and to measure integrated doses. These monitors must be placed near enough to the patient so that effects due to beam scattering by the monitor are tolerable. This also may entail a scheme of reliably switching between different monitors if there are multiple treatment or experimental rooms.

CONCLUSIONS

With the addition of a dc current monitor, the synchrotron and its injector will be well instrumented for intensity and longitudinal parameter measurements. The exception, only if it should become necessary to measure bunch shapes with bandwidths greater than ≈ 25 Mhz, is the absence of a good wall current monitor.

The extraction system is not so well off. Spill regulation using signals from one of several distant treatment rooms is a workable but less than desirable mode of operation. While development of a satisfactory non-intercepting monitor near the extraction point would require a substantial effort, it would offer the distinct advantage of separating both the function and reliability requirements of the accelerator from those of the treatment rooms.

BEAM POSITION AND TRANSVERSE PARAMETER MONITORS

Ion Source and 30 KeV Transport Line

An emittance probe is located midway between the two solenoid lenses in the 30 KeV transport line (See Figure 13.1). The probe can measure ≈ 40 mrad and scans 2.125 inches in the horizontal plane. It consists of a

0.003 inch slot in a 0.005 inch thick tungsten mask followed 2 inches downstream by 20 collectors subtending approximately 4 mrad each. Signals from the collectors are amplified and sampled and then digitized and read by the control system to be used by existing display and analysis software. On the same mechanism with the emittance probe is a pair of orthogonally crossed wires for rough profile measurements and a fixed round aperture stop to reduce the beam emittance for machine studies. Separate, but unused, provisions are made for the application of bias voltages to the emittance probe and the crossed wires.

2 MeV Line

Four multiwire grids are planned for the 2 Mev transport line, to be located immediately upstream and downstream of both the debuncher and the 180° bend magnet. These will be used for beam profile and position measurements. The multiwires at the debuncher are installed and have the wire pattern as shown in Figure 13.2. The 180° bend downstream multiwire is installed at this time; the upstream multiwire is not. They have a wire pattern as shown in Figure 13.3. Signals from the wires are amplified, sampled, and digitized in the same manner as those from the 30 Kev emittance probe. Information can be displayed on either a dedicated monitor or the control console display.

There are no non-intercepting beam position monitors in the 2 Mev line.

SYNCHROTRON RING

Profile Monitor

One multiwire grid profile monitor of the type shown in Figure 13.3 is planned for the Long 2 straight section of the ring. The monitor is built, but has yet to be installed. Signals will be handled in the same manner as those from the 2 Mev line multiwires. This device, though destructive, can monitor beam profiles for the first few turns in the ring. This will be useful to understand transverse matching between the 2 Mev line and the ring.

Beam Position Monitors

The ring is instrumented with a beam position monitor (BPM) at each long and each short straight section, as shown in Figures 13.4 and 13.5. The monitors are of the capacitive pick-up variety, consisting of an open-ended rectangular box cut diagonally in both the horizontal and vertical planes. The resulting four electrode geometry is sensitive to beam position in both planes. The pick-ups are 4.5 inches long with horizontal and vertical dimensions of 4.5 and 2.0 inches respectively. Signals are picked off each electrode at the top or bottom center, with leads about 2.5 inches long to output connectors near one end of the housing.

Figure 13.6 schematically shows the loading of each electrode to obtain an output signal. The 4:1 impedance transformer presents 200Ω to the electrode which combines with 65 pf of electrode and cable capacitance to give a 12 Mhz corner frequency. This represents a design compromise necessitated by a desire for best signal sensitivity and bandwidth constrained by signal transmission requirements and inaccessibility of the monitor output connectors. The four signals from each location are carried to beam position electronics modules in the equipment room by 3/8 inch heliax type cables matched in electrical length to approximately 50 psec.

Eight BPM electronics modules, Figure 13.7, one for each pick-up location, are housed in a single Eurocard crate in the equipment room. Each module consists of a four channel input stage and three output processing circuits which generate the SLOW, FAST, and FIRST TURN outputs described below. Each module functions independently except for a common control of the input stage attenuators.

Each channel of the BPM module input stage presents a 50Ω load to the pick-up electrode signal and contains a 20 db attenuator which may be switched in or out of the signal path depending on the beam intensity. The attenuator is followed by a 10 Mhz lowpass filter and an input stage amplifier. The filter kills high frequencies that might otherwise cause non-linear operation in the amplifier. A front panel switch on a narrow card in the center of the BPM crate controls attenuators in all BPM modules in common. The high gain setting (attenuators switched out) should be used for accelerated beam intensities less than about $4E9$, while the low gain setting is good up to $\approx 5E10$. Higher intensities will require hardware modification to reduce the input stage amplifier gain, thereby shifting the entire operating range. The slow sum signals (described below) are the best indicators that the position electronics is operating with appropriate signal levels. The slow sum signals should be between 0.5 and 10 volts for the position signals to be meaningful. At any attenuator setting, the usable dynamic range of the electronics is approximately 26 db. About 14 db of this range is eaten up by signal growth during the acceleration cycle, since the electrode signals are roughly proportional to beam current which increases with particle velocity. Accelerated beam intensities down to $1E9$ or less can be accommodated at the present high gain setting.

The first output processing section performs amplitude detection of the four input stage signals using wideband op-amp precision diode circuits. These detected signals are then filtered and appropriate sum and difference terms are produced in op-amp circuits. Difference to sum normalization is performed by an analog divider. The three resulting outputs, the SLOW SUM, SLOW HORIZONTAL POSITION, and SLOW VERTICAL POSITION, have useful bandwidth from dc to 10 Khz. They are available on a multipin connector on the BPM crate doghouse for position monitoring and closed orbit measurements by the control system, and on SMA connectors at the module rear panel for general usage. The slow outputs are intended to drive high impedance ($>2 K\Omega$) loads. The position outputs are scaled as 6.35 mm/volt horizontally and

2.54 mm/volt vertically. One of the slow sum signals is typically used for relative intensity measurements as described above. One of the slow horizontal position signals is used for real time radial feedback to the low level rf system.

The second output circuit utilizes 200 KHz to 220 Mhz current transformers to produce wideband sum and un-normalized horizontal and vertical difference signals. For equal inputs, the difference outputs are down 240 db from the sum output for frequencies up to and beyond 20 Mhz. The outputs of this wideband summing and differencing circuit can be no better than the relative timing of the inputs will allow, hence the aforementioned electrical length matching requirements on the cables from the beam pick-ups. These FAST SUM and FAST DIFFERENCE signals, intended to drive 50 Ω , are available on SMA connectors on the module rear panel. They are scaled as $x = (\text{hor.diff/sum}) * 63.5 \text{ mm}$ horizontally and $y = (\text{ver.diff/sum}) * 25.4 \text{ mm}$ vertically. The fast difference signals find application in tune measurements and are a source of turn-by-turn position information. It was expected that these signals would provide useful turn-by-turn position measurements at injection time. This would be an important injection tuning diagnostic. To date, understanding these signals early in the machine cycle has been frustrated by beam loss on the pick-up electrodes, the dynamic longitudinal structure of the beam, and perhaps other unknowns.

The third output circuit contains triggering and sample and hold features intended to produce normalized FIRST TURN sum and positions. This section has not been implemented for reasons related to the confusing injection time signals noted above.

The slow sum and position signals are read into the control system via Data Translation, Inc. DT-1492 VME cards. One card reads the 16 positions; a second card reads the 8 sums. On-card memory stores 4096 readings per signal at a programmable digitization rate of up to 15.6 KHz per signal. Existing software allows display of closed orbits and time plots of acquired data. Save files are available for storing closed orbit data and facilitate the plotting of differences between orbits.

Extraction Line

Several wire profile monitors have been available in the extracted beam line while the machine has been operating at Fermilab. Three such devices, appropriately placed so as to allow measurement of the extracted beam emittance, have recently been inserted into the beam line in the cave. This measurement has been performed and preliminary results, according to Martin Schultz, are consistent with predictions by Lee Teng.

Beam monitoring in the extraction line and switchyard at the hospital is not within the scope of Fermilab's responsibility. SAIC does have plans to instrument these beam lines with wire profile monitors similar to those used at Fermilab.

Beam Loss Monitors

There are presently beam loss monitors instrumenting each long and each short straight section of the ring, the extraction septum, lambertson magnet, and the front end of the extraction line. The monitors are of the glass envelope ion chamber type as used in the Fermilab Tevatron and Main Ring. They are of no use to see the low energy beam losses at injection, but have proven valuable for high energy losses and extraction monitoring.

Making Measurements

There are constraints (some fundamental, some practical, some by design) on measurements that can be made on this machine. These include:

1) Space charge forces within the beam are strong at low energy creating a dynamic situation

2) Beam lifetime in the ring at 2 Mev is the order of 200 msec

3) Apparent beam loss on the BPM pick-up electrodes results in confusing signals near injection time

4) The beam must be bunched for the Beam Position Monitoring System to work properly

5) During normal acceleration, the frequency of the beam and all its associated signals is changing rapidly ≈ 10 KHz/msec

6) Space in the ring for insertion of additional diagnostic devices is virtually non-existent

7) The number and placement of trim quadrupoles constrains independent adjustment of horizontal and vertical tunes

8) The number and placement of trim dipoles, coupled with the need for rf radial feedback, make attempts to explore machine aperture with "local" orbit bumps difficult and complex

9) There is no transverse kicker or shaker in the ring for stimulating beam motion; there are no momentum scrapers either in the ring or the 2 Mev line to allow controlled definition of the momentum spread of the beam

Momentum Spread

Several methods have been used with varying degrees of success attempting to measure the momentum spread of the beam in the ring immediately after injection.

The earliest method used on this machine involved gating on a small (compared to the expected machine acceptance) fixed frequency rf bucket 10 msec after injection into a fixed magnetic field. The delay was intended to allow the notch in the circulating beam due to the injection kicker to wash out. The modulation on the beam at the rf frequency was measured using a spectrum analyzer in the zero span mode looking at either the Long 2 toroid signal or a fast BPM sum signal. On successive injections, the rf frequency was stepped over a range to cover the frequency width of the aperture. A plot of signal strength vs. frequency should contain momentum spread information. The method was not as clean as one would hope, being sensitive to the time after rf turn-on at which the signals were measured. Results consistently showed asymmetric profiles and "holes" in the frequency space.

More recently, measurements have been made using an HP 3562A signal analyzer in the triggered frequency response mode. The 0 to 100Khz noise source from the analyzer is externally up converted to about 1 Mhz to span the frequency aperture of the machine at a fixed injection field and is applied to the beam via the rf system amplifier and cavity. The beam response signal, from the Long 2 toroid or a fast BPM sum signal, is in turn mixed back down to baseband frequencies for analysis by the 3562A. This method yields both amplitude and phase information in a measurement window of 8 msec, triggered at any selected time after injection. This method seems to produce cleaner results and is accomplished more automatically than the first method. Measurements using this scheme have repeatedly indicated changes in the momentum acceptance of the machine as large as 50%, depending on the manner in which the magnets are ramped down from flattop and returned to the injection level. This indicates the possibility of significant residual fields and may point to an area which deserves further study when the final magnet supplies are operational. The supply used at Fermilab does not accommodate accurate magnet current regulation during ramp-down and return to injection level.

BETATRON TUNE AND CHROMATICITY

The synchrotron has no dedicated provisions for stimulating the beam to facilitate transverse tune measurement.

During commissioning, one of the BPM pick-ups has been disconnected from the normal electronics so as to be used as a kicker. Three of the four electrodes of that BPM are terminated in 50 Ω ; the other is driven by a 100Mhz bandwidth 200 watt ENI 3200L amplifier. The one electrode couples to the beam simultaneously in both transverse planes. Beam response is observed using a fast difference signal (both horizontal and vertical signals are available) from any other BPM module. The characteristics of the fast difference signals are such that signal strength rolls off slowly above 10 Mhz and the accuracy of the differencing begins to deteriorate above about 25 Mhz. This sets limits on which revolution harmonics and associated betatron sidebands are sensible to use for these measurements.

Two different instruments have been utilized to make the tune measurements. A frequency response measurement with an HP 3577A network analyzer, triggered to sweep through a betatron sideband frequency, is the simplest and most direct technique to use. The swept rf source from the network analyzer drives the ENI and a BPM fast difference signal is returned to the analyzer. The several hundred millisecond minimum sweep time of the instrument restricts application of this method to beam on a long, high energy flattop where conditions are stable and beam lifetime is long. The HP 3562A dynamic signal analyzer setup, described above for longitudinal measurements, is also useful for tune measurements. In this case, the 0 to 100 KHz noise source of the instrument must be mixed up in frequency, to cover the band containing the desired betatron sideband, before it is applied to the beam through the ENI. The BPM fast difference signal must then be mixed back down to baseband for analysis. The primary advantage of this scheme is the short, 8 msec, sweep time of the instrument which permits tune measurement at injection energies when the beam lifetime is short.

Chromaticity measurements typically involve tune measurements as described above made while the beam is positioned at different radii with the rf radial offset program. The betatron sideband widths also contain chromaticity information, but good accuracy with such measurements is difficult to achieve.

The tune measurement techniques above produce good results for the beam at fixed energy. Tune measurements up the ramp are exceedingly difficult because of the range and rate of the frequency change during acceleration. At a nominal revolution frequency rate of change of 10 KHz/msec even the horizontal tune line at $.6 * \text{frev}$ will move 48 KHz in the 8 msec sweep time of the 3562A analyzer. This is equivalent to a tune change of about 0.05 units, not very satisfactory resolution. We have no good solution for this difficulty at this time.